UNIVERSITY OF SOUTHAMPTON

FACULTY OF ENGINEERING AND PHYSICAL SCIENCES

Electronics and Computer Science

Data Driven Transformer Thermal Modelling for Identification of Thermal Issues

by

Atip Doolgindachbaporn

Thesis

December 2021

UNIVERSITY OF SOUTHAMPTON

ABSTRACT

FACULTY OF ENGINEERING AND PHYSICAL SCIENCES

Electronics and Computer Science

Doctor of Philosophy

Data Driven Transformer Thermal modelling for identification of Thermal Issues

By Atip Doolgindachbaporn

Electricity demand is increasing because of global decarbonisation efforts to reduce emissions that have an impact on climate change. Climate change also impacts the operation of electrical networks due to increasing ambient temperatures and extreme weather conditions. It is therefore a challenging time for power system owners to operate their assets as efficiently as possible. Power transformers are key components in the transmission systems and expensive assets. Due to economic and technical aspects, there has been much research studied to maximize their life expectancy while maintaining the reliability and stability.

The two key aims of this thesis are to develop accurate transformer thermal models, utilising a range of operational data, and to assess the thermal performance of aged units. A top-oil thermal model is developed using thermal-electrical analogy and heat transfer principles that captures thermal influence of prevailing winds and solar radiation. The key improvements of the proposed thermal model are calculating the heat transfer coefficient of the radiator on the air side using the heat transfer coefficient of combined forced and natural convection and including the solar radiation as an addition heat source. The proposed model is validated against operational measurements. The results are also compared with the predictions based on the IEEE-Annex G model. The proposed model is generally more accurate in all periods, especially windy and sunny periods as expected.

Condition monitoring of power transformers, which are key components in the systems, is essential to identify incipient faults and avoid catastrophic failures. Machine learning algorithms, i.e. nonlinear autoregressive neural networks with external inputs and support vector machine for regression are used to capture dependency of the transformer temperature on loading and weather conditions for purpose of monitoring. These thermal models are trained using historical measurements. The results are validated against field measurements and it clearly demonstrated that the alternative algorithms surpass the IEEE Annex G thermal model. An incipient thermal fault identification algorithm is then proposed and successfully used to identify an issue using measurements taken in the field. This algorithm could be used to alert the operator and plan interventions accordingly.

Table of Contents

Research Thesis: Declaration of Authorship

Print name: ATIP DOOLGINDACHBAPORN

Title of thesis: Thermal Condition Assessment of Large High Voltage Transformers

I, Atip Doolgindachbaporn, declare that this thesis and the work presented in it are my own and has been generated by me as the result of my own original research.

I confirm that:

1. This work was done wholly or mainly while in candidature for a research degree at this University;
2. where any part of this thesis has previously been submitted for a degree or any other qualification at this University or any other institution, this has been clearly stated;
3. where I have consulted the published work of others, this is always clearly attributed;
4. where I have quoted from the work of others, the source is always given. With the exception of such quotations, this thesis is entirely my own work;
5. I have acknowledged all main sources of help;
6. where the thesis is based on work done by myself jointly with others, I have made clear exactly what was done by others and what I have contributed myself;
7. parts of this work have been published as:

   1. A. Doolgindachbaporn, N. H. Nik Ali, G. Callender, J. A. Pilgrim, P. L. Lewin and G. Wilson "Identification of Fault of Pumps and Fans in Transformer Cooling System Using Winding Temperature Indicator and Load Data." Universities High Voltage Network Colloquium UHVnet, 15-16 January 2019 Manchester, UK. (Only Poster)

   2. A. Doolgindachbaporn, N. H. Nik Ali, G. Callender, J. A. Pilgrim, P. L. Lewin and G. Wilson. "Detection of Forced Cooling Faults in Power Transformers based on Winding Temperature Indicator and Load Data." IEEE Electrical Insulation Conference, 16-20 June 2019, Calgary, Alberta, Canada.

   3. A. Doolgindachbaporn, G. Callender, J. A. Pilgrim, P. L. Lewin and G. Wilson. "The Use of Thermal and Load Data to Identify Large Autotransformers that Have Aged and Degraded Electrical Insulation." IEEE Electrical Insulation Conference, 22 June – 03 July 2020, Virtual Event.

   4. A. Doolgindachbaporn, G. Callender, P. L. Lewin and G. Wilson. "Estimation on Degradation Rate of Insulating Paper in Power Transformers Using Historical Load and Thermal Data." IEEE Electrical Insulation Conference, 7 - 28 June 2021, Virtual Event.

5. G.M. Callender, A. Doolgindachbaporn, P. L. Lewin and G. Wilson. “Impact of Climate Change on the Power Flow Capacity of Transformers.” CIGRE Symposium Ljubljana 2021, 21 - 24 November 2021, Ljubljana, Slovenia. (Accepted)

There is one journal paper that has been accepted in peer reviewed academic journal:

6. A. Doolgindachbaporn, G. Callender, P. L. Lewin, E. Simonson and G. Wilson. “A top-oil thermal model for power transformers that consider weather factors”. Submission to IEEE Transaction on Power Delivery. (Accepted)

There is one journal paper under production at the point of submission of the report:

7. A. Doolgindachbaporn, G. Callender, P. L. Lewin, E. Simonson and G. Wilson. “Data-Driven Transformer Thermal Model for Condition Monitoring” Submission to IEEE Transaction on Power Delivery. (Awaiting decision)

Signature: .....

Date: ……. .....

Acknowledgements

I would like to acknowledge a number of people that support me throughout pursing my PhD and writing my thesis. Firstly, I would like to acknowledge the Royal Thai Government for financial support and National Grid Electricity Transmission for supporting the project and agreeing to the publication of results. Project Condition and Climatic Environment for Power Transformer (NIA_NGET0213) was made possible through the Network Innovation Allowance.

I am thankful that I am part of Tony Davies High Voltage Laboratory where provides friendly and professional environment. I am grateful to my main supervisor, Prof. Paul Lewin, for his encouragement, professional support and kindness. I am indebted to my secondary supervisor, Dr George Callender, who always supported and challenged me to make me a better researcher. I would like to thank my supervisor, Dr James Pilgrim, for his discussion and advice.

I would also like to thank several great engineers who supported me and make sure that my work is interesting to those who work in industry, including Dr Gordon Wilson of National Grid Electricity Transmission and Dr Edward Simonson of Southampton Dielectric Consultants.

Finally, I am very grateful to my friends and family who always cheer me up and give me their kind support. I would like to eternally thank my wife, Sukanya Nambandit, who is always with me and encourage me to complete the thesis.

Nomenclature and Abbreviation

θ_{H}	The hot-spot temperature [°C]
θ_{A}	Ambient temperature [°C]
θ_{O}	The top-oil temperature [°C]
θ_{W}	The wall temperature [°C]
H	Hot-spot factor
g_{R}	Average winding gradient at rated load [K]
h	The convective heat transfer coefficient [W/(m^{2}K)]
Q_{Fe}	Core losses or no-load losses, [kW]
Q_{Cu}	Copper losses or load losses, [kW]
Q_{Solar}	The total received solar radiation [W]
C_{O}	Thermal capacitance of top oil, [J/K]
R_{O}	Thermal resistance of top oil, [K/W]
K	The ratio of current load to rated load, per unit
$\Delta\theta_{\mathrm{O,R}}$	The top-oil temperature rise at rated load [K]
$\tau_{\mathrm{O,R}}$	Oil time constant [s]
μ_{pu}	The relative oil viscosity
n	Oil circulation exponent
$R_{\mathrm{M,A}}$	thermal resistance due to forced and natural convection of the air [K/W]
R_{R}	thermal resistance due to radiative heat transfer of the radiator wall [K/W]
$R_{\mathrm{MR,A}}$	the thermal resistance between the exterior of the radiator and ambient comprised of the forced and natural convection due to the air ($R_{\mathrm{M,A}}$) and the radiation from the wall (R_{R}) [K/W]
$R_{\mathrm{N,O}}$	thermal resistance between the oil and the interior of the radiator which considers the natural convection of the oil [K/W]
A_{C}	Cooling area due to convection [m^2]
$\overline{Nu}$	the Nusselt number
k	thermal conductivity of the fluid [W/(m·K)]
Pr	the Prandtl number
Re_L	the Reynold number
u	wind speed [m/s]
L_{F}	characteristic length for forced convection [m]
ρ	density of the fluid [kg/m^3]
μ	dynamic viscosity of the fluid [kg/(m·s)]

α	thermal diffusivity of the fluid [m^2/s]
Ra_L	the Rayleigh number
g	gravitational constant [m/s^2]
β	thermal expansion coefficient of the fluid [1/K]
c_p	specific heat of the fluid [W·s/(kg·K)]
L_{N}	characteristic length for natural convection [m]
$h_{\mathrm{F,A}}$	heat transfer coefficient of forced convection of air [$W/(K \cdot m^2)$]
$h_{\mathrm{N,A}}$	heat transfer coefficient of natural convection of air [$W/(K \cdot m^2)$]
$h_{\mathrm{M,A}}$	heat transfer coefficient of mixed convection of air [$W/(K \cdot m^2)$]
A_{R}	radiating area [m^2]
ε	emissivity
σ	Stefan-Boltzmann constant [$W/(m^2 \cdot K^4)$]
q_{global}	the global solar radiation of a tilted surface [W/m^2]
q_{dir}	the direct radiation on a horizontal surface [W/m^2]
q_{indir}	the indirect radiation on a horizontal surface [W/m^2]
R_b	the ratio of the direct radiation on the tilted surface to that on a horizontal surface
p_{gr}	albedo factor
$\emptyset$	tilted angle with respect to the ground [rad]
ZN	zenith angle [rad]
AZ	azimuth angle [rad]
ϑ	the surface azimuth rotation angle [rad]
$\bar{k}_{\mathrm{indir}}$	the monthly-averaged ratio of the indirect to global radiation
$\bar{k_t}$	the monthly-averaged clearness index
r_s	the ratio of the shadow to the total area
α_{solar}	the solar radiation absorption
ONAN	Oil-Natural-Air-Natural Transformer
OFAF	Oil-Forced-Air-Forced Transformer
ODAF	Oil-Directed-Air-Forced Transformer
WTI	Winding Temperature Indicator
WTI temperature	The winding hot-spot temperature read by WTIs
ANN	Artificial neural network
SVM	Support vector machine
MLR	Multi linear regression

Chapter 1

Introduction

1.1 Background

Electricity demands are increasing because of global decarbonization efforts to reduce emissions that have an impact on climate change [1]. Climate change also impacts the operation of electrical networks due to increasing ambient temperatures and extreme weather conditions [2, 3]. It is therefore a challenging time for power system owners to operate their assets because maximum capacity of power transformers is reduced with increasing ambient temperature. Due to economic and technical issues, research areas regarding the management and operation of power transformers, which are expensive assets in power systems, are of interest to many researchers and industry.

Power transformers are key apparatus used to transfer electricity from power plants to the transmission system, and from the transmission system to the distribution system, see Figure 1.1 for a photograph of a large power transformer. The reliability and robustness of these transformers is highly important [4]. They are designed to withstand a high electrical and thermal stresses over a long period of time, typically 20 – 30 years. However, transformers are inevitably subject to ageing processes, a key factor is the use of organic compounds in insulating material such as Kraft paper and mineral oil [5]. It is well known that the deterioration rate of such cellulosic electrical insulation is exponentially dependent on the operating temperature [6].

Power transformers consist of a tank containing a magnetic core with metal coils wound around it. Current passing through the windings causes Joule heating, and the changing magnetic flux causes hysteresis and eddy current losses within the core. The transformers are usually filled with refined mineral oil, which aids heat transfer and acts as an electrical insulator. Hot oil from the tank is passed via pipes to cooler banks, transferring the heat generated by the transformer to surrounding environment. Cold oil from the bottom of the cooler banks is then transferred back to the tank. The temperature distribution inside the transformer tank is important factor for safe operation, because, as previous discussed, insulation degradation increases with temperature. Therefore, a transformer thermal model is necessary for predicting the temperature inside the transformer tank to avoid overheating issues which can eventually shorten the transformer's lifetime [6].

Figure 1.1 A large power transformer, used with permission from National Grid Electricity Transmission

Conventionally, power transformers are type tested to guarantee that a temperature rise between the peak transformer winding temperature and ambient temperature must not exceed 78°C at their nameplate power rating [7]. In a type test, a transformer is subjected to its maximum current by a short-circuit method to replicate heat losses generated by the transformer at nameplate power rating. There are several temperature measurements recorded during the test, such as the oil temperature at the top of the tank and average winding temperature [7].

In a normal situation, transmission transformers are expected to operate below their nameplate power rating because of contingency plans. Nevertheless, any transmission transformer could be temporarily subject to a higher current than the nameplate capacity due to an outage of another transformer. To calculate to what extent a transformer could be overloaded safely, a transformer thermal model is required. Transformer thermal models are usually semi-empirical [8, 9]. This means that a governing equation of the thermal model is based on heat transfer principles, but thermal constants of the governing equation are experimentally derived from a type test. Transformers are also protected from overheating by sensors, often an oil temperature indicator (OTI) and a winding temperature indicator (WTI). These are used to measure transformer temperature, control cooling systems and protect transformers from overheating issues [10]. They have been used for many decades to monitor the transformer temperature. They can be set to alert the operator and trip the transformer at specific temperature levels.

The transformer temperature is also affected by environmental conditions. A higher ambient temperature in summer may decrease maximum power rating of the transformer by reducing the thermal headroom. Typically, the maximum hot-spot temperature for design and testing is calculated using the monthly average temperature of the warmest month. However, it is preferrable to use real-time ambient temperatures for the thermal calculations in terms of monitoring and short-time emergency

loading [9]. In addition to ambient temperature, solar radiation and prevailing wind could also affect the transformer temperature and the maximum power rating.

To improve cooling performance of transformer, which determines the maximum capacity, there are fans and pumps installed at the cooler banks to increase air flow and raise oil flow, respectively. For example, the maximum power rating of transformers considered in this thesis is double when the cooling system is in operation. Transformers can still work even when pumps and fans are out of order. However, any reduction in their cooling performance can lead to overheating issues, until the fault has been detected [11, 12]. Pumps and fans which are not operating at all are easily detected by checking the current drawn. A more minor fault in the system may be less obvious while still reducing cooling efficiency. It is necessary for the operators to detect such issues to avoid overloading transformers.

Due to ageing processes, the transformer thermal performance could be gradually degrading over a long period of operation. For example, degradation of the transformer oil causes oil sludge that could block cooling ducts in the winding and pipes between the transformer tank and the radiators. Therefore, it is necessary to ensure that the parameters within a thermal model are still representative of current thermal performance to avoid miscalculation. In theory, these parameters could be updated by doing a heat run test again, but this is expensive and difficult because a tested transformer has to be disconnected from the system [13].

1.2 Research Motivation and Objectives

To operate transformers effectively, an accurate transformer thermal model is essential. It can be used to aid transformer rating calculations and thermal condition monitoring. Traditionally, a transformer thermal model is building on thermal constants derived from a type test that is carried out at commissioning. Due to ageing process, it cannot be guaranteed that the cooling performance is unaffected unless thermal behaviour of transformer is re-evaluated. The two key aims of this thesis are to develop accurate transformer thermal models, utilising a range of operational data, and to assess the thermal performance of aged units so that aged transformers with anomalous thermal behaviour could be identified. An accurate transformer thermal model will aid the operators to identify transformers that have anomalous thermal behaviour by comparing measurements of the transformer temperature with the predictions made by the model. If a significant reduction in cooling performance of transformers is detected, proper intervention could be undertaken.

As transformers are usually equipped with either OTI or WTI or both, and load profiles are regularly recorded, it is feasible to develop a method that leverage those thermal and load measurements in terms of condition monitoring. It should be note that all of units considered in this thesis only have WTIs.

Besides, influences of weather factors, prevailing wind and solar radiation will be considered in a transformer thermal model. As most power transformers are outdoor units, ignoring weather influences may lead to misunderstand that changes in the transformer temperature that are indeed caused by the environmental conditions were caused by a fault instead. This will also benefit thermal condition monitoring.

The objectives of the thesis are as follows:

1. Identifying faulty WTIs using the load profile and WTI measurements.
2. Developing a thermal model for power transformers that consider weather factors based on heat transfer principles.
3. Developing an alternative thermal model for power transformers using machine learning techniques.
4. Exploiting the thermal model in term of condition monitoring, especially thermal issues such as changes in the cooling performance.

To meet these objectives, it will be necessary to leverage the load profile and winding temperature indicator (WTI) measurement to facilitate operate and manage power transformers. In addition, weather data is also required to develop a transformer thermal model. Summary of data used in this thesis is proved in Appendix A.

1.3 Contributions

There are three significant contributions made by this thesis to the area of the thermal modelling and condition monitoring for power transformers. Firstly, an algorithm to identify faulty WTIs using time series decomposition is proposed and tested against field measurements, which addresses the first objective. The algorithm is able to identify WTIs, which exhibited load and ambient temperature independency. This is important to ensure that measurement collected by WTIs are reasonable because WTIs are primary sources of thermal data for further analysis.

Secondly, a thermal model for power transformers considering wind speed and solar radiation is introduced and validated against field measurements, which fulfils the second objective. To be able to predict the transformer temperature more accurately, it is necessary to estimate influences of the weather factors, wind speed and solar radiation because power transformers are usually outdoor units. A more accurate thermal model improves calculation of the cumulative loss of insulation life and ratings.

The third contribution is development of alternative algorithm to model transformer thermal behaviour using machine learning, which addresses the third objective. A comprehensive analysis of the

ability of the data-driven model to predict the transformer temperature over various loading conditions and an analysis of sensitivity on the model accuracy to inputs are undertaken. It was found that the root mean squared errors of the prediction made by alternative algorithm is only 1.5°C while the root mean squared errors of the prediction made by a traditional thermal model is 2.5°C. Furthermore, an algorithm for incipient thermal anomaly identification is proposed using the data-driven model, which fulfils the fourth objective. It helps to alert the operator it is likely that there is a presence of an incipient thermal fault so that proper intervention could be planned accordingly.

1.4 Thesis Structure

Chapter 1 presents a short introduction of the subject and provides details about the motivation for the research and the aims and objectives of the project.

Chapter 2 provides a summary of traditional and modern condition monitoring techniques for power transformers. A summary of thermal network models for power transformers and their limitations are also discussed.

Chapter 3 presents a time series analysis of operational measurements associated with the transformers. The measurements consist of load profile, the winding temperature indicator (WTI) temperature and ambient temperature. Time series of load profile and the WTI temperature rise above ambient temperature are decomposed into distinct components. Cycle patterns of the time series illustrated by the seasonal components are discussed. An algorithm to identify faulty WTIs using the time series decomposition is proposed. In addition, dependency of the WTI temperature on wind speed and solar radiation are identified. This does motivate us to develop a transformer thermal that considers the weather factors, which is discussed in the next chapter.

Chapter 4 presents a thermal model for power transformers considering environmental factors. Many traditional transformer thermal models do not include wind or solar radiation [9, 14, 15]. As large power transformers are usually outdoor units, they could be subjected to substantial prevailing wind and solar radiation. This could have significant effects on the transformer temperature. The wind could be considered as external forced convection. For solar radiation, it could be considered as an additional heat source. The model is based on electrical-thermal analogy and principles of heat transfer. An equivalent circuit and a governing equation of the thermal model are proposed and tested against field measurements across numerous units. The prediction made by the proposed algorithm is similar to the prediction made by a traditional thermal model for normal weather conditions, but the prediction is significantly more accurate on windy and sunny periods.

Chapter 5 provides a discussion of development of data driven thermal model for power transformers. The following are the candidates of the data-driven algorithms that are implemented: 1) Artificial neural networks (ANN), 2) Support vector machine for regression (SVM) and 3) Multiple linear

regression (MLR). Input data are comprised of load profile, WTI measurement, ambient temperature, wind speed, wind direction and solar radiation. The sensitivity of input data to the model performance is also investigated. The performance of the model over different loading conditions is analysed.

Chapter 6 presents applications of the data driven thermal model in terms of condition monitoring. The thermal models could be used to estimate the cumulative loss of insulation life given loading conditions. Thermal anomaly of an ageing transformer among transformer family could be identified using the thermal model. Furthermore, an algorithm to identify incipient thermal faults using the thermal models developed in the previous chapter. The algorithm could help the maintenance team to target faulty transformers for repair based on their conditions.

Chapter 7 presents a conclusion and highlights key findings of this report.

Chapter 2

Transformer Condition Monitoring Techniques and Thermal Network Models

Power transformers must be able to withstand a high level of thermal stress. The temperature of oil-filled transformer is mainly limited by maximum operating temperature and ageing rate of the cellulosic insulation and the mineral oil [8]. The heat inside transformers is mainly generated by the core and winding losses. The temperature rise of cooling medium (mineral oil) occurs due to the heat transfer between the heat sources (windings and core) and the heat sink (ambient air) [16]. There are two key thermal indicators inside a transformer that are measured, i.e. the oil temperature at the top of the tank, namely called top-oil temperature, and the hottest temperature of the winding in proximity to insulating materials, namely hot-spot winding temperature [9]. There has been much research on how to improve top-oil models and hot-spot models [14, 17, 18]. In this section, a review of the top-oil and the hot-spot thermal network models and condition monitoring techniques for power transformers is provided.

2.1 Introduction

According to IEC 60076-1 2011 [19], a power transformer is defined as "a static piece of apparatus with two or more windings which, by electromagnetic induction, transforms a system of alternating voltage and current into another system of voltage and current usually of different values and at the same frequency for the purpose of transmitting electrical power". They are used to increase effectiveness of transmitting electrical power from power plants, which are usually in remote areas, to end users by stepping up a voltage from a power plant before connecting to the transmission system in order to minimise losses. Clearly, there are power transformers at other points of the transmission system to step down the voltage to a range that customers can safely use. Power transformers could be classified by capacity, electrical insulation type and winding configuration. This work focuses on 180 – 1000 MVA mineral oil-immersed power transformers in transmission systems and therefore the discussion will be limited to these cases.

2.2 Transformer Failure

The life expectancy of typical transformers is approximately 20-35 years. Reliability of large power transformers are considerably high with a general failure rate of 2% per annum [20]. An international survey conducted by the international council on large electric systems (CIGRÉ) in 1983 revealed that for the transformers with an on-load tap changer (OLTC), 41.4% of the total failure were caused by OLTC, 19.2% were due to the windings, 12.9% were accounted by failure of the tank and insulating fluid, 12.3% were caused by bushing, 11.6% were due to accessories and 7.6% were due to the magnetic circuit [20]. In terms of failure modes, mechanical, dielectric and thermal failures accounted for 53%, 31% and 9% of the total failures, respectively.

A more recent worldwide transformer reliability survey conducted by CIGRÉ in 2015 showed that the major failure rate was 0.58% of the participants in the survey [21]. The dielectric failure had the highest contribution to the total failures, followed by the mechanical, electrical and thermal failures [21]. Due to development of a vacuum OLTC, it significantly reduces the number of outages or maintenance for OLTC. This is because an arc takes place in a designed vacuum chamber instead of a transformer tank where the insulating oil could be contaminated.

The dielectric failure is caused by the fact that the insulating material is not able to withstand the electric field. There are many reasons causing the dielectric failures such as poor design, defective manufacturing or ageing insulation. Ageing processes accelerated by temperature can lead to dielectric failures [6]. The ability to distinguish an anomalous increase in temperature will avoid unusual ageing and eventually reduce risk of dielectric and thermal failures.

2.3 Ageing of Insulating Material

New transformers can more easily accommodate a high level of mechanical and electrical stresses. As a result of ageing of the solid insulation system, which is usually made of cellulose, mechanical and electrical strength declines to the end of life by approximate 20 years at the operating temperature of 98°C for Kraft paper and at the operating temperature of 110°C for thermally upgraded paper, and the ageing rate increases exponentially with temperature [5]. Ageing mechanism involves three reactions, hydrolysis, pyrolysis and oxidation [6]. The oxidation could be reduced by using inhibited oil in which an antioxidant is added [22]. The moisture content is usually low for hermetically sealed transformers as there is no exchange air between a transformer tank and the atmosphere. For free breathing transformers a silica filter is equipped to filter out water while drawing air from the atmosphere. Despite that, the degradation of the internal cellulosic insulation produces water as a by-product, with degradation increasing at higher temperatures [23, 24].

The dielectric strength of the insulating paper insignificantly degrades while the mechanical strength does decrease significantly over the life expectancy of the unit. However, due to fragility of the

degraded insulating paper, the dielectric integrity could be compromised by mechanical damage [8]. As a result of the deterioration of the insulating material, there is a higher risk of the catastrophic failure during severe conditions such as a short-circuit, or lightning strike because the aged insulating paper is not able to withstand mechanical stresses caused by short-circuit faults and dielectric stress generated by lightning strikes. Many studies showed that there is a clear relationship between decrease in degree of polymerisation of the insulating paper and reduction in mechanical properties [25, 26, 27]. The degree of polymerisation of the cellulosic insulation is representative of the number of the glucose units chained together [5]. The initial degree of polymerisation of Kraft paper is usually around 1100 – 1200 [5]. According to IEEE Std C57.91-2011 [8], the remaining degree of polymerization of the insulating material should be greater than 200 after being continuously subjected to temperature at 110°C with well-dried and oxygen-free condition for 150,000 hours or 17.12 years. For thermally upgraded paper, temperature of 110°C is used as a reference temperature while temperature of 98°C is used for non-thermally upgraded paper. The ageing rate varying with the operating temperature for thermally upgraded paper is as follows [9]:

$$AR = \exp\left(\frac{15000}{383} - \frac{15000}{\theta_{\mathrm{H}} + 273}\right) \tag{2.1}$$

For non-thermally upgraded paper, the ageing rate is as follows [9]:

$$AR = 2^{\left(\frac{\theta_{\mathrm{H}} - 98}{6}\right)} \tag{2.2}$$

where θ_{H} is the hot-spot winding temperature [°C] and AR is ageing rate relatively to the reference temperature.

Studies regarding variations in relative ageing rate due to oxygen and water levels were conducted in [23, 24]. They showed that the higher oxygen and water levels could accelerate the degradation rate significantly. Controlling the oxygen and water contents in permissible levels is necessary to maximise the transformer life expectancy. The hydrolysis of the insulating paper catalysed by low molecular acids were studied in [28, 29]. It was found that the formic acid has the highest acceleration factor followed by acetic and levulinic acids. This means that the hydrolysis of the insulating paper is an auto accelerative process, which means that the hydrolysis is catalysed by its own by-product. A comprehensive discussion regarding those factors that accelerate the degradation rate of the insulating paper can be found in [10].

Ageing transformers need to be monitored carefully to avoid an unexpected failure. As not only do unexpected failures result in costly maintenance and replacement, but operators also have to pay a penalty charge for unexpected power outages and contingency costs. Many condition monitoring techniques have been developed to detect incipient faults and prevent transformers from catastrophic failures such as partial discharge (PD) measurement, dissolved gas analysis (DGA) and thermogra-

phy, see [30], [31] and [32] for detailed discussion regarding PD measurement, DGA and thermography techniques, respectively. In this thesis the focus is on thermal condition monitoring techniques because only the thermal performance of transformers is of interest.

2.4 Thermal Condition Monitoring Techniques

The transformer temperature is an essential parameter for condition monitoring. An excessive operating temperature leads to gas generation and accelerates the ageing rate in the insulation system, which jeopardises the transformer integrity. Identification of anomalous thermal behaviour would help the operators to manage their assets and plan intervention accordingly.

2.4.1 Thermography

Transformer surface temperatures can be obtained by measuring infrared emission. The testing can be performed on-line without an outage. Abnormalities which are close to transformer's surface can be detected such as clogged oil pipe or poor electrical connection [32]. Although a hot-spot location inside a transformer tank could not be directly detected by this method, it can be a useful tool to narrow a possible hot-spot location. An infrared image may be taken at the beginning of its operation as a reference and then it is used to compare with another to investigate thermal issues. As the transformer temperature vary with loading conditions, the comparison needs to be carried out carefully. It could be improved by continuously monitoring and recording the surface temperature rather than routine schedules.

2.4.2 Oil temperature indicator and Winding temperature indicator

Transformers usually have separate oil pockets in the top of the tank for temperature measurements. The oil pockets enable the operator to measure indirectly top-oil temperature without contaminating the oil inside the tank. It is easy for maintenance. Oil temperature indicator (OTI) is usually installed in the oil pocket to measure the top-oil temperature [10]. The temperature could be measured mechanically using capillary tube, which is based on the fact that the pressure of a fluid changes with temperature. Alternatively, the temperature could be measured electrically using resistance temperature detector (RTD) which is based on changes in electrical resistance with temperature. PT100, a temperature sensing probe made of platinum that has resistance of 100 Ω at temperature of 0°C, has been widely used to measure the transformer temperature [33]. OTIs can send a signal to control cooling pumps and fans and disconnect the transformer from the service based on the measured temperatures.

A winding temperature indicator (WTI) is similar to an OTI, but also captures the temperature rise of the winding above top oil through the use of a heating coil, see Figure 2.1. The heating coil is supplied with a proportional current to the winding current via a current transformer to replicate the

heat inside the winding [34]. The simulated heat is calibrated to make similar the hot-spot temperature rise over the top oil temperature at rated current measured during the heat run test in accordance with [8]. WTIs can also control cooling systems and disconnect units, in a similar manner to OTIs.

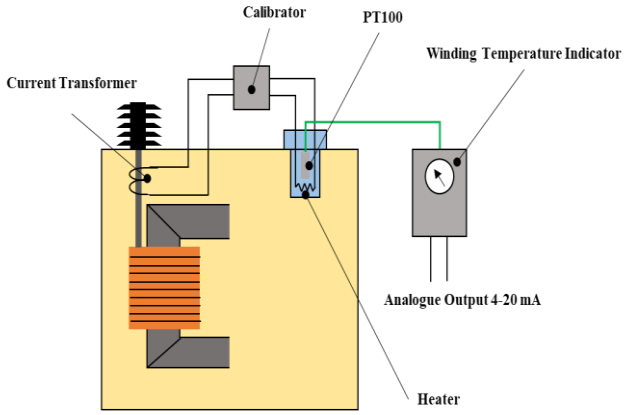

Figure 2.1 Traditional winding temperature indicator

2.4.3 Direct temperature measurement

Direct measurement on a transformer winding hot-spot temperature using fibre optic sensors was introduced over many decades ago [35]. Temperature measurement using fibre optic sensors for power transformers is usually based on changes in the light absorption properties of semiconducting crystals, which are usually made of gallium arsenide (GaAs) [36]. Fibre optic sensors were used to measure the transformer winding temperature directly for confirmation of a new transformer design where the conventional method could not work due to electromagnetic interference [37]. A number of sensors would need to be installed to measure the temperature distribution along the winding [38, 39]. The sensors are installed at the hot-spot location as near as possible regarding transformer design and simulation results. However, there are some limitations. It is difficult to install the sensors once the transformer has been already assembled [10]. Therefore, this method is not recommended for transformers which are already in service. The cost of fibre optic sensors is high, and it is likely that a number of them are required to measure the temperature at the hot-spot location [10]. Another limitation is vulnerability to physical damage. The maintenance and replacement of the sensors is also difficult due to their location within the windings.

2.5 Computational Fluid Dynamics (CFD)

Computational fluid dynamics (CFD) is a numerical method that is used to solve the Navier-Stokes equations by turning a combination of the differential equations to algebraic equations. By simultaneously solving the heat equation, it is in theory possible to determine the oil velocity and temperature anywhere in a transformer. Instead of conducting many experiments for developing a new trans-

former, design engineers could adjust transformer parameters in CFD models to simulate their designs and then conduct an experiment to validate the simulation. The majority of research to date focuses on the thermal behaviour at the windings and cooler bank where the majority of the generation and removal of the heat takes place [40, 41, 42]. CFD research has also considered the location of the peak winding temperature [43, 44]. In [43], it was found that the location of the hottest winding temperature for transformers which is in an oil-natural-air-natural (ONAN) state is at the top of the winding of each cooling pass, which is a stack of disc windings and cooling ducts, and at the middle for transformers which is either in an oil-forced-air-forced (OFAF) or oil-directed-air-forced (ODAF) state. Later on, studies based on CFD have shown that with high oil velocity, the location of the hot-spot temperature for direct forced oil (OD) could move to the bottom horizontal duct of a cooling pass due to a reverse oil flow [45, 46]. A relationship between a reverse oil flow and dimensions of the discs and ducts in the windings for OF and OD cooling modes was studied using the CFD model [47, 48]. A correlation between the hot-spot factor (H) and the Prandtl and Reynolds numbers for power transformers which are in an OD cooling mode was investigated [49]. There are many efforts try to improve the heat transfer coefficient of cooler bank by adjusting positions of cooling fans horizontally and vertically in CFD models [50, 51]. One of advantages of CFD modelling is that temperature profiles in any location could be determined. One of disadvantages of CFD is that it needs high computational resources and time. For example, the computational time for a complex 3-D system, solved by an ordinary computer, could be weeks [40]. Due to the long computational time, the CFD approach is not preferred for dynamic transformer thermal modelling.

2.6 Thermal-Hydraulic Network Models (THNM)

Thermal-hydraulic network models (THNMs) for transformers are fundamentally based on the law of conservation of heat and mass and pressure equilibrium in closed loops [52]. The hydraulic model considers flow and temperature distribution of the oil while the thermal model is representative heat exchange between the oil and the windings regimes. Unlike CFD approach that describes a system using partial differential equations, THNM utilise a combination of simple algebraic equations to determine oil flow and temperature distribution. These assumptions simplify the model to reduce computational time. The boundary of the surface temperature for each disc is assumed to be constant in [53]. In [54], the winding structure was simplified to rectangular ducts. Advantages of this approach are that the flow and temperature distribution for each section of the winding could be calculated, and the computational time is relatively faster than the CFD approach. A study showed that typical average temperature differences between measurements and prediction made by THNM did not exceed 5°C, while the calculation of hot-spot location in a transformer is more complicated and still needed to be improved [55].

2.7 Thermal Network Models

Based on the information presented in section 2.5 and 2.6, it appears that a key limitation of those approaches is computational time. This is a reason why those methods are not appropriate for condition monitoring and dynamic rating calculations. The industry standard approach is to use thermal network models, they are also used in international guidance, and offer a low computational cost approach for determining transformer temperatures [40].

A basic oil-filled transformer thermal model at steady state is shown in Figure 2.2 [9]. The aim of transformer models is to determine a maximum power rating thermally limited by the hot-spot winding temperature [56]. The hot-spot winding temperature is usually expressed as combination of three components: ambient temperature, top-oil temperature rise above ambient temperature, which is the oil temperature rise at the top of the tank, and the hot-spot temperature rise above the top-oil temperature, which is the winding temperature rise at the hottest location [8, 9]. Traditionally, the hot-spot temperature rise is estimated using a "winding gradient", which is the temperature difference between average winding and oil temperature because a direct measurement of the hot-spot temperature could not be undertaken. This winding gradient is likely to be higher for the top of the winding because there are additional losses due to the leakage flux at the top of the winding, and the oil flow may be restricted [40].

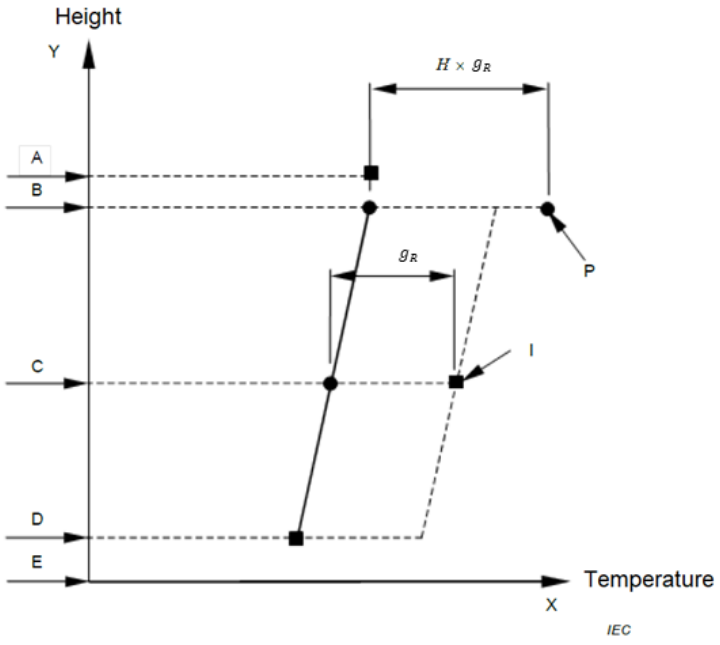

A Top-oil temperature derived as the average of the tank outlet oil temperature and the tank pocket temperature
B Mixed oil temperature in the tank at the top of winding
C Temperature of the average oil in the tank
D Oil temperature at the bottom of the winding
E Bottom of the tank
g_R Average winding to average oil (in tank) temperature gradient at rated load
H Hotspot factor
P Hotspot temperature
I Average winding temperature determined by resistance measurement

Figure 2.2 A basic transformer thermal model [9].

The higher temperature rise has led to the introduction of a hot-spot factor, H, applied to the winding gradient to determine the rise of the hot-spot above the top-oil temperature. Hence, the hot-spot temperature is defined as follows:

$$\theta_{\mathrm{H,R}} = \theta_{\mathrm{A}} + \Delta\theta_{\mathrm{O,R}} + H g_{\mathrm{R}} \tag{2.3}$$

$\theta_{\mathrm{H,R}}$ is the hot-spot temperature at rated load [°C]. $\Delta\theta_{\mathrm{O,R}}$ is the top-oil temperature rise above ambient temperature at rated load [°C]. θ_{A} is ambient temperature [°C]. H is hot-spot factor and g_{R} is the average winding gradient at rated load [°C].

Thermal network models can be considered as a lumped element model similar to electrical problems [14]. The analogy between lumped thermal and electrical elements is shown in Table 2.1. The temperature differences between two considered points is equivalent to the electric potential difference and the heat transfer rate is equivalent to electric current. There are also equivalent expressions for thermal resistance and capacitance. It is worth to note that some types of thermal resistances have a strong non-linear temperature dependency, especially for natural convective resistances which mainly contribute to the thermal resistance of oil-immersed power transformers that are in an ONAN state.

Table 2.1 The Lumped Electrical and Thermal Elements.

Electrical element	**Thermal elements**
Voltage (V [V])	Temperature (θ [°C])
Current (I [A])	Heat transfer rate (Q [W])
Electrical resistance ($R_{electrical}$ [Ω])	Thermal resistance ($R_{thermal}$ [K/W])
Electrical capacitance ($C_{electrical}$ [F])	Thermal capacitance ($C_{thermal}$ [W·s/K])

A simplified top-oil model could be considered as a thermal RC circuit with a heat source as shown in Figure 2.3 [14]. The heat sources comprise of the core and winding losses [57]. The core losses mainly depend on the supplied voltage and frequency, and are therefore assumed to be constant [57]. The winding losses are proportional to the square of the flowing current through the winding. The winding losses also depend on temperature because of changes in electrical resistance. Thermal capacitance is due to the thermal mass of the core, tank and oil [8]. The thermal resistance describes the heat transfer due to the cooling air and oil [14]. The radiation from the tank wall is neglected in a simplified top-oil model. Hence, the governing equation of the simplified top-oil model is given as follows [14]:

$$Q_{\mathrm{Fe}} + Q_{\mathrm{Cu}} = C_{\mathrm{O}} \frac{d\theta_{\mathrm{O}}}{dt} + \left(Q_{\mathrm{Fe,R}} + Q_{\mathrm{Cu,R}}\right)\left(\frac{\theta_{\mathrm{O}} - \theta_{\mathrm{A}}}{\theta_{\mathrm{O,R}} - \theta_{\mathrm{A}}}\right)^{\frac{1}{n_1}} \tag{2.4}$$

where Q_{Fe} is the core losses (no-load losses) [W], Q_{Cu} is the winding losses (load losses) [W], θ_{O} is the top-oil temperature [°C], $R_{\mathrm{O,R}}$ is the top-oil thermal resistance at rated conditions [K/W], C_{O} is the top-oil capacitance [W·s/K], n_1 is an exponent depending on cooling modes and θ_{A} is the ambient temperature [°C].

Approximately, the top-oil temperature can be determined as follows:

$$\theta_{\mathrm{O}}(t+\Delta t) \approx \frac{\Delta t}{C_{\mathrm{O}}}\left(Q_{\mathrm{Fe}} + Q_{\mathrm{Cu}} - \left(Q_{\mathrm{Fe,R}} + Q_{\mathrm{Cu,R}}\right)\left(\frac{\theta_{\mathrm{O}}(t)-\theta_{\mathrm{A}}}{\theta_{\mathrm{O,R}}-\theta_{\mathrm{A}}}\right)^{\frac{1}{n_1}}\right) + \theta_{\mathrm{O}}(t) \quad (2.5)$$

where Δt is time interval [s].

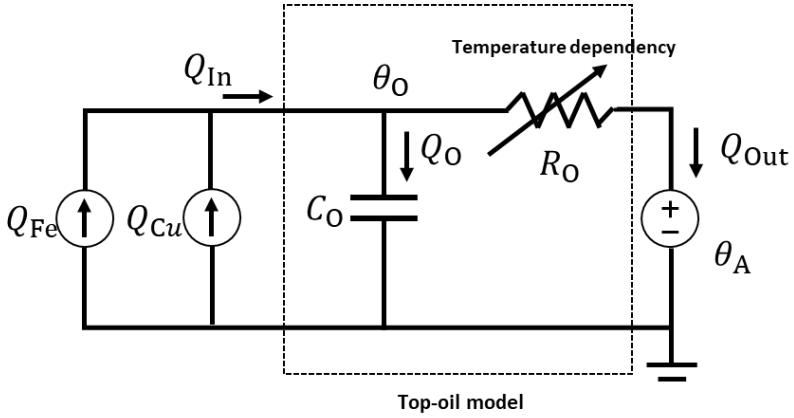

Figure 2.3 The simplified equivalent circuit of the transformer thermal model [14].

A thermal model for power transformers that is proposed by Pierce [58] is in similar approach to the previous equation, assuming the oil temperature at any location in a transformer obeys the same form of the equation, but the top-oil temperature is replaced with the average oil temperature. Subsequently, the top-oil temperature is then calculated using a proportion of the top-oil temperature rise above the bottom-oil temperature at rated load as follows:

$$\Delta\theta_{\mathrm{T/B}} = \left(\frac{\theta_{\mathrm{AO}}-\theta_{\mathrm{A}}}{\theta_{\mathrm{AO,R}}-\theta_{\mathrm{A,R}}}\right)^{\frac{1}{n_2}} \Delta\theta_{\mathrm{T/B,R}} \quad (2.6)$$

$$\theta_{\mathrm{O}} = \theta_{\mathrm{AO}} + \frac{\Delta\theta_{\mathrm{T/B}}}{2} \quad (2.7)$$

where θ_{AO} is the average oil temperature [°C], $\theta_{\mathrm{AO,R}}$ is the average oil temperature at rated load [°C], $\theta_{\mathrm{A,R}}$ is the ambient temperature at rated load [°C], n_2 is an exponent depending on cooling modes, $\Delta\theta_{\mathrm{T/B}}$ is the top oil temperature rise over the bottom-oil temperature [°C], $\Delta\theta_{\mathrm{T/B,R}}$ is the top-oil temperature rise over the bottom-oil temperature at rated load [°C].

Pierce's method also considers type of insulating liquid, changes in viscosity and winding losses due to temperature, and cooling modes. This method is widely accepted and included in the Annex G of the IEEE standard, which is referred to as IEEE-Annex G method. [8]. The method will be used to calculate the top-oil temperature as a reference method in Chapter 4 and Chapter 5 as it has been commonly used as a reference [18, 59, 60].

Over recent decades, the concept of top-oil model represented by an equivalent circuit has been unchanged. However, there are many researchers attempting to improve the accuracy of the model by considering the temperature dependency of the thermal resistance of the moving air and oil [14, 15, 61, 62]. G. Swift et.al argued that the exponent applied in the heat source should be rearranged to the oil temperature according to heat transfer principles [14], whereas the exponent is applied to the total losses in the governing equation used in the IEC guidance [9]. Changes in oil viscosity due to temperature have been explicitly included the top-oil model [15, 61]. Furthermore, the variation in the winding losses with temperature was discussed in [60].

The hot-spot temperature is determined in similar manner to the calculation of the top-oil temperature, excepting only the winding losses are considered. The hot-spot temperature rise is estimated as follows [8]:

$$\Delta\theta_{\mathrm{H}}(t+\Delta t) \approx \frac{\Delta t}{C_{\mathrm{H}}}\left(Q_{\mathrm{Cu}} - Q_{\mathrm{Cu,R}}\left(\frac{\theta_{\mathrm{H}}(t)-\theta_{\mathrm{O}}}{\theta_{\mathrm{H,R}}-\theta_{\mathrm{O,R}}}\right)^{\frac{1}{n_3}}\left(\frac{\mu_{\mathrm{H,R}}}{\mu_{\mathrm{H}}(t)}\right)^{\frac{1}{n_4}}\right) + \Delta\theta_{\mathrm{H}}(t) \qquad (2.8)$$

where θ_{H} is hot-spot temperature [°C], C_{H} is the hot-spot winding capacitance [W·s/K], μ_{H} is the oil viscosity [kg/(m·s)], $\mu_{\mathrm{H,R}}$ is the oil viscosity at rated load [kg/(m·s)], n_3 is an exponent depending on cooling modes and n_4 is an exponent depending on cooling modes.

Since fibre-optic technology has been developed as a temperature sensor, a number of investigations onto hot-spot temperature under different load conditions have been reported [17, 37]. It was found that there is an overshoot response of the hot-spot temperature rise for large power transformers due to relatively slow changes in the oil circulation especially, ONAN transformers [17]. Later, the overshoot responses of the hot-spot temperature rise above top oil temperature has been included into the IEC model by using two temperature gradients describing the hot-spot temperature rise, which consider the slow changes in the oil circulation.

Furthermore, a simple thermal model for the absolute hot-spot temperature was proposed in [63]. The differences are that the thermal model considers the ambient temperature at the reference temperature rather than the top-oil temperature. The second difference is that the thermal time constant switches between the winding time constant and the oil time constant dependent on specified thresholds. When the oil time constant is used, it means that the remaining change in the absolute hot-spot

temperature is caused by only a change in the top-oil temperature because the hot-spot temperature rise above the top-oil temperature, which has a faster time constant, has already reach an ultimate value.

In addition, environmental factors, solar radiation and wind, could also impact on the transformer temperature and loading capacity [64]. A study showed that the oil temperature for a distribution transformer in Iran could be increased by 3.7°C due to the high intensity of the solar radiation [65]. Another study conducted in Bahrain showed that the hot-spot temperature of a 15-MVA unit could be increased by 9°C in summer and 6°C in winter due to the solar radiation [66]. Effects of the solar radiation on the transformer temperature vary with the location of transformers, time of the year and the ratio of the total losses generated by the transformer to the received solar radiation. There is limited explicit literature about the impact of prevailing wind on transformer temperature. However, studies undertaken to improve heat transfer rate at the transformer radiators could provide relevant information. Based on simulation results, air velocity due to natural convection is within 1 m/s and air velocity could be improved to approximately 10 m/s by cooling fans [67, 68]. The air flow direction is vertical because the cooling fans are typically installed at the bottom of the radiators and the natural convection is caused by the buoyancy force. For prevailing wind, typical average wind speeds in the substation analysed are between 2 m/s and 5 m/s depending on substation and it should be noted that the typical direction of the prevailing wind on transformer substations analysed in this work is horizontally southwest, see Table 5.2 for average wind speeds and direction for each transformer considered in this work.

2.8 Data Driven Thermal Models

Alternatively, a transformer thermal model could be developed using historical measurement of load profiles, transformer temperature and weather factors instead of physical models. The performance of computers has improved significantly in recent decades, enabling researchers to develop transformer thermal models utilising machine learning techniques. In early work, feedforward artificial neural networks (ANNs) were used to develop a transformer thermal model by learning historical measurements consisting of load, ambient temperature and the top-oil temperature [69]. In [70] a comparison between feedforward and recurrent ANNs was undertaken. This showed that the recurrent ANNs, where the top-oil temperature at the previous time step is used as an input for predicting the top-oil temperature at the next time step, was superior to the feedforward approaches. In a more recent work, a transformer hot-spot thermal model was developed using recurrent ANNs [71] and it showed promising results. Furthermore, development of a transformer thermal model using a support vector machine (SVM) approach was also carried out [72]. Based on the review undertaken, a key limitation is the limited size of the datasets, less than a month, so it is impossible to evaluate error variation throughout a year and to determine the size of training datasets required to create a robust

model. Moreover, weather factors, such as wind and solar radiation have not been considered in these models to date.

2.9 Summary

Based on the literature undertaken, it appears that there has yet to be a thermal model for power transformers that considers prevailing wind and solar radiation. Typically, thermal models only include solar radiation and ambient temperature as weather inputs. Theoretically, a substantial wind would improve the cooling performance of transformers. It is noted that the wind speed is dependent on seasons, location and might not persist for extended periods of time. It is of interest that to what extent prevailing wind could improve the cooling performance, especially for those transformers that are in windy location, e.g. wind farms and offshore substations. This motivates the development of a thermal model for power transformers that considers those weather factors to improve the accuracy of the prediction. The discussion and results are provided in Chapter 4.

Although there are earlier transformer thermal models developed using machine learning techniques, there has yet to be a comprehensive analysis due to the limited data available. As historical load and WTI measurements collected by National Grid Electricity Transmission are available for long periods, 5 years of data, and across many transformer units, it enables the author to investigate a possibility of creating transformer thermal models using machine learning techniques in greater detail, see Appendix A. In this thesis, detailed discussion of development of transformer thermal models using data driven techniques are provided in Chapter 5.

Based on the review undertaken, the IEEE-Annex G method will be used as a reference thermal model throughout this thesis.

Chapter 3

Operational Measurements and Time Series Analysis

In this chapter, historical operational measurements considered in this work are presented and discussed. A time series decomposition technique is used to investigate distinct characteristics of the data. An algorithm that could identify faulty winding temperature indicators (WTIs) with load and ambient temperature dependency issues is proposed using a time series decomposition technique and correlation coefficients. Limitations of traditional transformer thermal models are also discussed.

3.1 Operational Measurements

In this chapter, three transformers are considered. Load and winding temperature indicator (WTI) measurements were provided by National Grid Electricity Transmission (NGET) as a part of Condition and Climatic Environment for Power Transformer (ConCEPT) project. The data are in an hourly interval format between 2013 and 2018 and 15-minute interval format since 2019. In addition, local substation weather stations have been installed at the substations as a part of ConCEPT project and the data are available since July 2019. The local substation weather stations have a sampling interval of 15 minutes, they measure and record: ambient temperature, wind speed, wind direction and solar radiation. As the weather information from the local substation weather stations does not cover the whole period of time, some of the weather information was derived from the nearest weather station of the UK meteorological office, referred to as the Met Office hereafter [73]. The data from the Met Office are only available in an hourly interval format. A summary of the data availability for the three transformers is provided in Table 3.1. Examples of load, WTI measurement, ambient temperature, wind speed, wind direction and solar radiation are shown in Figure 3.1. A picture of the local substation weather station for Transformer A is shown in Figure 3.2. Overall transformer specifications are provided in Appendix B in Table B.1. Transformer A and B are in the same family and at the same substation. Their main tanks are indoors while the radiators are left outdoors. They are in an urban area, surrounded by concrete walls. It is reported by a NGET operator that cooling pumps and fans of Transformer B are operating continuously regardless of the transformer temperature. Transformer C is an outdoor unit, with its main tank and radiators outdoors in a rural area, with another transformer next to it.

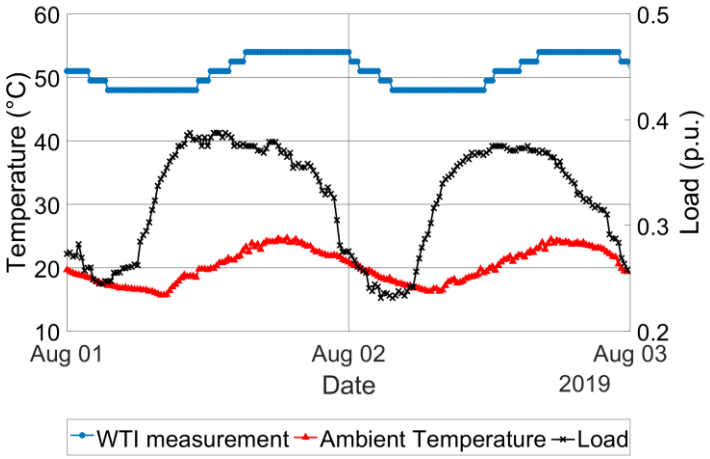

(a) Load, WTI measurement and ambient temperature

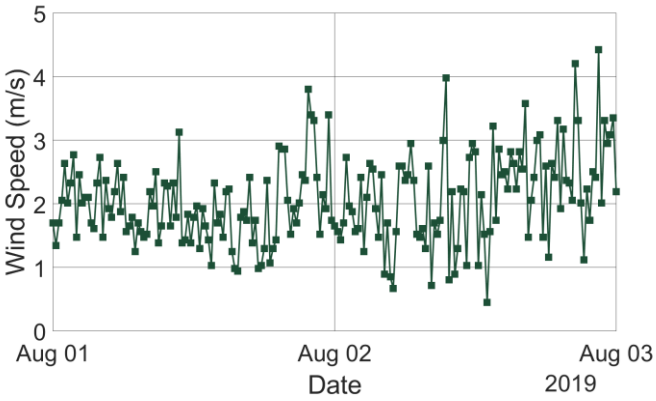

(b) Wind speed

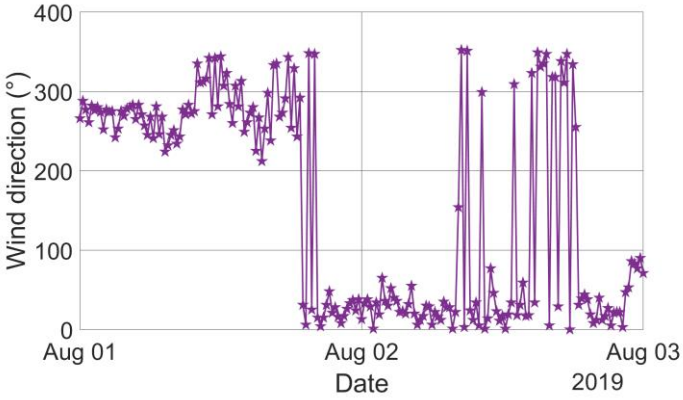

(c) Wind direction (0° = North, 90° = East, 180° = South and 270° = West)

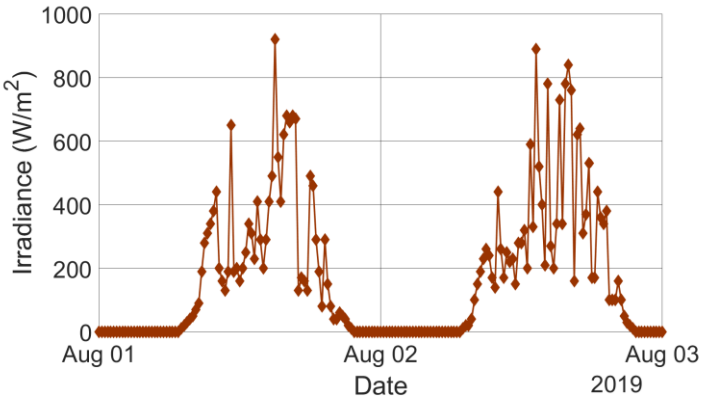

(d) Solar radiation

Figure 3.1 Example of Load, WTI measurement, wind speed and solar radiation data for the local substation weather station.

Table 3.1 Availability of load, WTI measurement and weather information

Transformer	WTI and load Measurement	Met Office	Local Substation
A	01/2013 to 05-2020	01/2013 to 05/2020	07/2019 to 05/2020
B	01/2013 to 05/2020	01/2013 to 05/2020	07/2019 to 05/2020
C	01/2013 to 05/2020	01/2013 to 05/2020	09/2019 to 05/2020

Figure 3.2 Weather station at substation of Transformer A.

3.2 Time Series Analysis

Time series analysis is a statistical technique for studying characteristics of time series. It is useful to split time series into a number of distinct independent component series. As changes in the transformer temperature driven by the loading conditions are considered, time series of the load and WTI temperature rise above ambient temperature are determined. It is expected that characteristics of the component series of WTI temperature rise should be similar with the components of the load with a time lag of several hours. The time lag is due to the thermal oil time constant which is dependent on transformer designs and the cooling state.

There are a plethora of component combinations that can be used. In the case of load and WTI temperature rise data it is appropriate to consider them as a multiplicative series (y_{m}), with a general trend (T_{m}), seasonal (S_{m}) and irregular components (I_{m}) as follows:

$$y_{\mathrm{m}} = T_{\mathrm{m}} \text{ x } S_{\mathrm{m}} \text{ x } I_{\mathrm{m}} \tag{3.1}$$

A multiplicative series is appropriate because the variability of the time series is roughly proportional to its magnitude. For example, the average load is typically smaller on weekends and has lower variability.

To calculate these components, logarithms of original data are first calculated as follows:

$$\log y_{\mathrm{m}} = \log T_{\mathrm{m}} + \log S_{\mathrm{m}} + \log I_{\mathrm{m}} \tag{3.2}$$

This means that the series become an additional series which is easier to calculate. A logarithm of a trend is then calculated as a moving average over a specified period as follows:

$$\log T_{\mathrm{m}}(t) = \frac{\sum_{i=0}^{8759} \log y_{\mathrm{m}}(t-i)}{8760} \; ; \qquad t \geq 8761 \tag{3.3}$$

The trend is calculated since the second year of the data because the first year of the data is used a base for calculating moving average. The size of moving window depends on time series characteristics. The window size is selected so that the trend is not comprised of any kind of cyclical patterns.

Following this, a logarithm of a detrended series which is then used to calculate logarithms of seasonal components could be determined as follows:

$$D_{\mathrm{m}} = \log y_{\mathrm{m}} - \log T_{\mathrm{m}} \tag{3.4}$$

A seasonal component is represented a repeated pattern which is occurs with a fixed period, e.g. yearly, weekly and daily. A logarithm of a yearly seasonal component is determined as follows:

$$\mathrm{S}_{1,\mathrm{yearly}}(\mathrm{t}) = \frac{\sum_{i=0}^{\mathrm{Year}} D_{\mathrm{m}}(t+(8760i))}{\mathrm{Year}} \; , 1 \leq t \leq 8760 \tag{3.5}$$

$$\mathrm{S}_{2,\mathrm{yearly}}(\mathrm{t}) = \mathrm{S}_{1,\mathrm{yearly}}(\mathrm{t}) - \overline{\mathrm{S}_{1,\mathrm{yearly}}(\mathrm{t})} \tag{3.6}$$

$$\log S_{\mathrm{yearly}}(t) = \begin{cases} \dfrac{\sum_{i=0}^{167-t} \mathrm{S}_{2,\mathrm{yearly}}(8760-i) + \sum_{i=0}^{t-1} \mathrm{S}_{2,\mathrm{yearly}}(t-i)}{168} & \text{if} \quad t \le 167 \\ \dfrac{\sum_{i=0}^{167} \mathrm{S}_{2,\mathrm{yearly}}(t-i)}{168} & \text{if} \quad t > 167 \end{cases} \tag{3.7}$$

where Year is the number of years of the data. It should be noted that the size of $\log S_{\mathrm{yearly}}(t)$ is 8760 data points.

A logarithm of a weekly seasonal component is determined as follows:

$$D_{\mathrm{m,weekly}} = D_{\mathrm{m}} - \log S_{\mathrm{yearly}} \tag{3.8}$$

$$\mathrm{S}_{1,\mathrm{weekly}}(\mathrm{t}) = \frac{\sum_{i=0}^{\mathrm{Week}} D_{\mathrm{m,weekly}}(t+(168i))}{\mathrm{Week}} \quad , 1 \le t \le 168 \tag{3.9}$$

$$\mathrm{S}_{2,\mathrm{weekly}}(\mathrm{t}) = \mathrm{S}_{1,\mathrm{weekly}}(\mathrm{t}) - \overline{\mathrm{S}_{1,\mathrm{weekly}}(\mathrm{t})} \tag{3.10}$$

$$\log S_{\mathrm{weekly}}(t) = \begin{cases} \dfrac{\sum_{i=0}^{23-t} \mathrm{S}_{2,\mathrm{weekly}}(168-i) + \sum_{i=0}^{t-1} \mathrm{S}_{2,\mathrm{weekly}}(t-i)}{24} & \text{if} \quad t \le 23 \\ \dfrac{\sum_{i=0}^{23} \mathrm{S}_{2,\mathrm{weekly}}(t-i)}{24} & \text{if} \quad t > 23 \end{cases} \tag{3.11}$$

where Week is the number of weeks of the data. The size of $\log S_{\mathrm{yearly}}$ is 8760 data points and it is replicated so that it has the same size as the detrend series. It should be noted that the size of $\log S_{\mathrm{weekly}}(t)$ is 168 data points.

A logarithm of a daily seasonal component is determined as follows:

$$D_{\mathrm{m,daily}} = D_{\mathrm{m}} - \log S_{\mathrm{yearly}} - \log S_{\mathrm{weekly}} \tag{3.12}$$

$$\mathrm{S}_{1,\mathrm{daily}}(\mathrm{t}) = \frac{\sum_{i=0}^{\mathrm{Day}} D_{\mathrm{m,daily}}(t+(24i))}{\mathrm{Week}} \quad , 1 \le t \le 24 \tag{3.13}$$

$$\log S_{\mathrm{daily}}(t) = \mathrm{S}_{1,\mathrm{daily}}(\mathrm{t}) - \overline{\mathrm{S}_{1,\mathrm{daily}}(\mathrm{t})} \tag{3.14}$$

where Day is the number of days of the data. The size of $\log S_{\mathrm{weekly}}$ is 168 data points and it is replicated so that it has the same size as the detrend series. It should be noted that the size of $\log S_{\mathrm{daily}}(t)$ is 24 data points.

A logarithm of an irregular component contains the remaining data which is not captured in the trend or seasonal components, e.g. uncertainty of electricity consumption, outages or overloading due to a failed transmission line or transformer and is determined as follows:

$$\log I_{\mathrm{m}} = \log y_{\mathrm{m}} - \log T_{\mathrm{m}} - \log S_{\mathrm{yearly}} - \log S_{\mathrm{weekly}} - \log S_{\mathrm{daily}} \tag{3.15}$$

It should be noted that the seasonal components are replicated so that their size are equal to the size of the trend.

Figure 3.3 to Figure 3.8 and Figure 3.9 to Figure 3.14 show the decomposition components for Transformer A which is in Westminster, Greater London, and Transformer C which is in Braintree, Essex, respectively. For Transformer A, it appears that the trend of load profile was quite constant at 50 MVA until 2018. Then the trend increased to about 70 MVA. The same behaviour was also observed for the trend of the WTI temperature rise as expected. While the trends of both load and WTI temperature rise for Transformer C did not vary significantly. It appears that the loads have a yearly, weekly and daily seasonal components for both Transformer A and C. The load and WTI measurements of Transformer A and C were provided for two different periods, i.e. 1st January 2013 to 31st January 2019 and 1st February 2019 to 1st May 2020. Missing data in late 2018 to early 2019 for Transformer A and C were because permissible amount of the data downloaded for each time had been reached. The author was unable to obtain data for the gaps because the load and WTI measurements had to be downloaded by an independent party. However, it is a sufficiently short period that it would make no difference.

Similar curves were also observed in the seasonal components of the WTI temperature rise, but there is a time lag between the load and the WTI temperature rise of about five hours, which is expected. Regarding the yearly seasonal component, it suggests that the load is strongly dependent on the ambient temperature. This is expected because the electricity demand for heating would be relatively low in summer. It is worth noting that the load drops noticeably during Christmas and New year holidays where most workplaces, supermarkets, schools, etc are closed. It appears that the yearly variation in the load of Transformer A is slightly lower than the load variation of Transformer C. This is probably because the ratio of industrial and commercial electricity demands to domestic demands is relatively higher for Transformer A (6.66:1 average between 2013-2017) than Transformer C (1.06:1 average between 2013-2017) [74]. It is plausible that industrial and commercial demand depends less on ambient temperature than domestic demand.

For the weekly seasonal components, it shows that the load demand for weekends is relatively lower for weekdays. This is because workplaces, schools and so on are closed. Regarding the daily seasonal components, the load peaks between 10:00 AM and 6:00 PM where they are working hours for Transformer A. While there are 2 peaks for Transformer C at 8:00 AM and 6:00 PM. These are common times for preparing breakfast and dinner in the UK where electrical cooking appliances are being used [75].

The seasonal and irregular components are divided by the trend component so that the values of those components are fractions of the trend component.

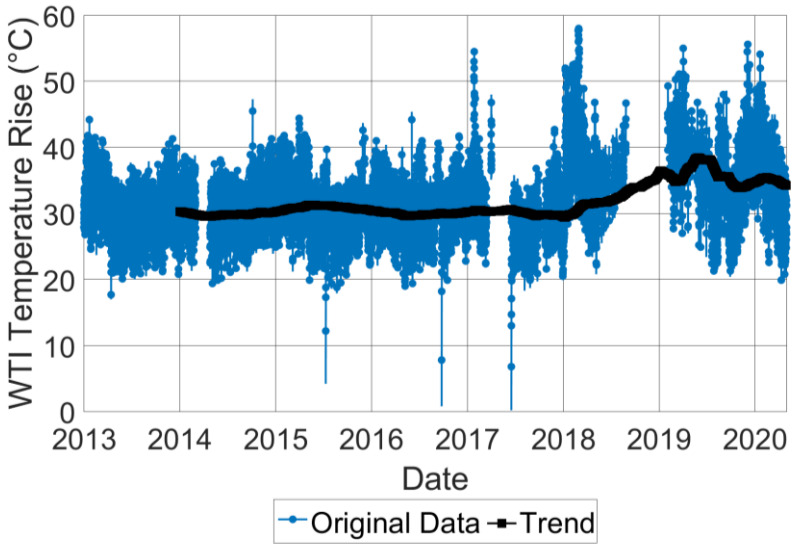

Figure 3.3 Original data and trend component of WTI temperature rise for a transformer in the central London (Transformer A). The gaps are either unavailable data or periods that the transformer is not in operation.

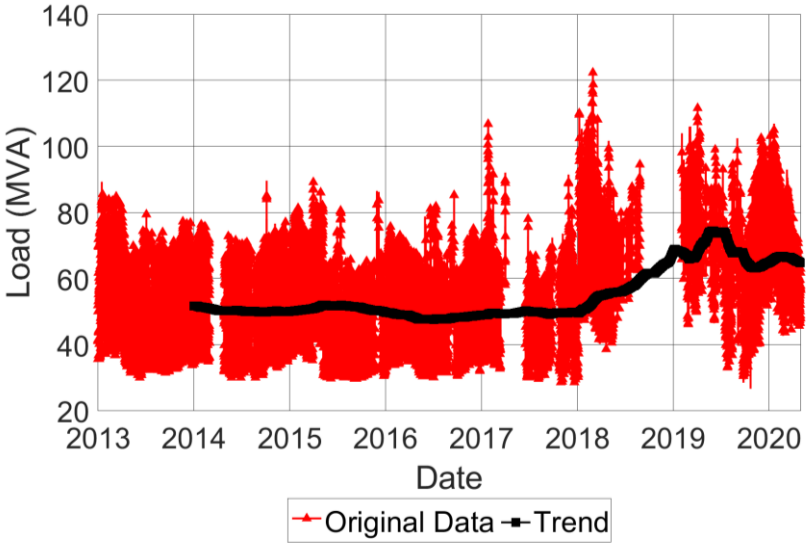

Figure 3.4 Original data and trend component of load for a transformer in the central London (Transformer A). The gaps are either unavailable data or periods that the transformer is not in operation.

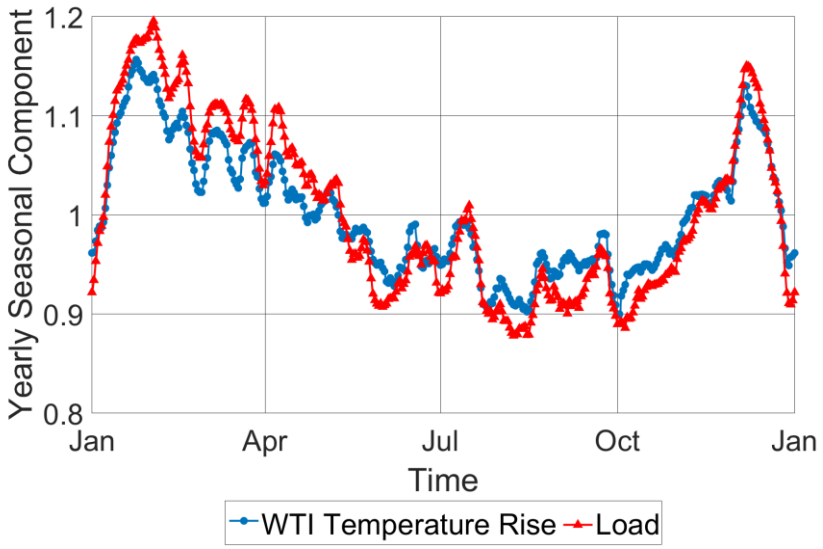

Figure 3.5 Yearly seasonal component of WTI temperature rise and load for a transformer in the central London (Transformer A).

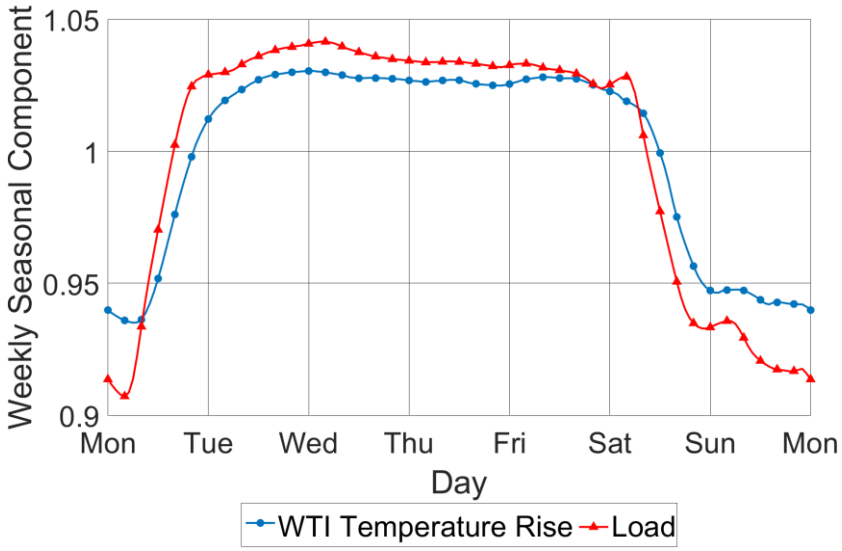

Figure 3.6 Weekly seasonal component of WTI temperature rise and load for a transformer in the central London (Transformer A).

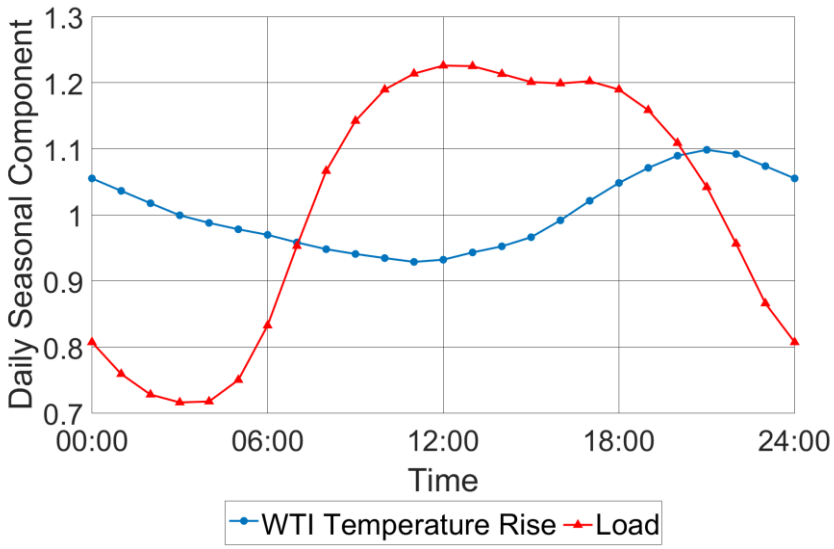

Figure 3.7 Daily seasonal component of WTI temperature rise and load for a transformer in the central London (Transformer A).

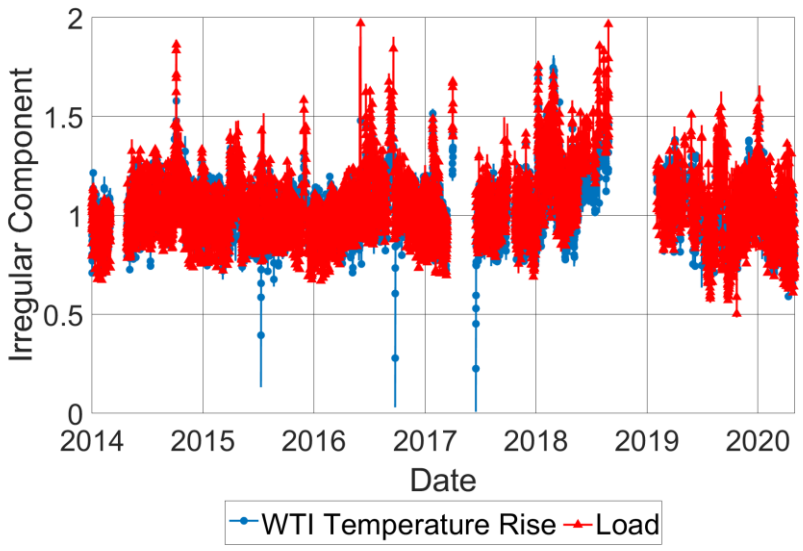

Figure 3.8 Irregular component of WTI temperature rise and load for a transformer in the central London (Transformer A). The gaps are either unavailable data or periods that the transformer is not in operation.

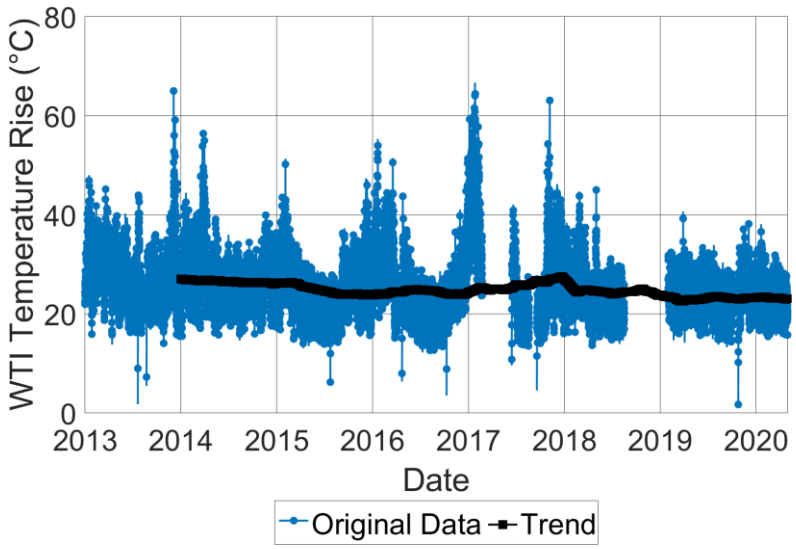

Figure 3.9 Original data and trend component of WTI temperature rise for a transformer in Braintree that is a residential area (Transformer C). The gaps are either unavailable data or periods that the transformer is not in operation.

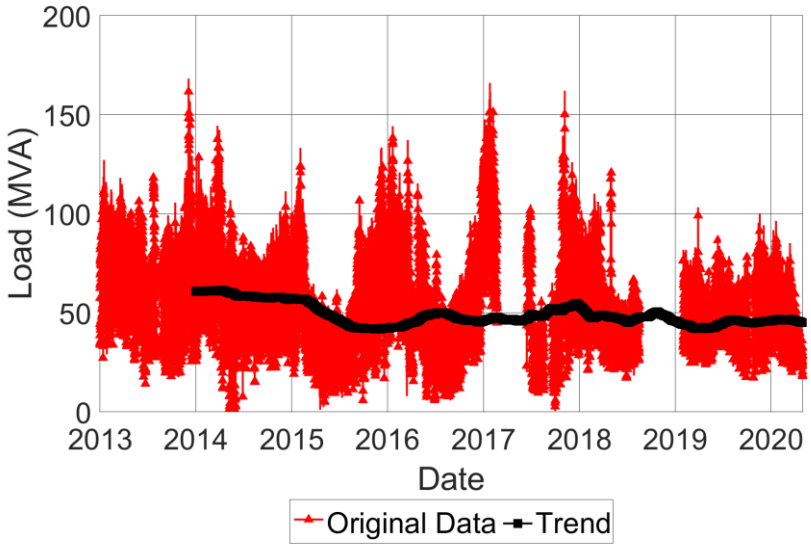

Figure 3.10 Original data and trend component of load for a transformer in Braintree that is a residential area (Transformer C). The gaps are either unavailable data or periods that the transformer is not in operation.

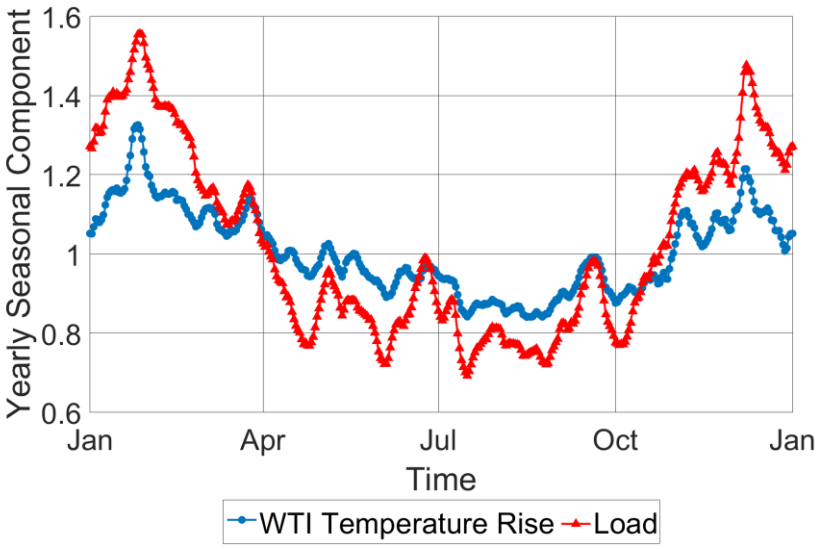

Figure 3.11 Yearly seasonal component of WTI temperature rise and load for a transformer in Braintree that is a residential area (Transformer C).

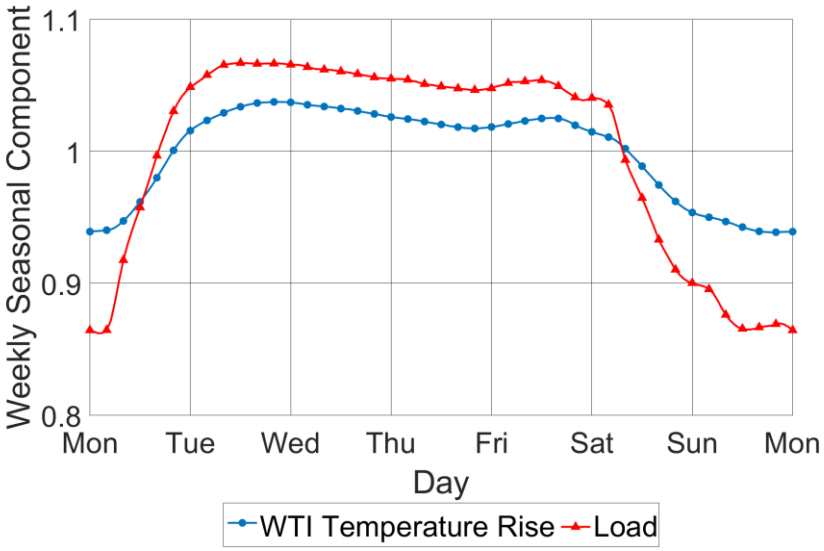

Figure 3.12 Weekly seasonal component of WTI temperature rise and load for a transformer in Braintree that is a residential area (Transformer C).

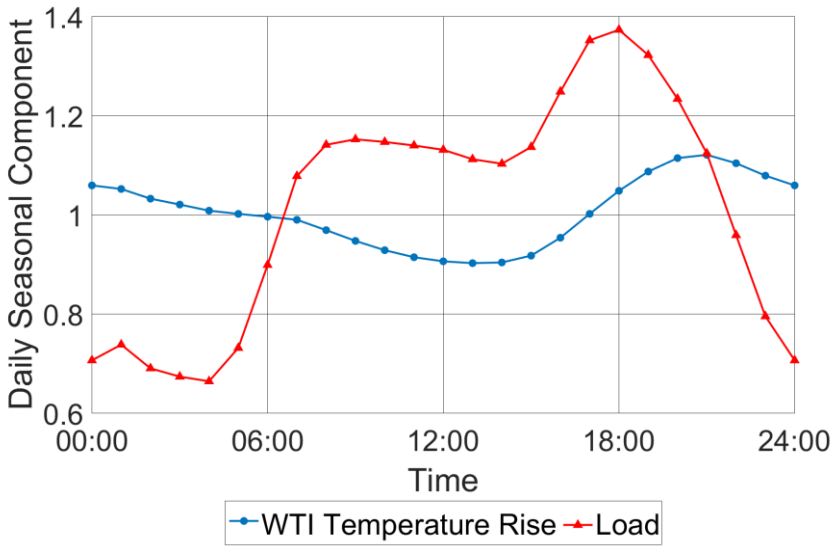

Figure 3.13 Daily seasonal component of WTI temperature rise and load for a transformer in Braintree that is a residential area (Transformer C).

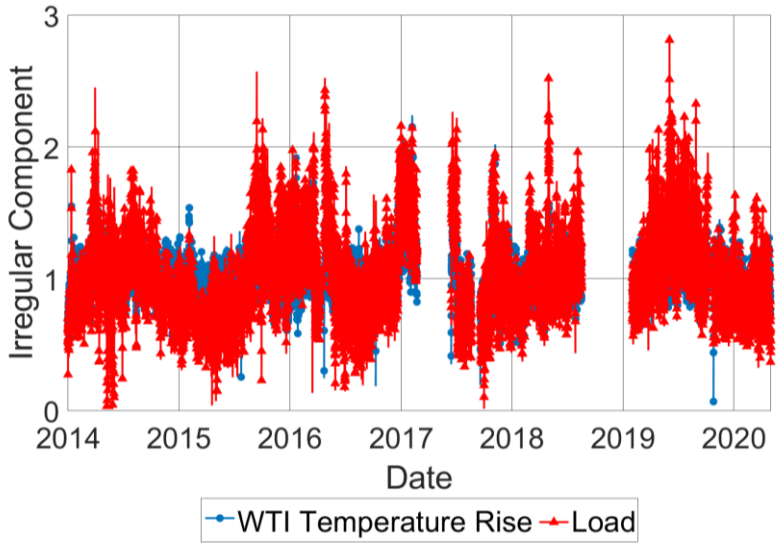

Figure 3.14 Irregular component of WTI temperature rise and load for a transformer in Braintree that is a residential area (Transformer C). The gaps are either unavailable data or periods that the transformer is not in operation.

3.3 Identifying Faulty WTIs using Time Series Decomposition

Winding losses in the transformer, which are correlated with load, and ambient temperature should lead to changes in the WTI temperatures. However, due to a failure of a WTI part, WTIs may no longer exhibit the intended load and ambient temperature dependency. Time series decomposition is a simple technique which can be utilised to easily check whether the data is correlated over different daily and weekly periods. It is worth noting that a limitation of this approach is WTIs with tracking top-oil temperature issues cannot be identified by this algorithm because they still exhibit load and ambient temperature dependency. WTIs with tracking top-oil temperature mean that there is a faulty part associated with a heater of a WTI that generates a temperature gradient between top-oil temperature and hot-spot temperature resulting in underestimating a hot-spot temperature. An algorithm that will be able to identify these issues will be discussed later in Chapter 6.

This section explains how faulty WTIs that do not have load and ambient temperature dependency could be identified using seasonal components between the load and WTI temperature rise and correlation coefficient. It is necessary to identify faulty WTIs because they control the cooling system of transformers and protect transformers from overheating. Typically, power transformers are equipped with two WTIs for LV and HV windings. As there are a sufficient large number of power transformers on the network, it is necessary to automate a process to detect faulty WTIs as much as possible.

Figure 3.15 shows a flow chart of a proposed algorithm for detecting faulty WTIs. First of all, the load, WTI temperature and ambient temperature measurements for the last 28 days are acquired to calculate the weekly seasonal components. This amount of the data provides sufficient information to calculate average values of the data for each time and day of weeks for weekly seasonal components, which is equal to 4 data points at any time of a week. The WTI temperature is subtracted with ambient temperature to obtain the WTI temperature rise.

The weekly seasonal components for both load and WTI temperature rise are calculated. Following that, the correlation coefficient between the load and WTI temperature rise for the weekly components is determined. If the correlation coefficient between the weekly components is less than 0.5, it indicates a faulty WTI with load dependency issue. Even when the coefficient of the weekly components is slightly higher than 0.5, there is probably an incipient fault. The daily correlation coefficients between the original load and WTI temperature rise, and between the ambient temperature and absolute WTI temperature for each single day are therefore determined for further investigation. If both daily correlation coefficients are less than 0.5 for three consecutive days, it indicates a faulty WTI with load and ambient temperature dependency issue. Typically, the correlation coefficients of healthy WTIs are between 0.8 and 1.0, see Figure 3.19. To reduce the number of fault positive results, the correlation coefficient of 0.5 is set as a threshold and it is also required to have three similar consecutive results. The reason why the correlation coefficient between the ambient temperature and

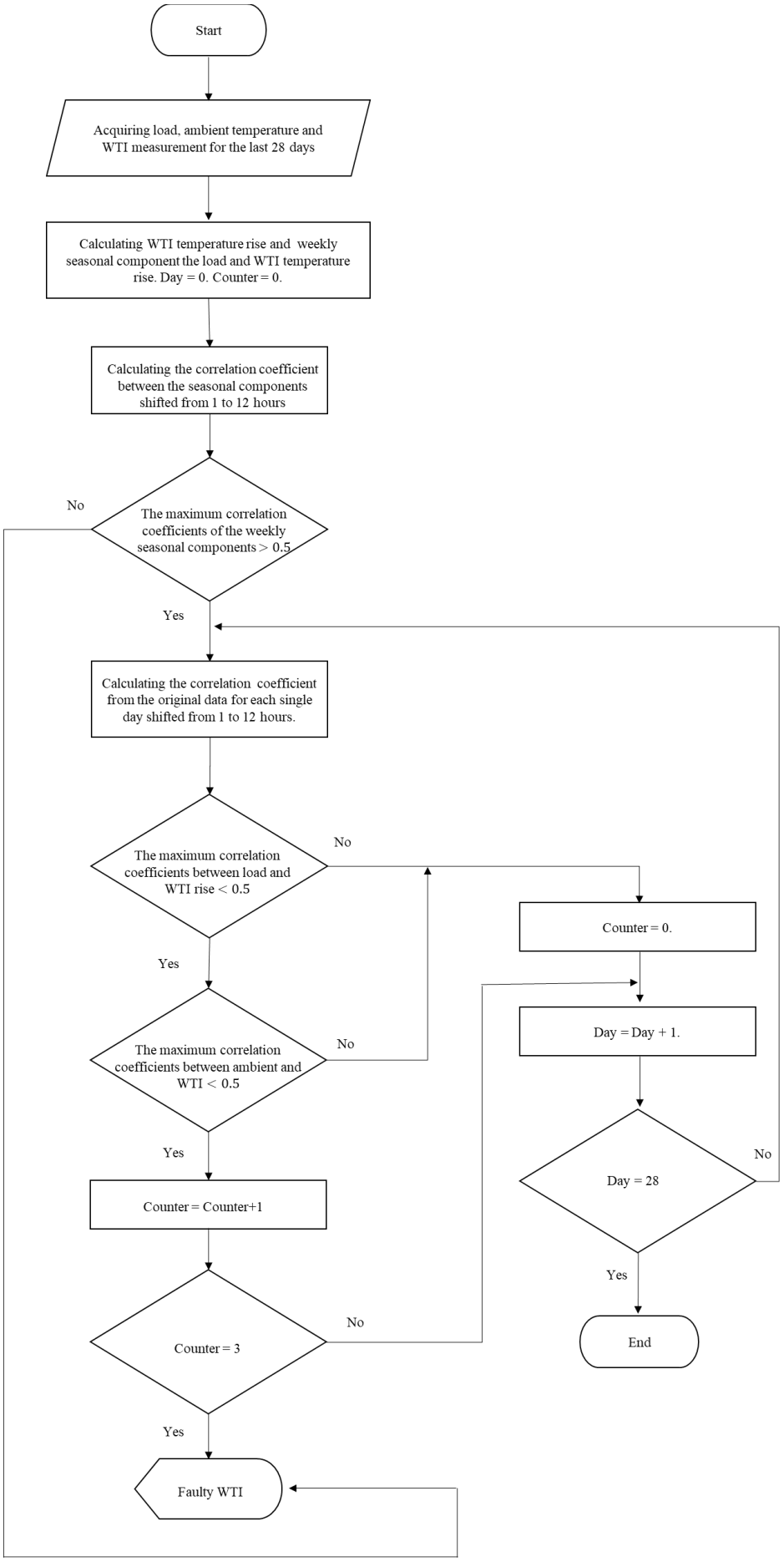

Figure 3.15 A flow chart of identifying faulty WTI with load and ambient temperature dependency.

the WTI temperature is also determined is that sometimes the load does not change significantly to cause a significant change in the WTI temperature, for example some weekends in summers. In contrast, the WTI temperature changes significantly because of ambient temperature, especially in summer. As there is a time lag from changes in the load and ambient temperature to changes in the WTI temperature, the temperature data are shifted backward so that the two data are in the same alignment. The correlation coefficients are calculated using the WTI temperature data shifted backward between 0 and 12 hours. The maximum coefficient is selected for judgement. The algorithm can be automatically and repeatedly applied over large periods of the data and identify a suspicious period when WTIs do not work properly. This helps maintenance team to target WTIs that need to be repaired effectively. The following are examples of the analyses of heathy and faulty WTIs. Figure 3.16 and Figure 3.17 show the original WTI temperature rise and load and their trend components for a healthy WTI, respectively. Figure 3.18 shows the weekly seasonal component for both the WTI temperature rise and load. The value of the correlation coefficient between them was greater than 0.95. In addition, the daily correlation coefficients were determined as shown in Figure 3.19. As either the daily correlation coefficients between load and WTI temperature rise or between ambient temperature and absolute WTI temperature had been greater than 0.5 over that periods, it indicated that the WTI was healthy.

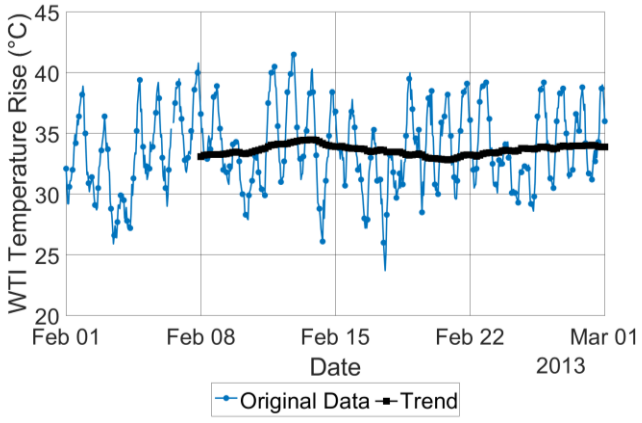

Figure 3.16 Original data and trend component of WTI temperature rise for a heathy WTI.

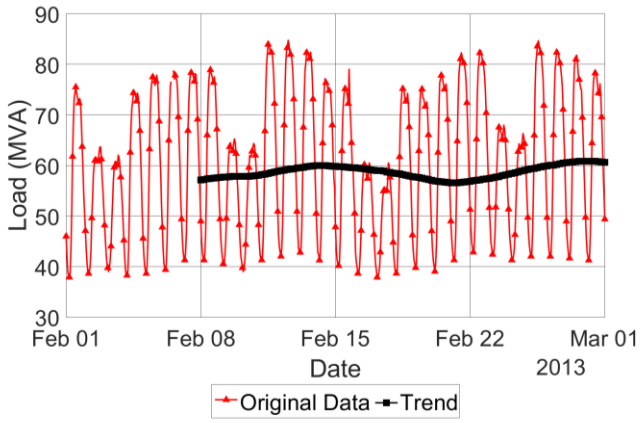

Figure 3.17 Original data and trend component of load for a heathy WTI.

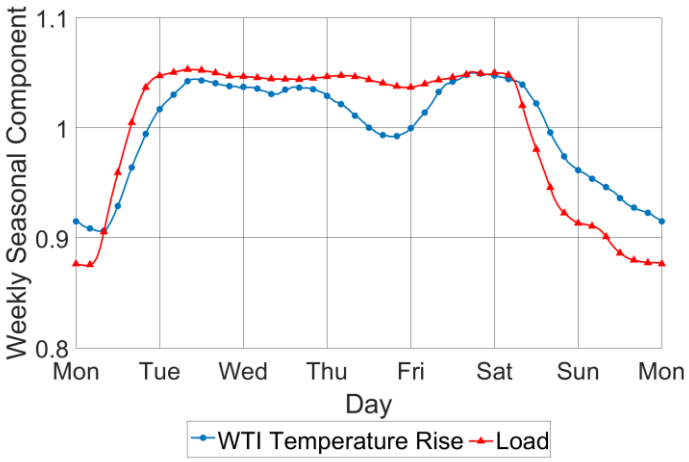

Figure 3.18 Weekly seasonal components of WTI temperature rise and load for a heathy WTI.

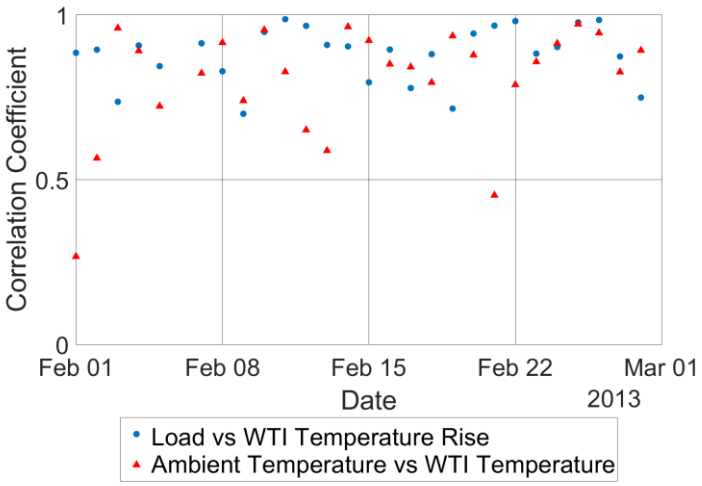

Figure 3.19 The daily correlation coefficients for a heathy WTI between load and WTI temperature rise and between ambient temperature and absolute WTI temperature.

WTIs of Transformer A, B and C are working properly. To demonstrate that the algorithm is able to identify a faulty WTI, a WTI measurement read by a real faulty WTI, from a transformer not considered thus far, is analysed. Analyses of a real faulty WTI that does not have load and ambient temperature dependency are shown in Figure 3.20 to Figure 3.23. It appears that the WTI was reading random values. The fault might be overlooked because the WTI was sending some values instead of being unresponsive. However, the fault will be detected by this algorithm as the correlation coefficient of the weekly seasonal components between the WTI temperature rise and load was less than 0.5. The values of the daily correlation coefficient also indicated a faulty WTI, see Figure 3.23. Absences of the values of the daily correlation coefficient on some days are due to missing data on those days.

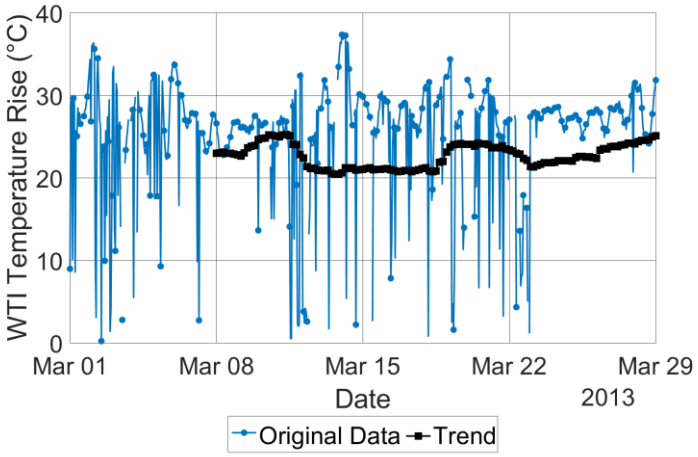

Figure 3.20 Original data and trend component of WTI temperature rise for a real faulty WTI with load and ambient temperature dependency issue.

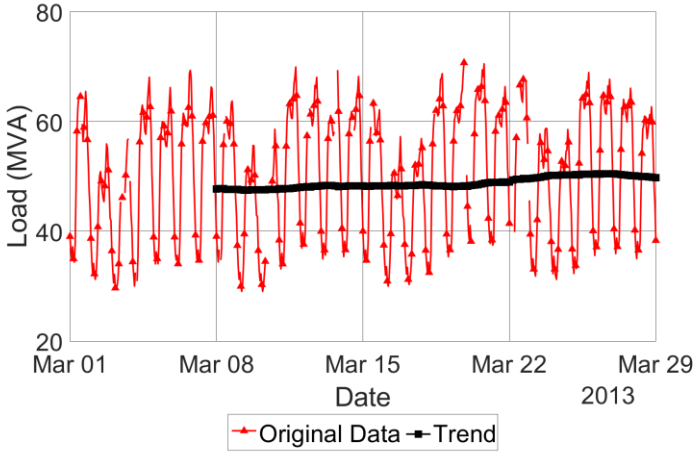

Figure 3.21 Original data and trend component of load for a real faulty WTI with load and ambient temperature dependency issue.

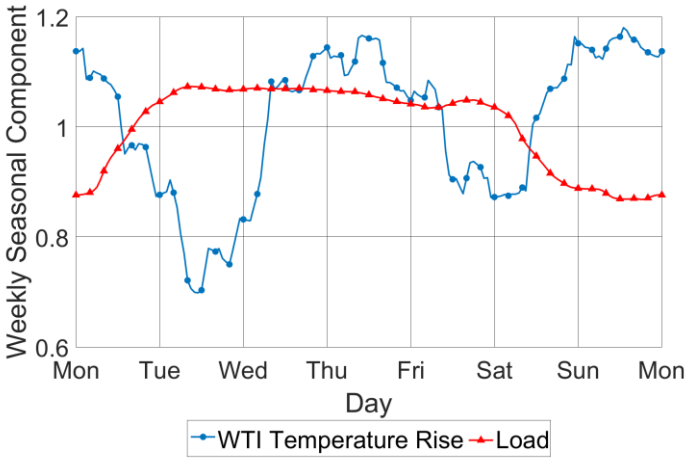

Figure 3.22 Weekly seasonal components of WTI temperature rise and load for a real faulty WTI with load and ambient temperature dependency issue.

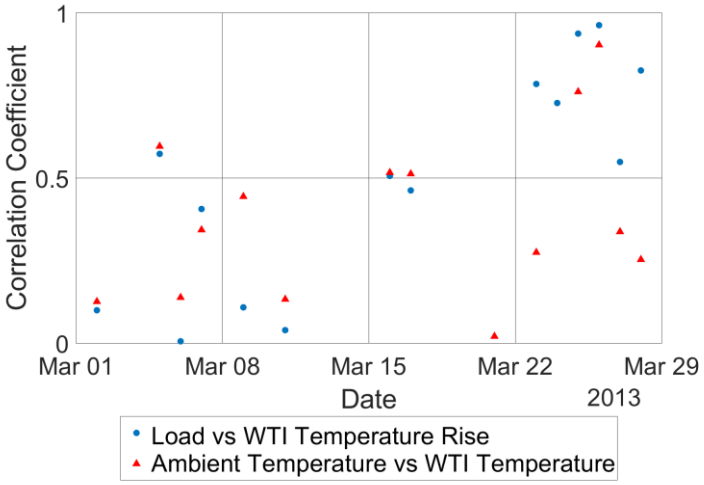

Figure 3.23 The daily correlation coefficients for a real faulty WTI between load and WTI temperature rise and between ambient temperature and absolute WTI temperature. Absences of the values of the daily correlation coefficient on some days are due to missing data on those days.

3.4 The IEEE-Annex G Model

Providing load profile, ambient temperature and transformer thermal parameters, the transformer temperature could be approximately determined using the IEEE-Annex G model [8]. Discussions of the results of the prediction made by the IEEE-Annex G model versus the measurement are provided in this section. The data were between July 2019 to April 2020 where weather stations have been installed at the substations as a part of ConCEPT project. Figure 3.24 to Figure 3.26 show examples of measurements and predictions made by the IEEE-Annex G model for Transformer A, B and C. Root mean squared errors (RMSEs) between the measurement and prediction for three transformers are provided in Table 3.2. The prediction of the model is fairly accurate, but it appears that the errors do vary with prevailing wind and solar radiation in some units. Impacts of prevailing wind and solar radiation are therefore investigated further in the next section.

Table 3.2 RMSE between measurement and prediction made by the IEEE-Annex G model.

Transformer	**RMSE (°C)**
A	1.96
B	2.10
C	2.96

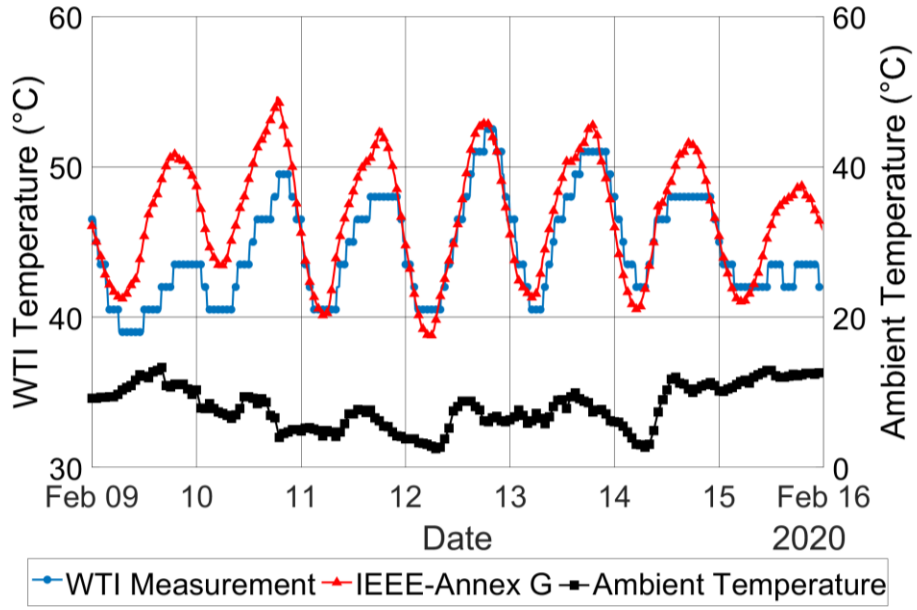

a) Measured and predicted WTI measurements and ambient temperature

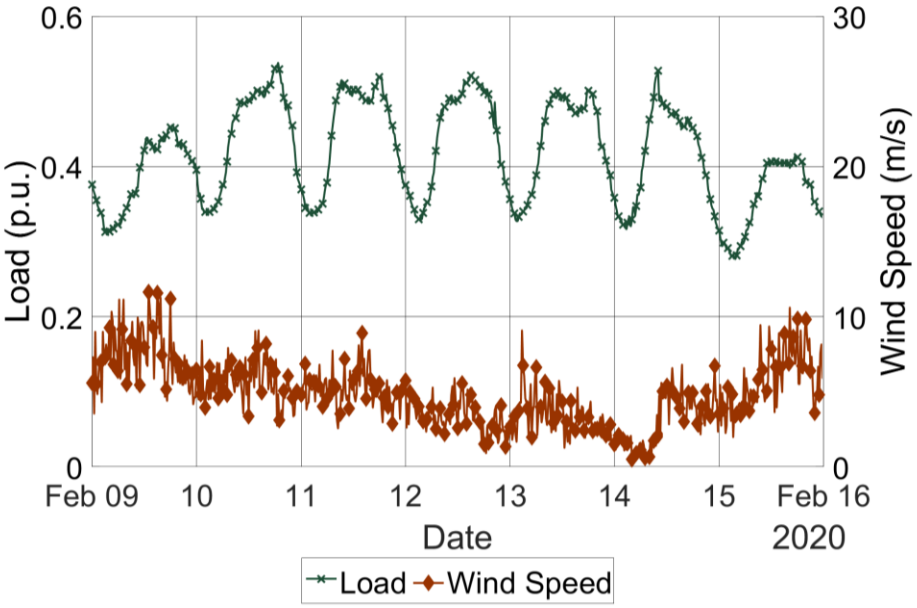

b) Load and wind speed profiles

Figure 3.24 WTI measurements and predictions made by the IEEE-Annex G model and load and wind speed profiles for Transformer A.

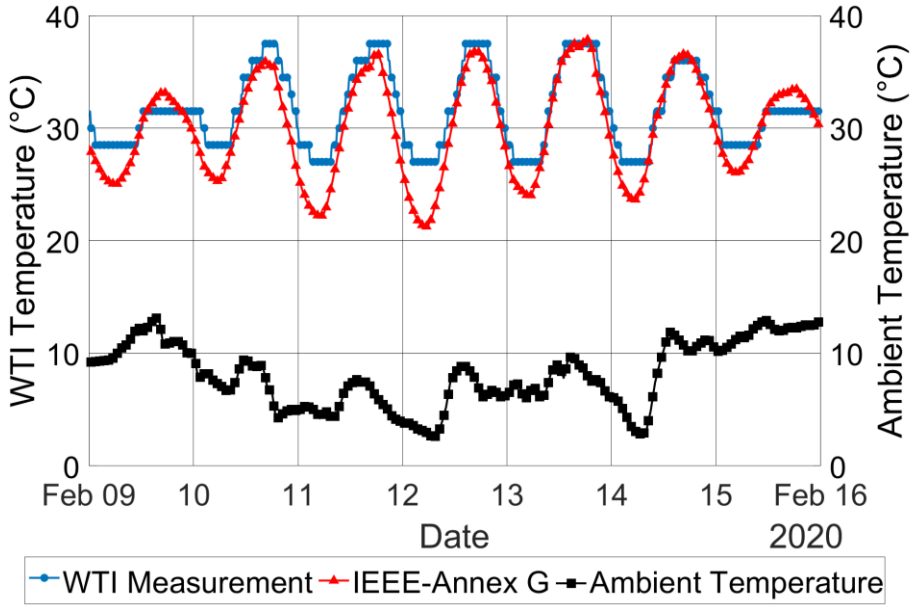

a) Measured and predicted WTI measurements and ambient temperature

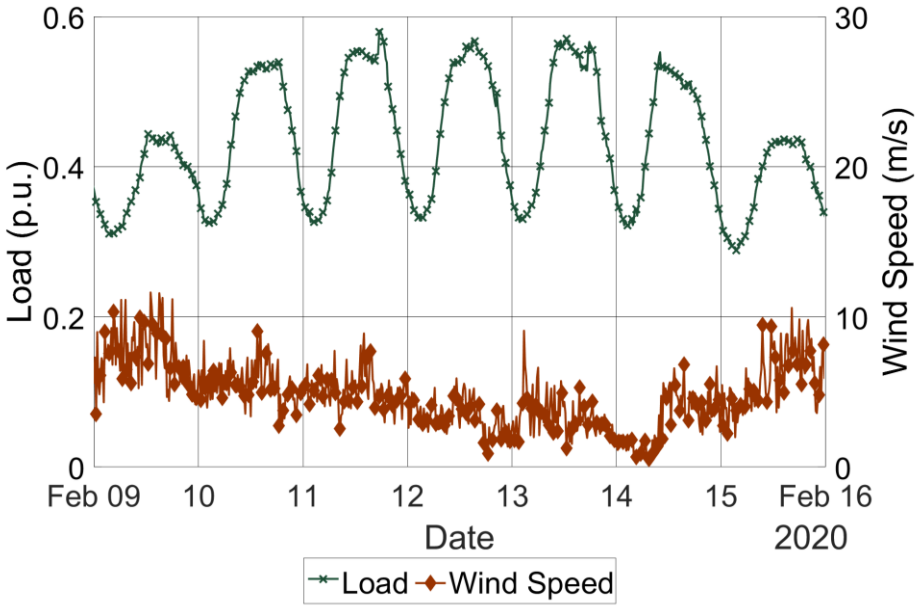

b) Load and wind speed profiles

Figure 3.25 WTI measurements and predictions made by the IEEE-Annex G model and load and wind speed profiles for Transformer B.

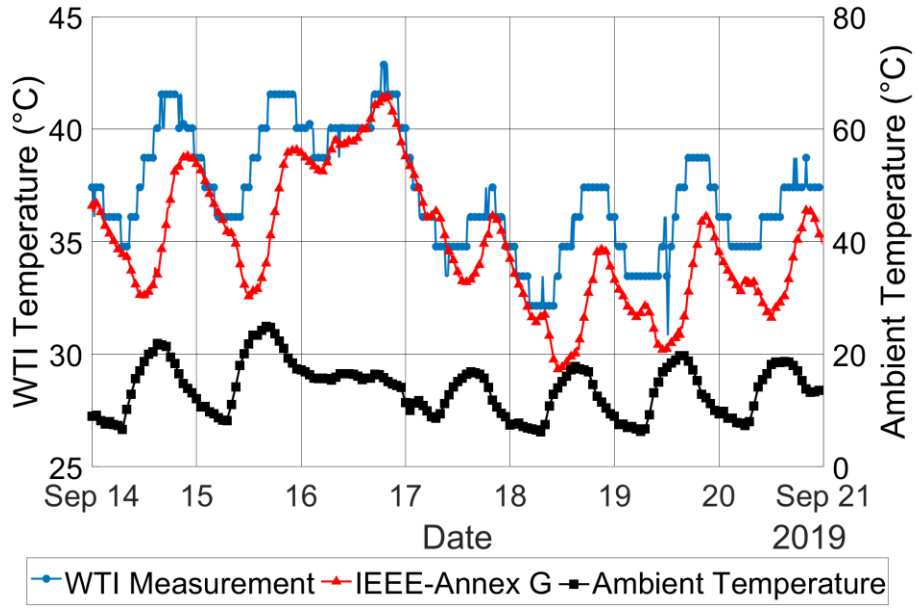

a) Measured and predicted WTI measurements and ambient temperature

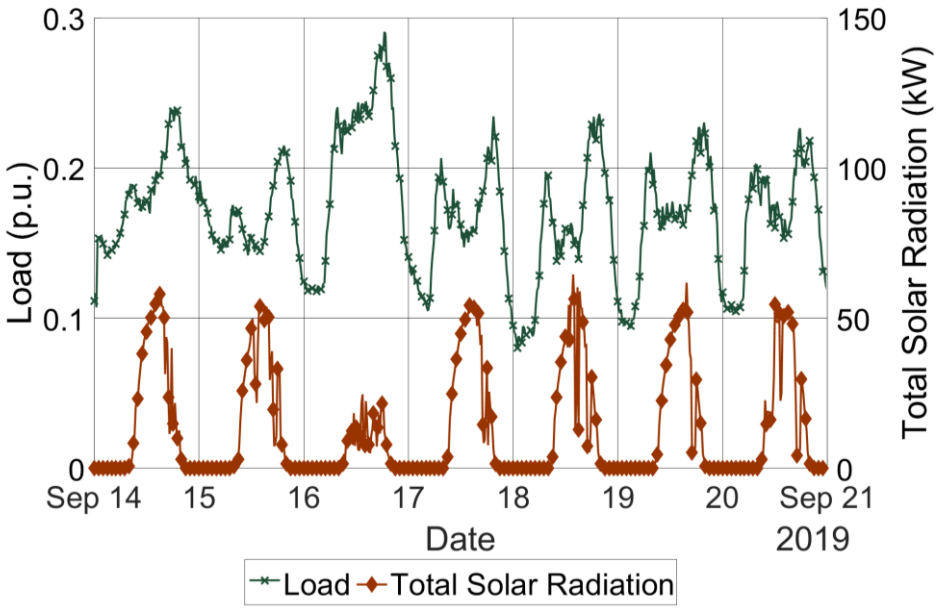

b) Load and wind speed profiles

Figure 3.26 WTI measurements and predictions made by the IEEE-Annex G model and load and solar radiation profiles for Transformer C.

3.4.1 Impacts of Wind and Solar Radiation

The daily average WTI temperature rise against load squared of Transformer A are plotted to illustrate an impact of prevailing wind as shown in Figure 3.27. It is evidenced that the daily average WTI temperature rise is usually cooler on windy days. Windy days are defined here as being those with a wind speed above 4 m/s. In addition, a plot of the RMSEs made by the IEEE-Annex G model against wind speed is provided in Figure 3.28. The results show that the errors rise with increasing wind speed. This supports that a presence of substantial wind could decrease the WTI temperature. Furthermore, the top-oil temperature rise at rated load and oil time constant, which are key parameters in the thermal model, are fitted for each single day. The rated top-oil temperature rise is supposed to be a constant, but it appears to decrease with increasing wind speed as shown in Figure 3.29.

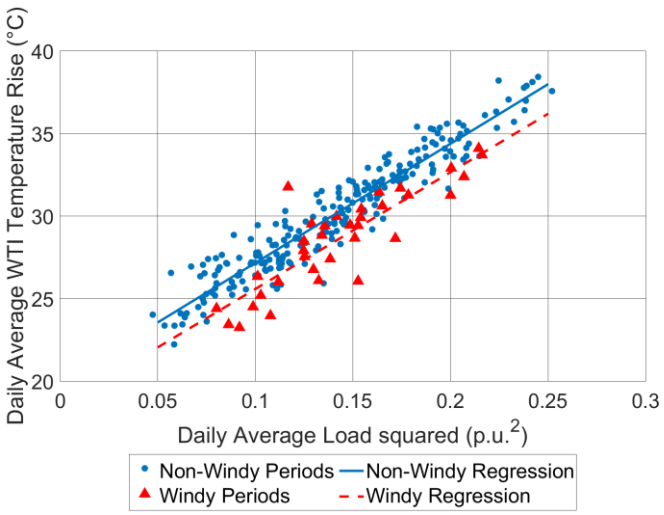

Figure 3.27 Daily average WTI temperature rise above ambient temperature against load squared for normal and windy periods for Transformer A.

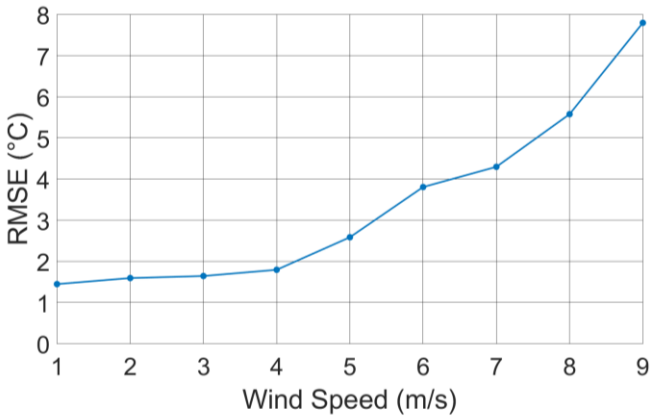

Figure 3.28 RMSEs mady by the IEEE-Annex G model agaist 6-hour average wind speeds for Transformer A.

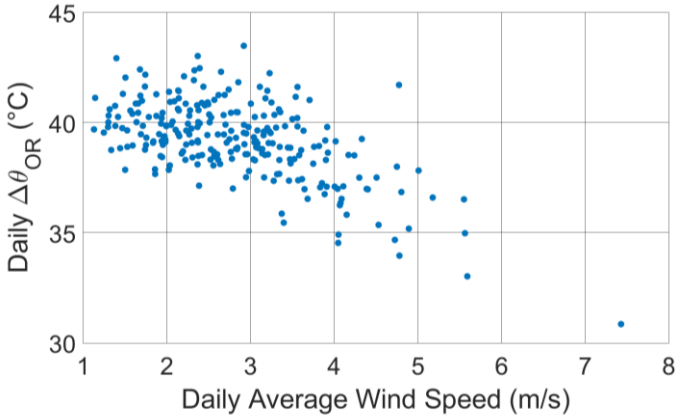

Figure 3.29 Daily rated top-oil temperature rise against daily average wind speed.

In addition to impacts of prevailing wind, the influence of solar radiation on the transformer temperature is also investigated. A plot of the daily average WTI temperature rise against load squared for Transformer C is shown in Figure 3.30. It also appears that the daily average WTI temperature is warmer during sunny days as shown in Figure 3.30. Plots of the RMSEs versus solar radiation and the fitted top-oil temperature rise also support this, see Figure 3.31 and Figure 3.32. As a transformer tank of Transformer A and B is indoor and only cooling banks are outdoor, it does not appear that the transformer temperature is warmer on sunny days which is as expected.

Based on the initial analysis, the weather factors do not have significant effects on Transformer B which is in an OFAF state. This is likely to be because the effect of wind cooling is small compared with forced air from fans and solar heating is only a small proportion of the total losses for this transformer which is more highly loaded. It is therefore excluded from further investigation. But this analysis does provide motivation for developing transformer thermal models for an ONAN state that can consider these weather factors.

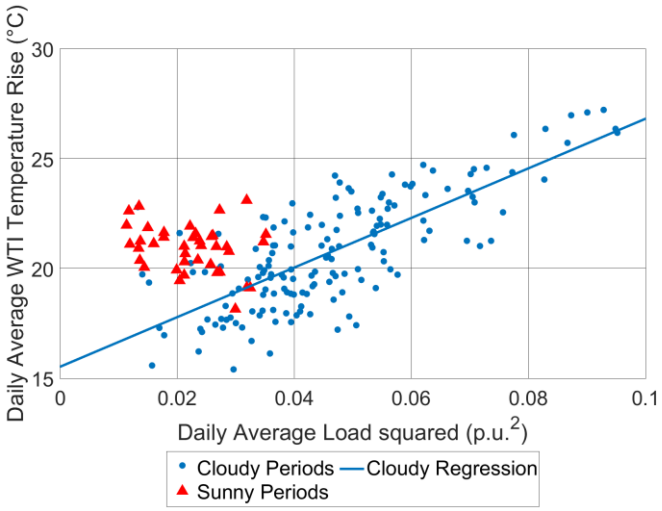

Figure 3.30 Daily average WTI temperature rise against load squared for normal and sunny periods for Transformer C.

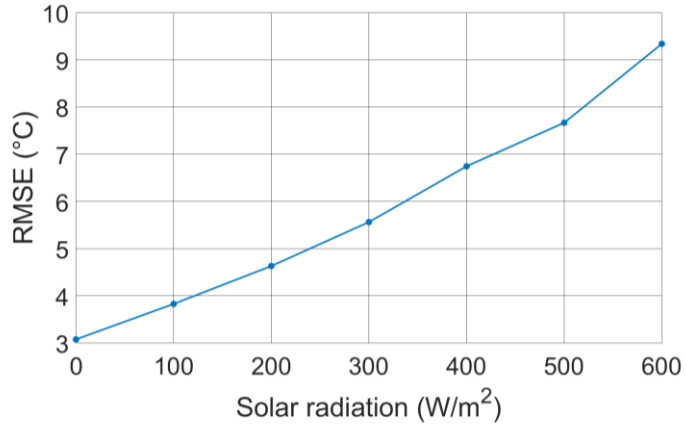

Figure 3.31 RMSEs mady by the IEEE-Annex G model agaist 6-hour average solar radiation for Tranformer C.

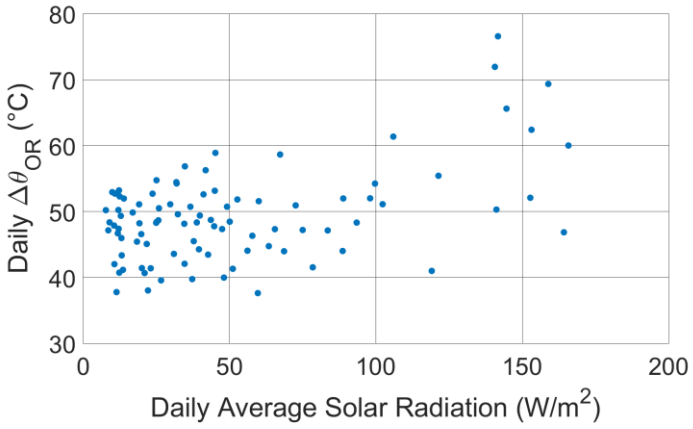

Figure 3.32 Daily rated top-oil temperature rise against daily average solar radiation.

3.5 Summary

Characteristics of time series of the load and WTI temperature rise have been investigated using the time series decomposition technique. It has been found there are yearly, weekly and daily seasonal components. The load appears to gradually drop from winter toward summer and then rise from summer to winter. It could be inferred that the load usually depends on ambient temperature as the electricity demand for heating would be reduced with increasing ambient temperature. The load demand is usually much lower on weekend. There is a time lag of about 5 hours between changing load and WTI temperature rise.

Faulty WTIs with load and ambient temperature dependency issues could be detected automatically using the time series analysis and correlation coefficient. The WTI temperature rise which is read by a healthy WTI should have a high correlation with the load. This algorithm helps maintenance teams

target faulty WTIs more effectively and reduce possibilities of overheating issues due to the faulty WTIs.

It appears that in some units the daily average WTI temperature rise is lower during windy days, while the daily average WTI temperature rise is warmer during sunny days. In addition, the errors between the measurement and prediction made by the IEEE-Annex G model that does not consider wind and solar radiation during windy and sunny periods are higher than average. According to this analysis, it is found that there is a dependency of the WTI temperature and wind speed for Transformer A, and dependency of the WTI temperature and solar radiation for Transformer C. This analysis does provide motivation for developing transformer thermal models for an ONAN state that can consider these weather factors. In Chapter 4, a top-oil transformer thermal model that considers wind and solar radiation will be discussed.

Chapter 4

A Top-oil Thermal Model for Power Transformers Considering Weather Factors

In this chapter, a top-oil thermal model for power transformers that considers weather factors is proposed to address the limitations of the traditional model discussed in the previous chapter. The thermal model is based on the thermal-electrical analogy and principles of heat transfer. Wind and solar radiation are explicitly included in a proposed differential equation. Prevailing wind is considered as a forced convection which improves the heat transfer rate while the solar radiation is considered as an additional heat source. The approach is validated using operational measurement from two different transformers. Effects of the weather factors on the loss of the solid insulation life and power flow capacity are also discussed.

4.1 Transformer Thermal Model

A novel transformer thermal model of the top-oil temperature is proposed by considering two environmental factors: prevailing wind and solar radiation. The thermal model is based on thermal-electrical analogy and heat transfer principle. The proposed model is designed for transformer units that are operating at an ONAN mode based on the analysis in the section 3.4.1. It clearly demonstrates dependency of the transformer temperature on wind speed and solar radiation, see Figure 3.27 and Figure 3.30. The novel contribution of the proposed thermal network model to the existing literature is that prevailing wind and solar radiation are both included in the governing equation for top-oil temperature.

The proposed model is based on Swift's model [14] but the top-oil thermal resistances are explicitly split into two regimes: between the oil and the radiator interior and between the radiator exterior and the ambient. For the interior regime, the thermal resistance depends on the oil movement. For the exterior regime, the natural and forced convection due to the air movement and the radiation from the radiator wall are explicitly considered simultaneously. This is especially necessary when the thermal resistance of the air and oil are similar. For example, it is a reasonable assumption to consider only thermal resistance of the air when operating in an ONAN mode because the oil has much lower thermal resistance than the air [14]. However, the situation has changed when fans are working or there is substantial wind as the air's thermal resistance is significantly decreased and is therefore

closer to the oil's thermal resistance. The thermal resistance of the radiator steel is neglected as the radiator wall is a good thermal conductor [14].The heat sources are comprised of the magnetic core, winding losses and solar radiation. Figure 4.1 illustrates the proposed top-oil thermal circuit.

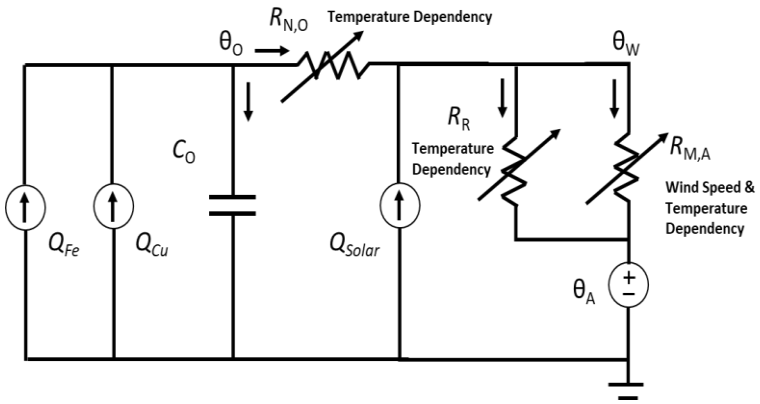

Figure 4.1 The proposed top-oil thermal model network that explicitly includes impacts of wind and solar radiation.

The governing differential equation is as follows:

$$Q_{\mathrm{Fe}} + Q_{\mathrm{Cu}} = C_{\mathrm{O}} \frac{d\theta_{\mathrm{O}}}{dt} + \frac{\theta_{\mathrm{O}} - \theta_{\mathrm{A}} - R_{\mathrm{MR,A}}(\theta_{\mathrm{O}}, \theta_{\mathrm{A}}) Q_{\mathrm{Solar}}}{R_{\mathrm{N,O}}(\theta_{\mathrm{O}}, \theta_{\mathrm{A}}) + R_{\mathrm{MR,A}}(\theta_{\mathrm{O}}, \theta_{\mathrm{A}})} \tag{4.1}$$

where Q_{Fe} are the magnetic core losses [W], Q_{Cu} are the winding losses [W], Q_{solar} is the total received solar radiation [W], C_{O} is thermal capacitance [W·s/K] and calculated in accordance with [8], $R_{\mathrm{N,O}}$ is the thermal resistance between the oil and the interior of the radiator which considers the natural convection of the oil [K/W], $R_{\mathrm{MR,A}}$ is the thermal resistance between the exterior of the radiator and ambient comprised of the forced and natural convection due to the air ($R_{\mathrm{M,A}}$) and the radiation from the wall (R_{R}), θ_{O} is the top-oil temperature [°C] and θ_{A} is the ambient temperature [°C]. Necessary thermal properties of the air and oil are derived from [76]. It should be noted that all thermal resistances are temperature dependent.

To calculate the effective thermal resistance on the air side and the oil side ($R_{\mathrm{MR,A}}$ and $R_{\mathrm{N,O}}$), it is necessary to calculate the temperature at the wall of the radiator (θ_{W}). This can be calculated by iteratively solving the following equation, which ensures the continuity of heat flux:

$$\frac{\theta_{\mathrm{O}} - \theta_{\mathrm{W}}}{R_{\mathrm{N,O}}} + Q_{\mathrm{Solar}} = \frac{\theta_{\mathrm{W}} - \theta_{\mathrm{A}}}{R_{\mathrm{MR,A}}} \tag{4.2}$$

4.1.1 Oil-to-Wall and Wall-to-Air Convection

The heat transfer due to convection exists as a result of fluid movement. Within the radiator, the convection occurs due to the oil movement while the convection arises between the exterior of the radiator and ambient due to air movement. The convection can be improved by applying external

force, e.g. pumps and fans. The prevailing wind could be considered as external force that improves the heat transfer rate of the radiator.

The thermal resistance due to convection is inversely proportional to heat transfer coefficient and cooling area, it is defined as [77]:

$$R = \frac{1}{hA_{\mathrm{C}}} = \frac{L}{A_{\mathrm{C}}k\overline{Nu}} \tag{4.3}$$

where h is a heat transfer coefficient [W/(K·m^2)], A_{C} is cooling area due to convection [m^2], L is characteristic length of heat transfer [m], k is thermal conductivity of the fluid which will be air or oil [W/(m·K)] and $\overline{Nu}$ is the Nusselt number.

The Nusselt number ($\overline{Nu}_{\mathrm{F}}$), Reynold number ($Re_L$), and Prandtl number ($Pr$) of forced convection for constant heat flux on a vertical plate with a laminar flow are based on empirical correlations as follows [77]:

$$\overline{Nu}_{\mathrm{F}} = D_1 Pr^{1/3} {Re_L}^{1/2} \tag{4.4}$$

$$Re_L = \frac{uL_{\mathrm{F}}\rho}{\mu} \tag{4.5}$$

$$Pr = \frac{\mu}{\alpha\rho} \tag{4.6}$$

where D_1 is an empirical constant, L_{F} is characteristic length for forced convection [m], u is wind speed [m/s], μ is dynamic viscosity of air [kg/(m·s)], ρ is density of air [kg/m^3] and α is thermal diffusivity of air [m^2/s].

The Nusselt number ($\overline{Nu}_{\mathrm{N}}$) and Rayleigh number ($Ra_L$) of natural convection on a vertical plate with a laminar flow based empirical correlations are expressed as [77]:

$$\overline{Nu}_{\mathrm{N}} = D_2 {Ra_L}^{\frac{1}{4}} \tag{4.7}$$

$$Ra_L = \frac{\mathrm{g}\beta c_p \rho^2 \Delta\theta {L_{\mathrm{N}}}^3}{\mu k} \tag{4.8}$$

where D_2 is an empirical constant, L_{N} is characteristic length for natural convection, μ is dynamic viscosity of the fluid which will be air or oil [kg/(m·s)], c_p is specific heat of the fluid [W·s/(kg·K)], g is gravitational constant [m/s^2], ρ is density of the fluid [kg/m^3], $\Delta\theta$ is the temperature difference over the fluid medium which will be a temperature difference of the oil above radiator wall for the interior of the radiator and a temperature difference of the radiator wall above air the exterior of the radiator [K]. β is thermal expansion coefficient of the fluid [1/K].

The heat transfer coefficient of mixed forced and natural convection of air is expressed as follows [78]:

$$h_{\mathrm{M,A}} = \left({h_{\mathrm{F,A}}}^{3.2} + {h_{\mathrm{N,A}}}^{3.2} \right)^{\frac{1}{3.2}} \tag{4.9}$$

where $h_{\mathrm{F,A}}$ is the heat transfer coefficient of forced convection of air [W/(K·m^2)] and $h_{\mathrm{N,A}}$ is the heat transfer coefficient of natural convection of air [W/(K·m^2)]. $h_{\mathrm{M,A}}$ is then used to determine the thermal resistance through (4.3).

As the radiators of transformers are not perfectly planar the values of empirical constants (D_1 and D_2) are treated as free parameters. The fitted values are determined using trust-region-reflective algorithms [79]. To avoid the fitted values becoming unrealistic, both constants are restricted to between 0 and 1. A comparison of the fitted values is made against literature values, [77], which are 0.68 and 0.59 for D_1 and D_2 respectively.

The wind direction will influence the extent to which it can penetrate the radiator. The reduction due to the alignment is considered by treating D_1 as a free parameter. Generally, the wind has a prevailing direction at any given site so the value of D_1 for any given location, radiator type and orientation should remain roughly constant.

$R_{\mathrm{M,A}}$ is expressed in terms of a combination of forced and free convective thermal resistance of the air ($R_{\mathrm{F,A}}$ and $R_{\mathrm{N,A}}$) by substituting (3) to (9) and then rearranging the equation as follows:

$$R_{\mathrm{M,A}} = \frac{1}{A_{\mathrm{C}} h_{\mathrm{M,A}}} \tag{4.10}$$

where A_{C} is cooling area [m^2] and $h_{\mathrm{M,A}}$ is the heat transfer coefficient of mixed convection of air [W/(K·m^2)].

$R_{\mathrm{N,O}}$ is calculated in the same way as $R_{\mathrm{N,A}}$, replacing the air's thermal properties with the oil's properties. $R_{\mathrm{MR,A}}$ is calculated as the total resistance of two thermal resistances connected in parallel as follows:

$$R_{\mathrm{MR,A}} = \left(\frac{1}{R_{\mathrm{M,A}}} + \frac{1}{R_{\mathrm{R}}} \right)^{-1} \tag{4.11}$$

where R_{R} is a thermal resistance due to radiative heat transfer of the radiator wall [K/W].

4.1.2 Radiative Heat Transfer

Transformers are not only receiving heat from the sun, but they also transfer heat to the surrounding environment via radiation. The radiative thermal resistance (R_{R}) is [12]:

$$R_{\mathrm{R}} = \frac{1}{\varepsilon\sigma A_{\mathrm{R}}[(\theta_{\mathrm{W}})^2 + (\theta_{\mathrm{A}})^2](\theta_{\mathrm{W}} + \theta_{\mathrm{A}})} \quad (4.12)$$

where ε is emissivity, σ is the Stefan-Boltzmann constant [W/(m^2·K^4)], A_{R} is the radiating area [m^2], θ_{W} is the radiator wall temperature [K] and θ_{A} is ambient temperature [K]. As the paint colour of the transformers is grey, a value of 0.9 for ε is considered reasonable [76].

4.1.3 Additional Heating Due to Solar Radiation

As the global solar radiation is only recorded on a horizontal surface, the global solar radiation on vertical surfaces is estimated based on the solar radiation on the horizontal surface. The global solar radiation of a tilted surface is estimated as follows [80]:

$$q_{\mathrm{global}} = q_{\mathrm{dir}} R_b + 0.5 q_{\mathrm{indir}}(1 + \cos\emptyset) + 0.5 p_{gr}(q_{\mathrm{dir}} + q_{\mathrm{indir}})(1 - \cos\emptyset) \quad (4.13)$$

where q_{dir} [W/m^2] and q_{indir} [W/m^2] are the direct and indirect radiation on a horizontal surface, respectively, $R_b$is the ratio of the direct radiation on the tilted surface to that on a horizontal surface, p_{gr} is albedo factor and $\emptyset$ is tilted angle with respect to the ground. A value of 0.3 for p_{gr} is typically found for weathered grey concrete [81].The R_b is dependent on the altitude and azimuth angles and the location of the surface and is expressed as follows:

$$R_b = \cos\emptyset + \sin\emptyset \tan(ZN) \cos(AZ - \vartheta) \quad (4.14)$$

where ϑ is the surface azimuth rotation angle [rad], ZN is zenith angle [rad] and AZ is azimuth angle [rad]. The azimuth and zenith angles are dependent on the time of the year and location of the transformer. Detailed calculation for the altitude and azimuth angles can be found [82].

The indirect radiation for the UK could be estimated as follows [83]:

$$q_{\mathrm{indir}} = q_{\mathrm{global\,H}} \bar{k}_{\mathrm{indir}} \quad (4.15)$$

$$\bar{k}_{\mathrm{indir}} = 0.89\overline{k_t^2} - 1.185\bar{k}_t + 0.95 \quad (4.16)$$

where $\bar{k}_{indir}$ is the monthly-averaged ratio of the indirect to global radiation, $q_{\mathrm{global\,H}}$ is the global radiation on a horizontal surface measured by the local substation weather station, and $\bar{k}_t$ is the monthly-averaged clearness index. $\bar{k}_t$ used in this work is derived from [80], see Table 4.1.

The direct radiation on a horizontal surface is expressed as follows:

$$q_{\mathrm{dir}} = q_{\mathrm{global\,H}} - q_{\mathrm{indir}} \quad (4.17)$$

where $q_{\mathrm{global\,H}}$ is the global radiation on a horizontal surface measured by the local substation weather station [W/m^2] and q_{indir} is indirect radiation on a horizontal surface [W/m^2].

Solar radiation is accounted for using the same approach suggested in [65], taking into account the fact that for the larger power transformers considered in this work comprise of a tank and a cooler bank. In [65] only smaller power transformers were considered, where solar radiation on a main tank and fins attached to it was considered. For the inner of radiator plates, the surface areas are decreased due to shadow of the adjacent plates. The value of the direct radiation on the remaining areas that are not in the shadows is corrected as follows [65]:

$$q_{\mathrm{diri}} = (1 - r_s) q_{\mathrm{dir}} \tag{4.18}$$

where r_s is the ratio of the shadow to the total area.

There are seven surfaces that receive the solar radiation in total: two vertical surfaces of the radiator, four vertical surfaces of the transformer tank and the horizontal surface of the transformer tank. The surfaces that are not facing to the sun only receive indirect solar radiation. This is shown in Figure 4.2. The total received solar radiation is:

$$Q_{\mathrm{Solar}} = \sum_{i=1}^{7} \alpha_{\mathrm{solar}} A_i q_{\mathrm{global}\ i} \tag{4.19}$$

where α_{solar} is the solar radiation absorption, A_i is the receiving area on each surface [m^2], $q_{\mathrm{global}\ i}$ is the global radiation on each surface [W/m^2]. A value of 0.9 for α_{solar} is considered reasonable for transformers painted with grey color [76]. If the transformer tank is indoors, the tank surface is excluded.

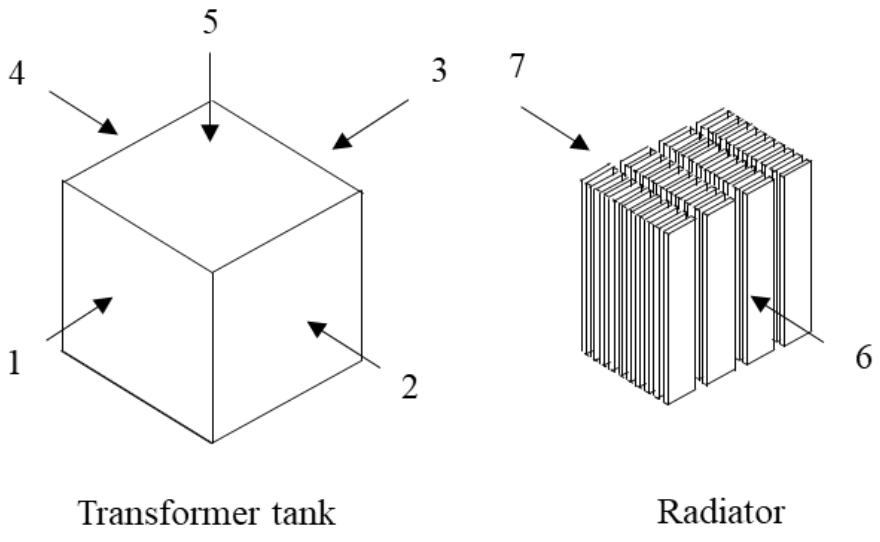

Figure 4.2 Surfaces of a transformer tank (left) and radiator (right) subjected to solar radiation. This figure is not drawn to scale.

Table 4.1 Monthly-Averaged Clearness Index for The UK [80]

Month	**Jan**	**Feb**	**Mar**	**Apr**	**May**	**Jun**
$\overline{k_t}$	0.24	0.29	0.34	0.35	0.39	0.43
	Jul	Aug	Sep	Oct	Nov	Dec
	0.4	0.39	0.39	0.35	0.31	0.25

4.2 Results and Discussion

The proposed model is validated with the operational measurement of Transformers A and C. The data comprised WTI measurement, load, tap position, ambient temperature, wind speed and solar radiation. The analyses have been carried out based on the measurements between July 2019 and May 2020 for Transformer A and C. The total numbers of the data points for Transformer A and C are 17796 and 25622 points with 15-minute sampling interval. The first half of the operational measurement is used to adjust the D_1 and D_2 and the other half is used to evaluate the accuracy. The results are provided and discussed in this section. Transformer A is in an urban area, surrounded by concrete walls. Transformer C is an outdoor unit, with its main tank and radiators outdoors in a rural area. Overall transformer specifications are provided in Appendix B in Table B.1.

4.2.1 Transformer thermal parameters

Table 4.2 shows the results of the thermal parameters derived based on the first half of the operational measurement. The value of D_1 of Transformer A is lower than the value derived from the literature. This is probably the transformer is surrounded by walls which could restrict prevailing wind. While the value of D_1 is similar to the recommended value for Transformer C in a rural area without surrounding buildings. The values of D_2 that are derived from the measurement are slightly higher than the value in the literature [77]. This is probably because the plates of the transformer cooler banks are optimized to increase heat transfer coefficient in comparison with a plain plate. The thermal parameters associated with geometry of transformer are provided in Table 4.3. It was found that the average contribution of the radiative losses from the tank and coolers for a whole year is about 2% and 12% to the total losses for Transformer A and B, respectively. The reason that the contribution of Transformer A is relatively smaller is because the main tank is indoors. The contribution of the radiative heat transfer to the total heat transfer varies with transformer designs and operating conditions.

Table 4.2 Thermal Parameters Derived from the Local Substation Data.

Transformer	Forced Convection (D_1)	Natural Convection (D_2)
A	0.45	0.85
C	0.69	0.62
Literature	0.68	0.59

Table 4.3 Thermal Parameters

Thermal Parameters	Transformer A	Transformer C
L_N [m]	3.74	2.09
L_F [m]	4.0	5.1
Cooling areas [m^2] [A_C]	2573.0	1364.5
North and south-facing radiator surface areas [m^2]	N/A	N/A
East and west-facing radiator surface areas [m^2]	14.96	10.66
North and south-facing Transformer surface areas [m^2]	11.6	24.8
East and west-facing transformer surface areas [m^2]	28.3	15.3
Top transformer surface areas [m^2]	22.6	28.6
Radiating areas [m^2] (A_R)	29.92*	130.12

For Transformer A, radiating areas are accounted for radiator surface areas only because the tank is indoors.

4.2.2 Comparisons between Measurement and Prediction

The other half of the operational thermal measurements of the two transformers is compared with the predictions made by the proposed model as well as the Annex G in the IEEE guide [8], referred to as the IEEE-Annex G model hereafter. To improve the accuracy of the IEEE-Annex G model the top oil temperature rise at rated load, a key model input, was adjusted to reduce the error between simulated and measured data instead of using the original value derived from the heat run test. This was based on previous investigations by the authors [84]. It should be noted that the set of equations

of the IEEE-Annex G model are not modified but only the top-oil temperature rise at rated load is tuned to fit the operational measurement.

Comparison of the accuracy of the predictions between the IEEE-Annex G and the proposed models on windy periods for Transformer A and their dependency on wind speed is provided in Table 4.4. The results on sunny periods for Transformer C and dependency on solar radiation are provided in Table 4.5. In general, the accuracy of the proposed model is not significantly different from the traditional model. However, the improvement of the prediction made by the proposed model is significant when the transformers are subjected to substantial prevailing wind or solar radiation for extend periods of time. The predictions made by the proposed model without considering solar radiation and wind speed intentionally are also included in the results to highlight the improvement due to the consideration of the weather factors.

Table 4.4 RMSE of Thermal Model for Transformer A.

Model	**All Periods**	**Windy Periods***
IEEE-Annex G (°C)	1.96	4.53
Proposed Model (°C)	1.77	1.99
Improvement (%)	9.5	56.1
Proposed Model (NW) (°C)	2.62	5.70

*Windy periods are defined here as being those with 6-hour average wind speed above 6 m/s and no weather (NW) means weather factors ignored intentionally.

Table 4.5 RMSE of Thermal Model for Transformer C.

Model	**All Periods**	**Sunny Periods****
IEEE-Annex G (°C)	2.96	5.92
Proposed Model (°C)	2.01	2.21
Improvement (%)	32.1	62.7
Proposed Model (NW) (°C)	2.78	4.06

**Sunny periods are defined here as being those with 6-hour average solar radiation above 0.4 kW/m^2 and no weather (NW) means weather factors ignored intentionally.

The root-mean-square errors (RMSEs) between the measurements and predictions based on the IEEE-Annex G and the proposed model over sunny and windy periods are used to evaluate the accuracy. Windy periods are defined here as being those with 6-hour average wind speed above 6 m/s and sunny periods are defined here as being those with 6-hour average solar radiation above 0.4 kW/m^2. The transformers were subjected with various load and ambient temperature.

The RMSEs made by the IEEE-Annex G and proposed models at various 6-hour average wind speeds of Transformer A are shown in Figure 4.3. For Transformer A, it appears that the errors between the measurement and prediction based on the IEEE-Annex G model increase with increasing wind speeds while the errors for the proposed model do not vary with the wind speeds.

Figure 4.4 shows the RMSE against the 6-hour average total receiving solar radiation for Transformer C. There is a significant correlation between the RMSE made by the IEEE-Annex G model and the solar radiation for Transformer C while there is not dependency of the RMSE made by the proposed model on solar radiation. The RMSE of the proposed model is around 3.0°C at the solar radiation of 55 kW while the RMSE of the IEEE-Annex G model is about 7.5°C.

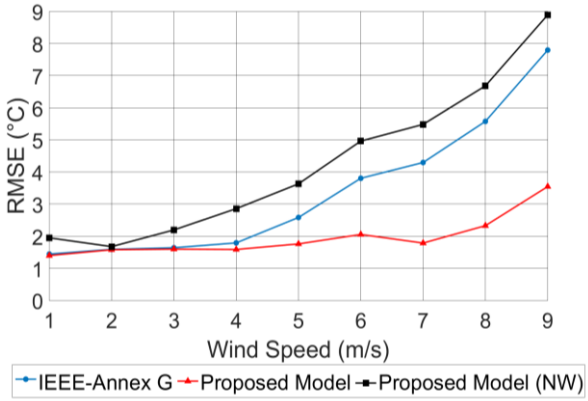

Figure 4.3 Statistical errors of the IEEE-Annex G and proposed models against 6-hour average wind speed for Transformer A.

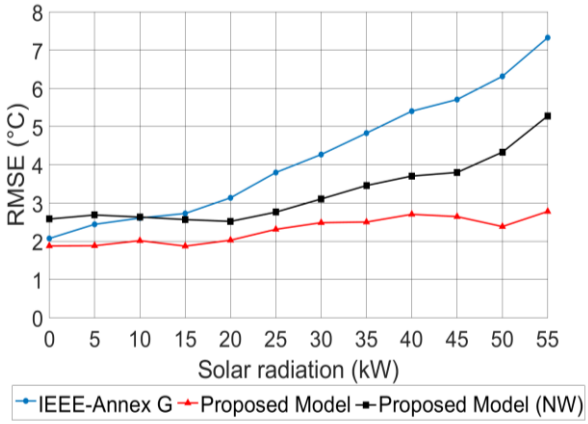

Figure 4.4 Statistical errors of the IEEE-Annex G and proposed models against the total 6-hour average receiving solar radiation for Transformer C.

Examples of WTI measurement and prediction made by the IEEE-Annex G and proposed models for Transformer A on a windy day and Transformer C on a sunny day are shown in Figure 4.5 and Figure 4.6. The prediction made by the proposed model is typically in closer agreement with the measurement compared with the prediction made by the traditional model. The RMSE of the traditional model is about 8°C at the wind speed of 9 m/s while the accuracy of the proposed model is higher at the RMSE of 3°C.

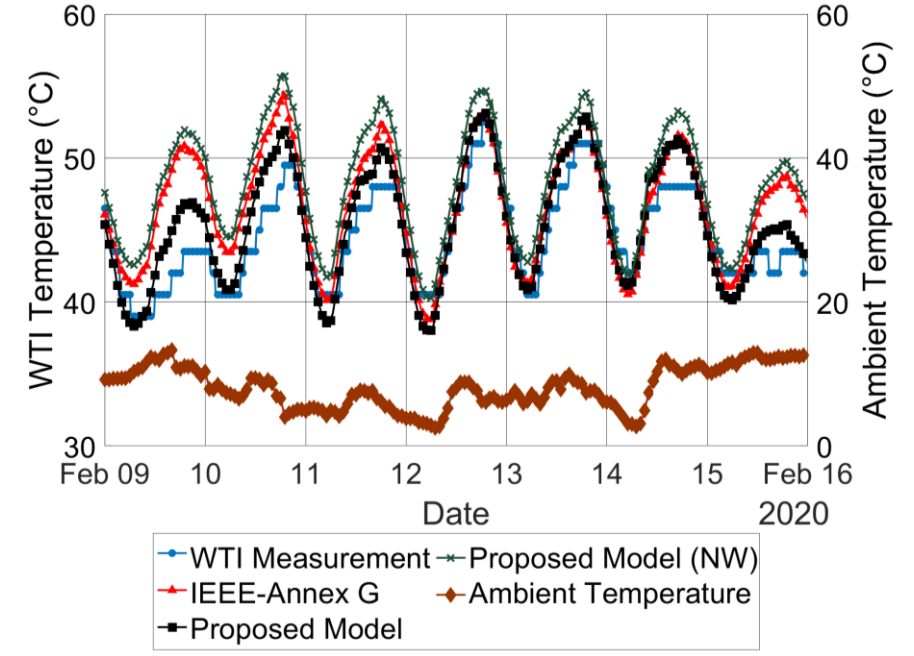

a) WTI measurement and predictions and ambient temperature

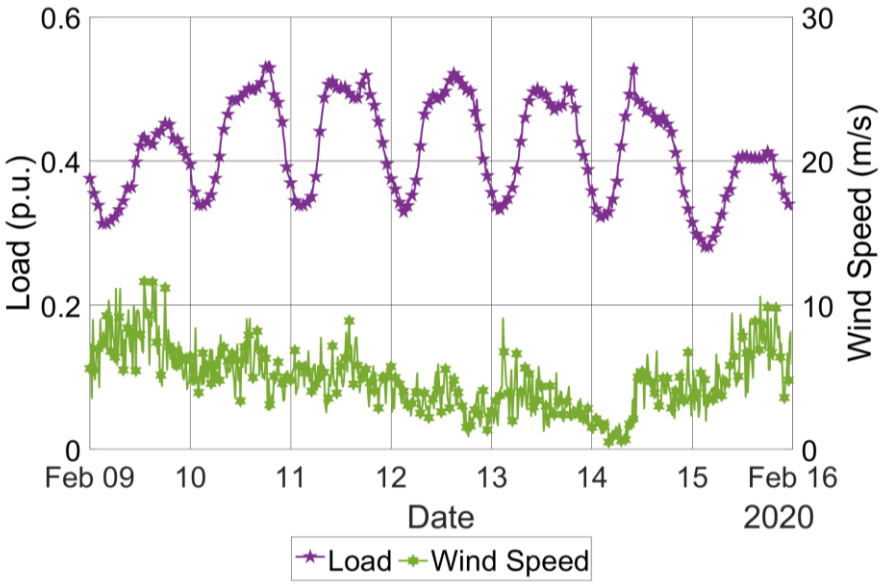

b) Load profile and wind speeds

Figure 4.5 Example of WTI measurement and prediction made by the IEEE-Annex G and proposed models on windy days for Transformer A.

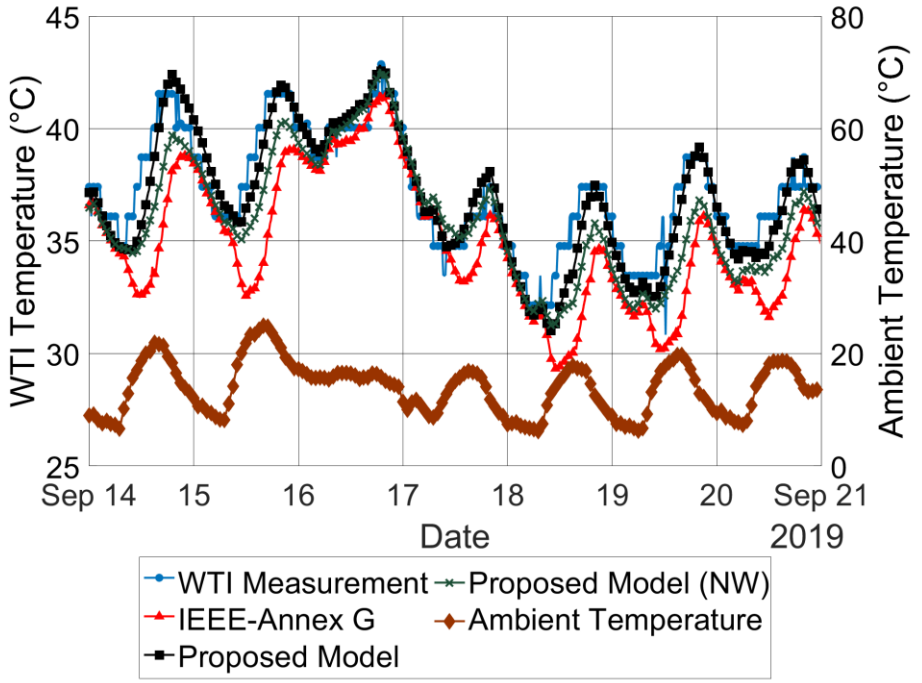

a) WTI measurement and predictions and ambient temperature

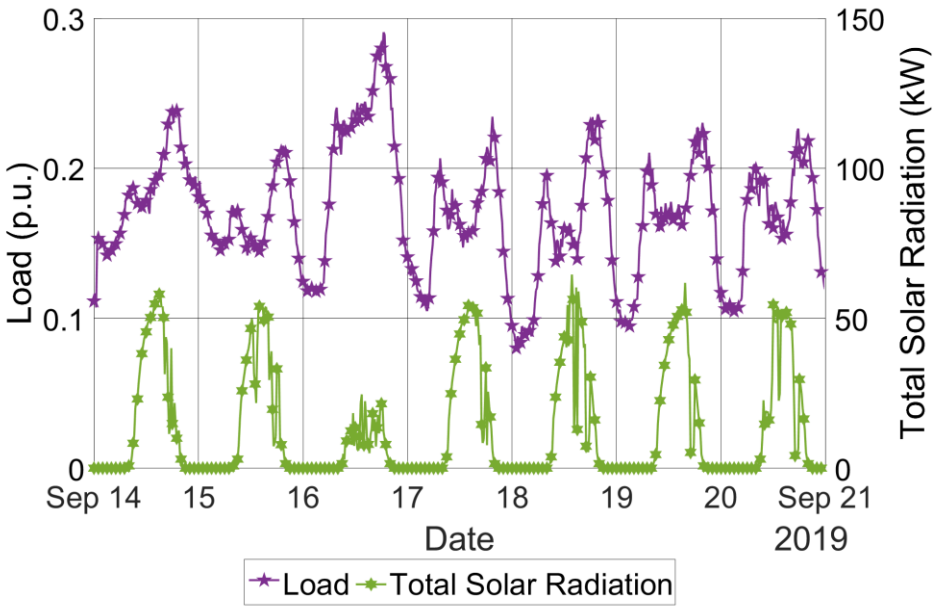

b) Load profile and solar radiation

Figure 4.6 Example of WTI measurement and prediction made by the IEEE-Annex G and proposed models on sunny days for Transformer C.

Figure 4.7 and Figure 4.8 show error duration curves of absolute errors between the measurement and predictions based on the IEEE-Annex G and proposed models over windy and sunny periods for Transformer A and C, respectively. It showed the prediction based on the IEEE-Annex G model is less accurate and always overestimated over windy periods for Transformer A. The highest error is about 9°C and the errors rise with increasing wind speed. The overall accuracy of the proposed model over windy periods is improved about 3°C for Transformer A. For sunny periods of Transformer C, the traditional model often underestimates the transformer temperature with the highest error of 11.5°C while the errors made by the proposed model are reduced by 4°C.

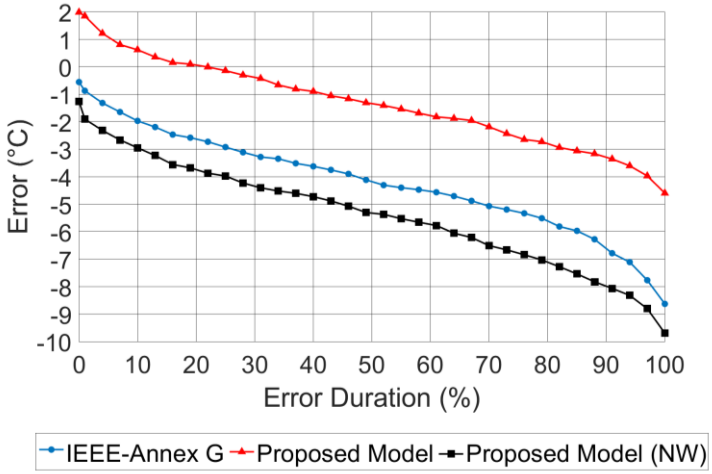

Figure 4.7 Error duration curve of errors between the measurement and prediction based on the IEEE-Annex G and proposed models over windy periods of Transformer A.

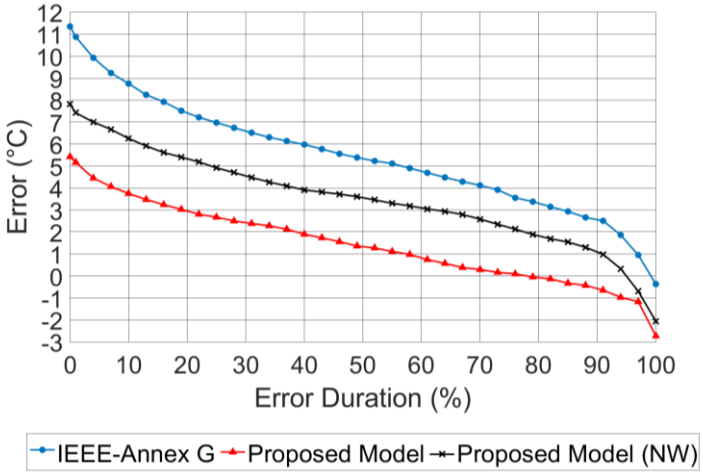

Figure 4.8 Error duration curve of errors between the measurement and prediction based on the IEEE-Annex G and proposed models over summer of Transformer C.

4.2.3 Effect of Weather Factors on Loss of Transformer Life

Loss of transformer insulation life is a useful indicator to estimate the remaining life of the solid insulation. Ageing rate of insulation life depends on the transformer hot-spot temperature. According

to the IEC guidelines [9], the nominal ageing rate for non-thermally upgraded paper is referenced to the hot-spot temperature of 98°C. The hot-spot temperature could significantly decrease on windy days. Ignoring the effects of wind could result in overestimating the loss of transformer life. To illustrate the influences of the weather on the ageing rate, the proposed model is used to determine the hot-spot temperature over different loading conditions.

It is assumed that Transformer C continuously carries a load of 1.0 p.u. of the ONAN capacity over 24 hours at daily average ambient temperature of 40°C. It is worth noting that the loading condition is a hypothetical example for the sake of simplicity. Under typical operation transmission transformers do not operate at this level for extended periods of time. The solar radiation profile is derived from a typical sunny day on summer periods of the historical measurement. The peak solar radiation is about 0.8 kW/m^2 on the horizontal surface. The hot-spot temperatures estimated by the proposed model are 99°C without solar radiation and 104.7°C with solar radiation respectively. It shows that the solar radiation could increase the hot-spot temperature by 5.7°C for Transformer C.

The hot-spot temperature and loss of life at 1.0 p.u. of the ONAN capacity and various wind speeds for Transformer A are also investigated. The aim is to demonstrate that a substantial prevailing wind could decrease the transformer temperature significantly. It is noted that the actual wind speed usually varies throughout a year and not sustained for extend periods of time. To estimate actual cumulative loss of life, the historical measurement of wind speed will be required. The results are shown in Figure 4.9. The transformer temperature and the loss of life for Transformer A is decreased by approximately 5% and 30% at wind speed of 5 m/s, and 15% and 60% at wind speed of 10 m/s, respectively. The calculation made by the IEEE-Annex G model may be a relatively conservative estimation for transformers in windy locations, e.g. wind farms and could lead to a decision to replace the transformers earlier than necessary on the loss of life criterion.

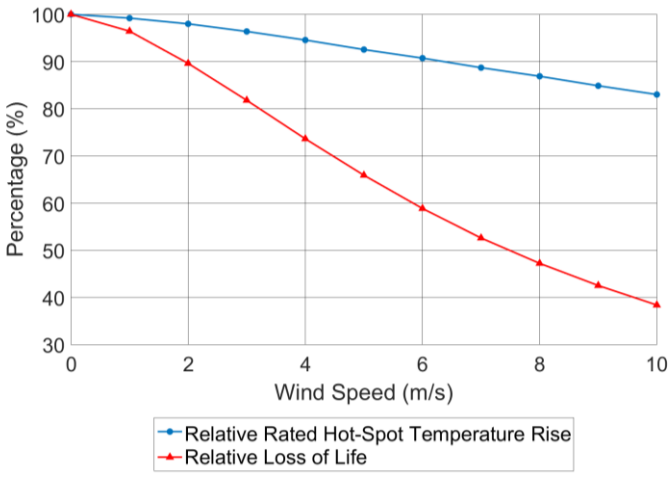

Figure 4.9 The calculated hot-spot temperature at rated and load loss of life against wind speeds based on the proposed model for Transformer A.

4.2.4 Utilisation of Weather Information from the Met Office

The feasibility of exploiting weather data from the Met office as an alternative is investigated. Not all the substations have a local substation weather station but there should be the Met office's weather station that is close to that area. The same analysis has been carried but the weather data derived from the local substation is replaced with the data derived from the Met office. As the Met office dataset is in hourly format, the data is interpolated into a 15-minute format so that the format of the weather data is the same format as the load and WTI measurements. A list of the nearest Met office weather station for each transformer is provided in Appendix B in Table B.2 .

The RMSEs between the measurement and predictions based on the Met office and local substation datasets against 6-hour average wind speed for Transformer A are provided in Figure 4.10. The thermal parameters that are derived from the datasets, D_1 and D_2, are provided in Table 4.6. The RMSEs of the thermal models for both the datasets over all periods and windy periods for Transformer A are provided in Table 4.7. A snapshot of the measurement and predictions on windy periods is provided in Figure 4.11. The error duration curve of the absolute error between the measurement and predictions are provided in Figure 4.12.

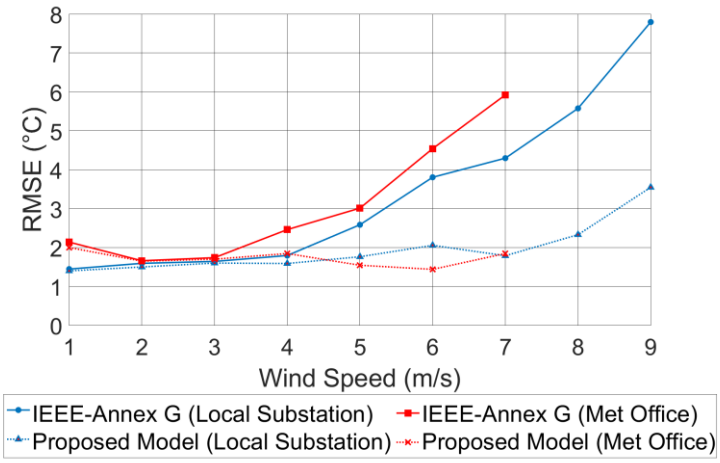

Figure 4.10 Statistical errors of the IEEE-Annex G and proposed models against 6-hour average wind speed for Transformer A.

Table 4.6 Thermal Parameters derived from the local substation and Met office station datasets for Transformer A

Dataset	Forced Convection (D_1)	Natural Convection (D_2)
Local Substation	0.45	0.85
Met Office	0.53	0.84

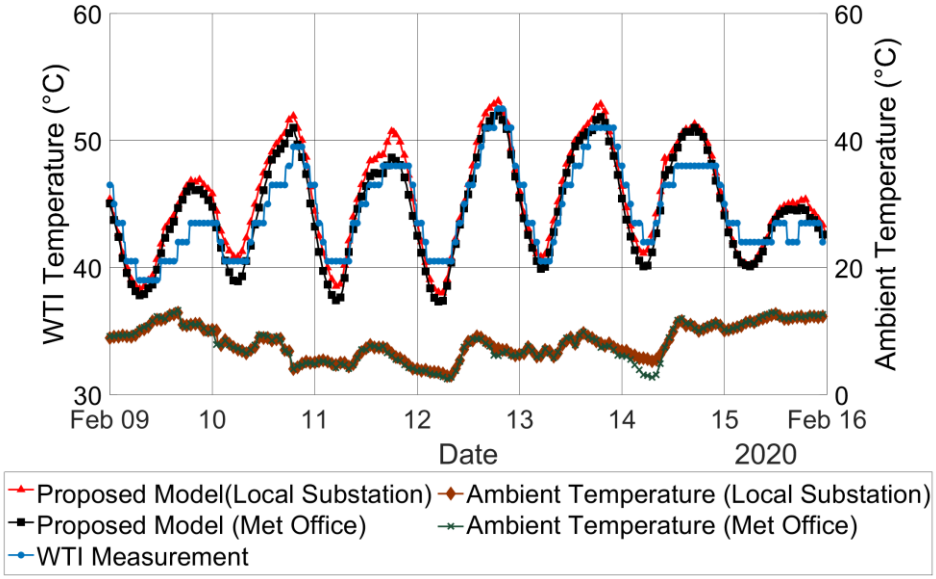

a) WTI measurement and predictions and ambient temperature

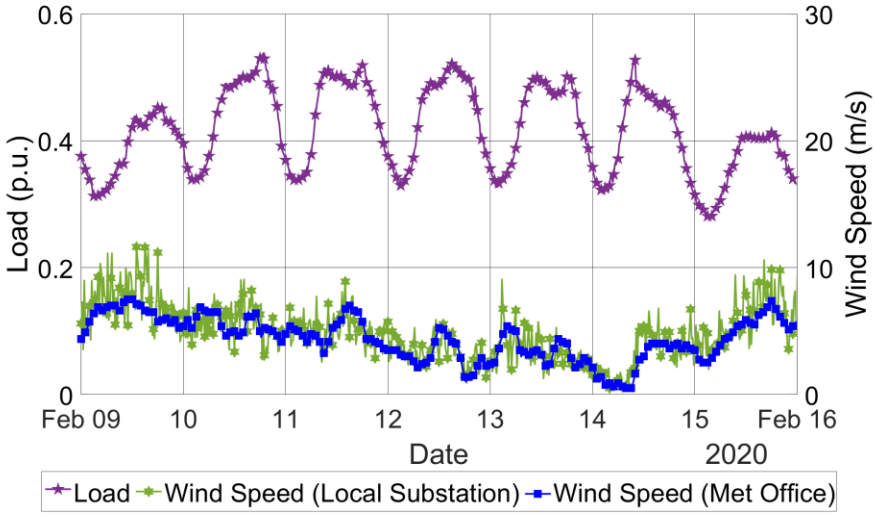

b) Load and wind speed

Figure 4.11 Example of WTI measurement and prediction based on the local substation and Met office station datasets on windy days for Transformer A.

Table 4.7 RMSE of Thermal Model for Transformer A

Model	Local Substation		Met Office	
	All Periods	Windy Periods*	All Periods	Windy Periods*
IEEE-Annex G (°C)	1.96	4.53	2.22	5.25
Proposed Model (°C)	1.77	1.99	1.91	1.55
Improvement (%)	9.5	56.1	14.0	70.5

*Windy periods are defined here as being those with 6-hour average wind speed above 6 m/s

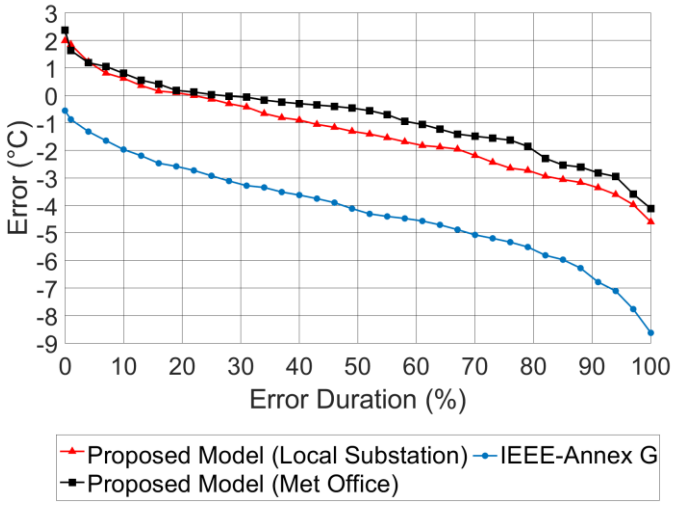

Figure 4.12 Error duration curve of errors between the measurement and prediction based on the local substation and Met office station datasets over windy periods for Transformer A.

It is shown that the results derived from the local substation and Met office datasets are comparable. The patterns of the ambient temperature and wind speed from the two datasets are relatively similar despite of spikes of wind speeds in the local substation dataset. Consequently, the Met office station dataset could be used as a substitute for the local substation dataset for Transformer A in case that the local substation dataset is not available.

The analysis has also been carried out for Transformer C that the dependency on solar radiation is identified. The RMSEs between the measurement and predictions based on the Met office and local substation datasets against 6-hour average solar radiation for Transformer C are provided in Figure 4.13. The thermal parameters that are derived from the datasets, D_1 and D_2, are provided in Table 4.8. The RMSEs of the thermal models for both the datasets over all periods and sunny periods for Transformer C are provided in Table 4.9. A snapshot of the measurement and predictions on sunny periods is provided in Figure 4.14. The error duration curve of the absolute error between the measurement and predictions are provided in Figure 4.15.

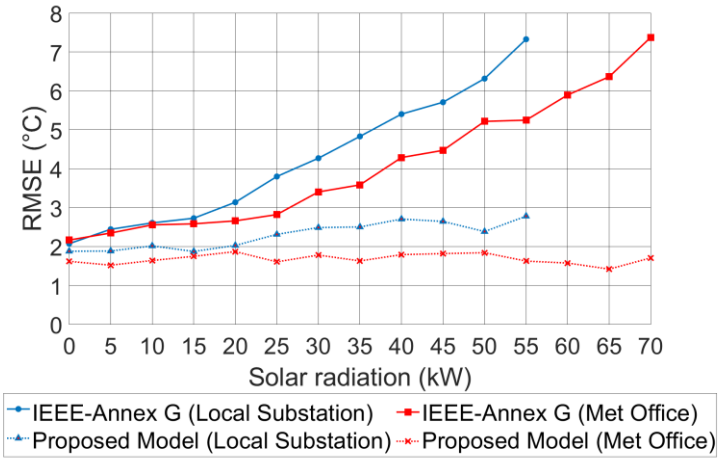

Figure 4.13 Statistical errors of the IEEE-Annex G and proposed models against 6- hour average solar radiation for Transformer C.

Table 4.8 Thermal Parameters derived from the local substation and Met office station datasets for Transformer C

Dataset	**Forced Convection (D_1)**	**Natural Convection (D_2)**
Local Substation	0.69	0.62
Met Office	0.48	0.60

Table 4.9 RMSE of Thermal Model for Transformer C

Model	**Local Substation**		**Met Office**	
	All Periods	Sunny Periods**	All Periods	Sunny Periods**
IEEE-Annex G (°C)	2.96	5.92	2.81	5.19
Proposed Model (°C)	2.01	2.21	1.65	1.86
Improvement (%)	32.1	62.7	41.3	64.2

**Sunny periods are defined here as being those with 6-hour average solar radiation above 0.4 kW/m^2

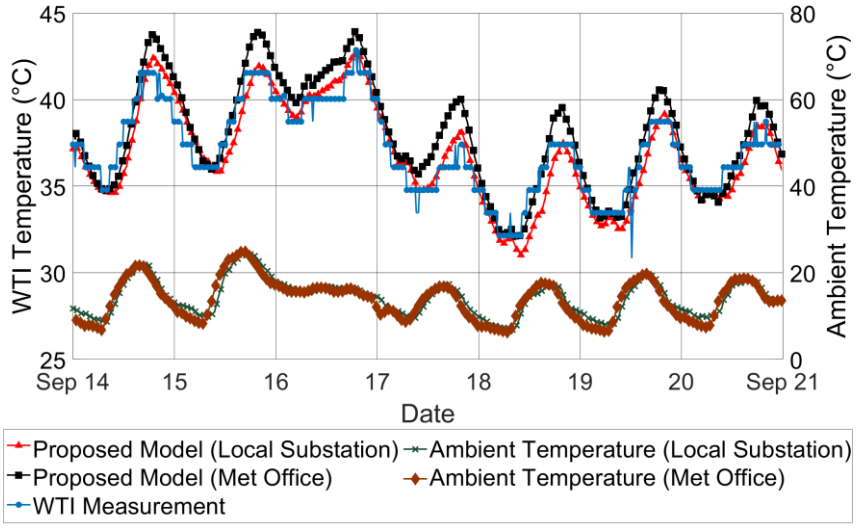

a) WTI measurement and predictions and ambient temperature

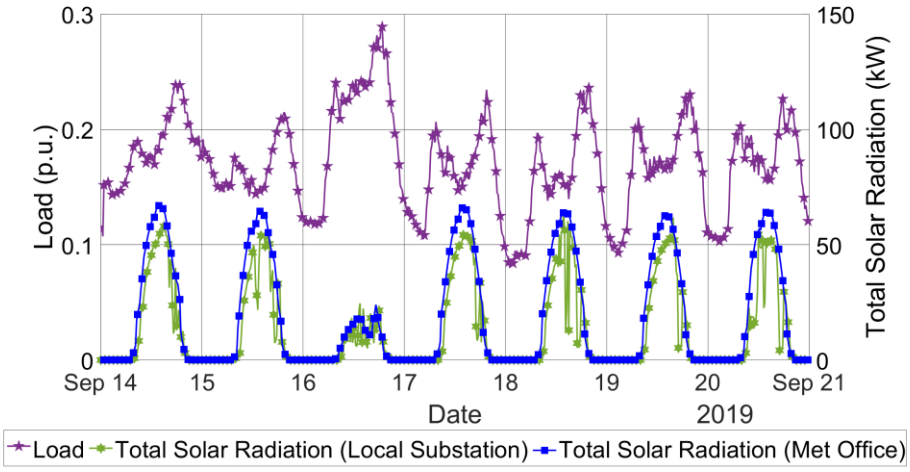

b) Load and solar radiation

Figure 4.14 Example of WTI measurement and prediction based on the local substation and Met office station datasets on sunny days for Transformer C.

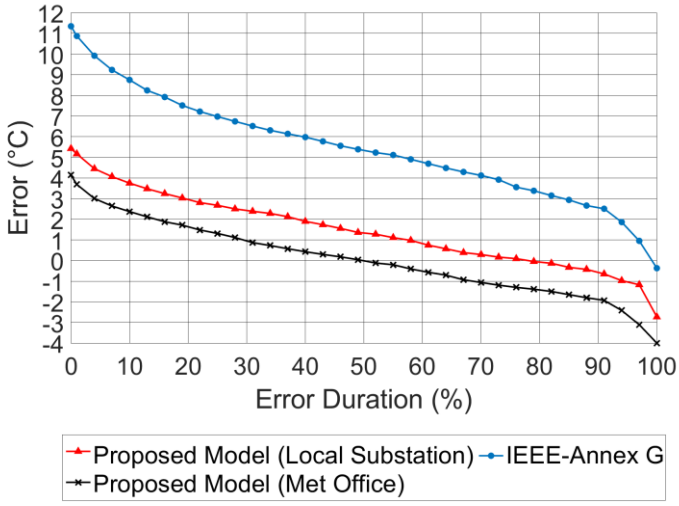

Figure 4.15 Error duration curve of errors between the measurement and prediction based on the local substation and Met office station datasets over sunny periods for Transformer C.

As the patterns of the ambient temperature and solar radiation between the local substation and Met office station datasets are relatively similar, the results based on the two datasets are relatively comparable. Therefore, the Met office station dataset could be used as a substitute for the local substation dataset for Transformer C in cases where the local substation dataset is not available.

It should be note that it is not always guarantee that the Met office dataset will be a good substitute for a local substation weather station. In case that the distance between the nearest Met office weather station and the substation is significantly high, it would be preferable to install the local substation weather station on that substation.

4.3 Summary

A top-oil thermal model that considers the thermal influence of prevailing wind and solar radiation is proposed. The thermal model is based on heat transfer theory and the thermal-electrical analogy. The prevailing wind is considered as an additional forced convection and solar radiation is treated as an additional heat source. The average heat transfer rate can be improved in windy periods resulting in transformer operating at a lower temperature than expected. Transformers subjected to solar radiation for extended periods can have a noticeable increase in the WTI temperature.

The IEEE-Annex G and proposed models are used to determine the hot-spot temperatures of two different transformers over various conditions. The results show the better agreement between the operational measurement and prediction made by the proposed model over all periods especially windy and sunny periods while the IEEE-Annex G model appears to overestimate the hot-spot temperature during windy periods and underestimate the hot-spot temperature over summer periods. The results show the prevailing wind has less effect when cooling fans are in operation. The similar results are also observed over extended periods using the Met Office weather information.

In general, environmental effects should be taken into account if attempting to compare the as-installed transformer performance with factory heat run measurements.

Chapter 5

Data Driven Thermal Models for Power Transformers

This chapter presents data driven alternative algorithms for calculating transformer thermal profiles: nonlinear autoregressive neural network with external inputs (ANN), support vector machine for regression (SVM) and multi linear regression (MLR). A summary of each algorithm is provided. Following this, a comparison of the performance between the traditional and the proposed algorithms is undertaken. Influences of weather factors, wind speed, wind direction and solar radiation, on the transformer temperature are also investigated. Abilities of the alternative thermal models to predict thermal profiles in different situations such as thermally stressful events or active cooling events are evaluated. The sensitivity of model performance to inputs is also investigated and discussed.

5.1 Introduction

As historical thermal, load and weather measurements for power transformers are increasingly available, it is of interest whether they can be leveraged to develop transformer thermal models using data driven modelling techniques. Data driven modelling allows the development transformer thermal models without considering physical principles. Thermal models could be developed using only the measured data.

As data driven modelling considers a transformer as a black box, there is no need to derive a differential equation. Weather factors can be easily added to a data driven model.

The data driven algorithms that are proposed in this thesis are as follows: nonlinear autoregressive neural network with external inputs (ANN), support vector machine for regression (SVM) and multi linear regression (MLR). These algorithms have been widely used in many applications and shown promising results [85, 86, 87].

5.2 Time Series Forecasting

This section provides a summary of the concepts behind each algorithm considered here: a nonlinear autoregressive neural network with external input (ANN), a support vector machine for regression (SVM) and a multiple linear regression (MLR) model.

5.2.1 Artificial Neural Networks (ANN)

The first algorithm investigated is a nonlinear autoregressive neural network with external input, referred to as ANN hereafter. Neural networks operate as a series of simple elements called neurons [88]. These neurons accept inputs and, using a defined transfer function, provide a certain output. Neurons are connected to each other, with most neurons passing their output data to become the input data of other neurons of the next layer. There are three main layers: an input layer, hidden layers and an output layer [88]. The input layer is a layer containing input features. The hidden layers contain a series of neurons, which could be a single layer or multiple layers. The output layer then sums up all the final information from the last hidden layers. Inputs are weighted regarding their contribution to the output data of each neuron. A bias is also associated with each neuron and the weighted inputs combined with the bias are then used to calculate the neuron output using its transfer function. A set of training data is used by the neural network to learn, adjusting the weightings between neurons, and their biases, such that when the training input data is inputted the output from the network is close to the training output data [89]. Figure 5.1 shows a basic feed-forward neural network architecture [90].

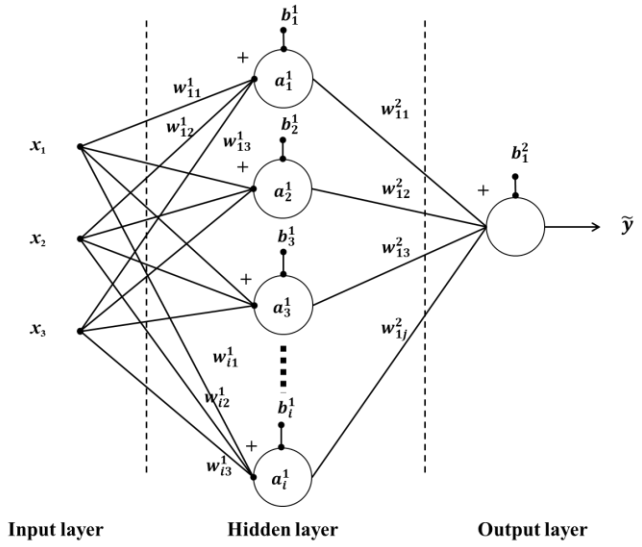

Figure 5.1 Neural network architecture [90]. x are inputs, w are weights, b are biases, a are the output from the activation function and $\tilde{y}$ are predicted outputs.

The neural network used in this report is a nonlinear autoregressive neural network with external input. Autoregressive means that predicted future value of variables is based on the known values at

earlier times. This means that inputs into the model include values of the prediction at earlier times. Nonlinearity means that the relationships between inputs and output are allowed to be nonlinear.

The following equations describe the process of a feedforward ANN. First each input is multiplied by its own weight and then they are added together with bias as a single input as given follows:

$$n^{k+1}(i) = \begin{cases} \sum_{j=1}^{N^k} w_{ij}^{k+1} a_j^k + b_i^{k+1} & \text{if } k > 0 \\ \sum_{j=1}^{N^k} w_{ij}^{k+1} x_j + b_i^{k+1} & \text{if } k = 0 \end{cases} \quad (5.1)$$

where x is an input vector, a is an output of the activation function, w is weight, b is bias, k is the index of the layer itself, i is the index of the neurons, j is the index of the input features to the activation function and N is the total number of the input features for each layer.

The outputs of each layer are passed to the next layer as input data until the output layer. The sum of squared errors (SSE) between the prediction and measurement is defined as follows:

$$SSE = \sum_{q=1}^{Q} (y_q - \tilde{y}_q)^2 = \sum_{q=1}^{Q} E_q^2 \quad (5.2)$$

where y_q are the measured outputs, $\tilde{y}_q$ are the predicted outputs, E_q^2 are the squared error between the measured and predicted outputs, q is the index of the points within dataset and Q is the total number of datapoints.

Weights and bias are adjusted to minimise the sum of squared errors. The numbers of hidden layers and neurons are pre-defined parameters by a user. There is not a set of optimal values that can fit all problems. If the number of the hidden layers and neurons is sufficiently large, it will result in the network memorising individual inputs and outputs rather than learning a pattern from the data. This is known as overfitting [89]. The key is to determine the number of hidden layers and neurons that will provide the lowest error when the model is tested against the testing data.

The network was trained in open loop form, which means that only the next time step of the output is predicted. A labelled schematic of the open loop network is provided in Figure 5.2. In order to predict multiple time steps ahead a closed loop form of the network, shown in Figure 5.3, is required. In a closed loop network predicted outputs are fed back into the network as inputs.

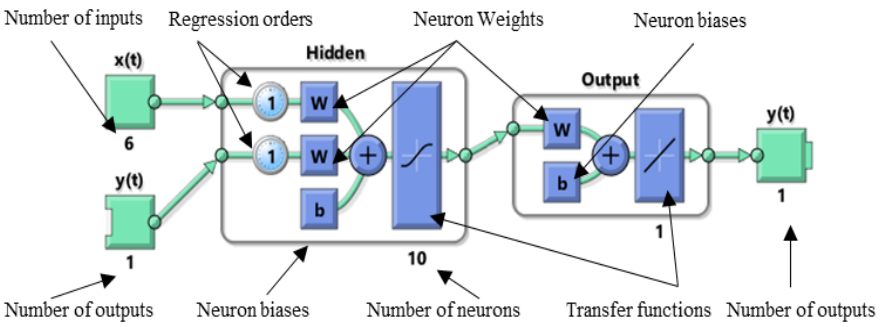

Figure 5.2 Labelled schematic of open loop form of the nonlinear autoregressive neural network used in this thesis. The number of the neurons are increased until the increase makes no significant difference to the model performance. The highest number of the neurons was 10 [91].

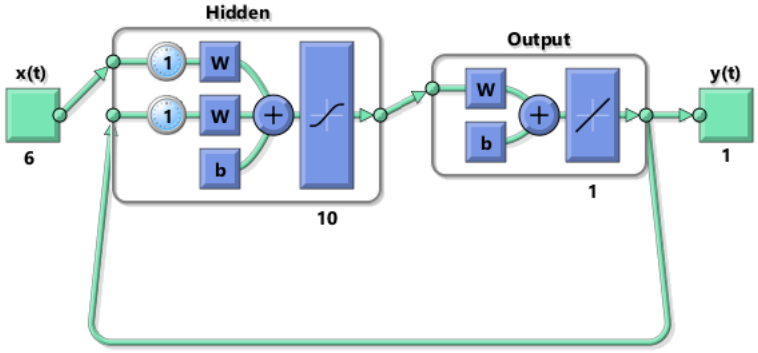

Figure 5.3 Schematic of the nonlinear autoregressive neural network in closed loop form. All components have the same meaning as those in Figure 5.2 [91].

The neural network was implemented using prebuilt functions in MATLAB. The weightings and bias are solved using Levenberg-Marquardt algorithm [92]. The Levenberg-Marquardt algorithm is a method for solving nonlinear least square problems so that the errors between measurement and prediction are minimised. An important point to note is that the initial values for weights and biases are randomly assigned, and as such the trained network, and the outputs from it, are not exactly reproducible.

5.2.2 Support Vector Machine for Regression (SVM)

In addition to the ANN algorithm, support vector machine for regression is also proposed as an alternative dynamic thermal modeling technique. The concept of SVM is to try to create a linear function between inputs and outputs by minimizing the loss function and ignoring errors below a specified margin, generally referred to as the error margin (ε) [93]. However, most systems have a non-linear relationship between inputs and outputs within the original space. In order to create a linear relationship between inputs and outputs, the data are mapped into a higher dimensional space using a kernel function. The kernel function is a technique for measuring similarity between two sets of data [94].

The kernel method is selected for SVM as it has a fast computational time. The algorithm is referred to as "support vector machine" because some input vectors in the training dataset are used as reference, or support, vectors in the kernel function to calculate the output prediction. A basic architecture of SVM regression is shown in Figure 5.4 [95].

The predicted output based on the SVM for regression is given as follows:

$$\tilde{y} = \sum_{m=1}^{S} \lambda_m k(\boldsymbol{x}, \tilde{\boldsymbol{x}}_m) + b \tag{5.3}$$

where $\tilde{\boldsymbol{x}}_m$ are the support vectors which are subsets of the input data in the training dataset, m is the index of the support vectors, S is the total number of the support vectors, λ_m are weights for each support vector and $k(\boldsymbol{x}, \tilde{\boldsymbol{x}}_m)$ is a kernel function. Similarities between an input vector ($\boldsymbol{x}$) and support vectors $\tilde{\boldsymbol{x}}_m$ are computed using a kernel function and then weighted and added with bias to form the predicted output.

There are many popular kernel functions such as linear, polynomial, Gaussian and hyperbolic tangent functions [93]. The Gaussian function has been widely used and shown to outperform the others in various applications [95]. Explicitly the kernel function is:

$$k(\boldsymbol{x}, \tilde{\boldsymbol{x}}_m) = \exp\left(\frac{-\|\boldsymbol{x} - \tilde{\boldsymbol{x}}_m\|^2}{\gamma}\right) \tag{5.4}$$

where γ is the kernel scale and $\|\ \ \|$ is Euclidean distance. The output of the kernel function is equal to one if an input vector is in the same position as the support vectors or decreases toward zero if an input vector is far away from the support vectors.

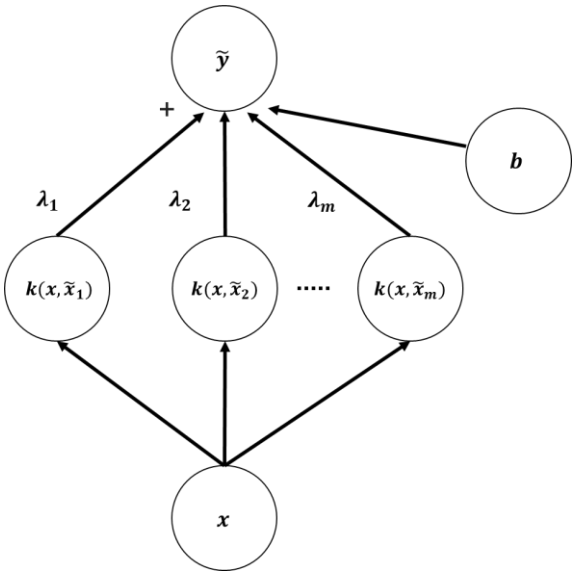

Figure 5.4 Architecture of SVM regression. The figure is adapted from [95]. x are inputs, λ are weights, b are biases, $k(\boldsymbol{x}, \tilde{\boldsymbol{x}}_m)$ is a kernel function and $\tilde{y}$ are predicted outputs.

The algorithm determines a set of support vectors from the training dataset, weight ($\lambda(m)$) and bias (b) by minimizing the following nonlinear least square problem:

$$\text{minimise} \qquad \frac{SSE}{2} + C\sum_{q=1}^{Q} E_{\varepsilon}\left(y_q - \tilde{y}_q\right)$$

$$\text{subject to } E_{\varepsilon}(z) = \begin{cases} |z| - \varepsilon & if\ |z| \geq \varepsilon \\ 0 & \text{otherwise} \end{cases}. \tag{5.5}$$

where C is the penalty factor and ε is the error margin.

The type of kernel function, kernel scale (γ), penalty factor and the error margin are needed to be specified by the user in order to optimize the accuracy of the model. These parameters are used to optimise the model errors mainly preventing overfitting problems. Higher value of the penalty factor can cause overfitting problem to the training dataset because it emphasises the model error of the training dataset and vice versa according to (5.5). Larger values of the kernel scale lessen the magnitude of the difference between 2 sets of data. As a single set of data can represent wider areas, this reduces the number of support vectors required to form a model [86]. Larger values of the error margin allow more errors not to be considered in the loss function, and the fewer number of support vectors are likely to be required to form a model which could underfit data [86].

The SVM was implemented using prebuilt functions in MATLAB. The Gaussian function is selected as a kernel function. The kernel scale, penalty factor and error margin are optimised for each model, see section 5.4 for detailed discussion.

5.2.3 Multiple Linear Regression (MLR)

A multiple linear regression model assumes that there are linear relationships between a dependent variable and functions of one or multiple independent variables. A general multiple linear regression model is [96]:

$$\tilde{y} = \beta_0 + \sum_{j=1}^{N} \beta_j f_j(x_j) + \epsilon \tag{5.6}$$

where $f_j(x_j)$ is a function of input feature of j^{th} index, ϵ is a random noise, β_j are coefficients and β_0 is a constant term that does not relate to any independent variables. The noise term should be random errors that have normal distributions with mean zero and constant standard deviation and independent correlation with the responses and predictors. The coefficients are adjusted to minimise the sum of square errors between the observation and prediction.

In this analysis, the transformer WTI temperature is assumed to have linear relationships with the square of load, a cosine function of angle differences between radiator and wind direction and linear functions of the other independent variables for simplicity as follows:

$$\theta_{\mathrm{WTI}} = \beta_0 + \beta_1 K^2 + \beta_2 \theta_{\mathrm{WTI,P}} + \beta_3 \theta_{\mathrm{A}} + \beta_4 u \cos(\emptyset_{\mathrm{R}} - \emptyset_{\mathrm{W}}) + \beta_5 q_{\mathrm{dir}} \quad (5.7)$$

where θ_{WTI} is the WTI temperature at the next time step [°C], $\theta_{\mathrm{WTI,P}}$ is the WTI temperature at the present time step [°C], K is the load factor at the present time step [p.u.], θ_{A} is the ambient temperature at the present time step [°C], u is the wind speed at the present time step [m/s], $\emptyset_{\mathrm{R}}$is direction of the radiator [°], $\emptyset_{\mathrm{W}}$ is wind direction [°] and q_{dir} is the solar radiation on a horizontal surface at the present time step [kW/m^2].

5.3 Operational Measurements

5.3.1 Sources of Weather information

There are 2 different sources of weather information: local substation weather stations and the Met office weather stations [73]. The weather datasets that are derived from the local substation weather station and the Met office are referred to as Local substation dataset and Met Office station dataset hereafter, respectively. The sampling intervals of the Local substation and the Met Office station datasets are every 15 minutes and 1 hour, respectively. The amount of Local substation dataset is limited by the commencement date of the local substation weather station, which is since mid-2019 and the load and WTI measurements provided by NGET which are available until mid-2020. The amount of the Met Office station dataset is restricted by the availability of the load and WTI measurements which are usually only stored by NGET for the last 7 years. There are 3 transformers in the local substation weather station, i.e. Transformer A, B and C which are investigated in Chapter 4. The Met Office station is comprised of the data of Transformer A, B and C and eight additional transformers. The aim of the Met Office station dataset is to investigate whether this approach can be generally applied to other transformers. Overall transformer specifications are provided in Appendix B in Table B.1.

5.3.2 Statistical Quantities of Inputs and Output

The data are comprised of seven measurements: load, tap position if it is available, WTI measurement, ambient temperature, wind speed, wind direction and solar radiation. All of them are used as inputs including the WTI measurement at the present time step. The WTI measurement at the next time step is an output. Examples of measurement for Local substation and Met Office station datasets

are shown in Figure 5.5 and Figure 5.6, respectively. The means and standard deviations of the measurements for each transformer are provided in Table 5.1 for Local substation dataset and Table 5.2 for Met Office station dataset.

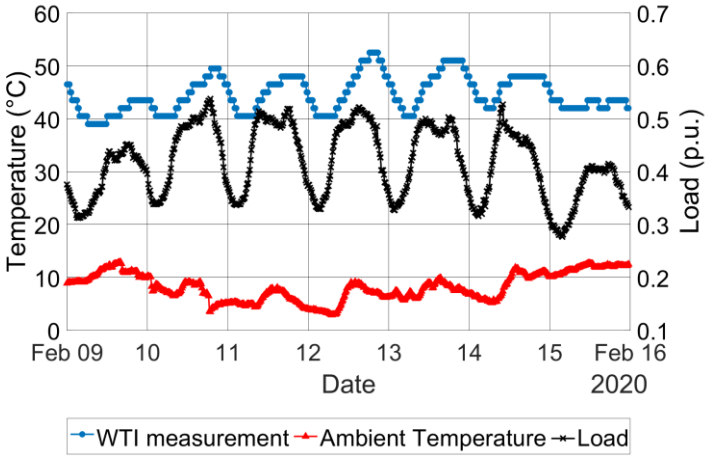

(a) Load, WTI measurement and ambient temperature

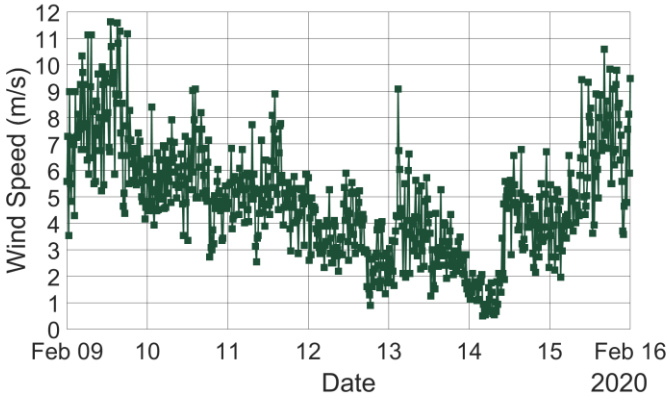

(b) Wind speed

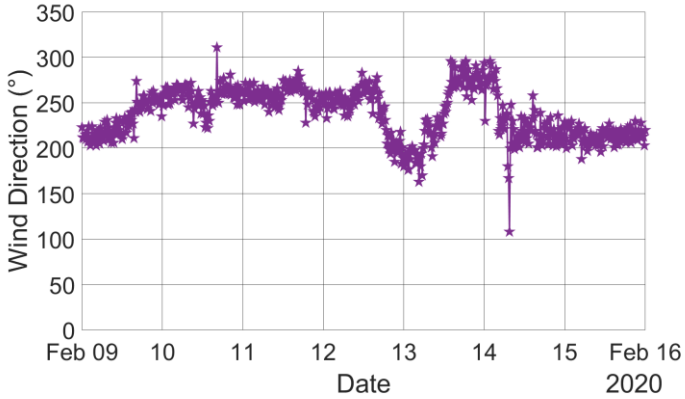

(c) Wind direction (0° = North, 90° = East, 180° = South and 270° = West)

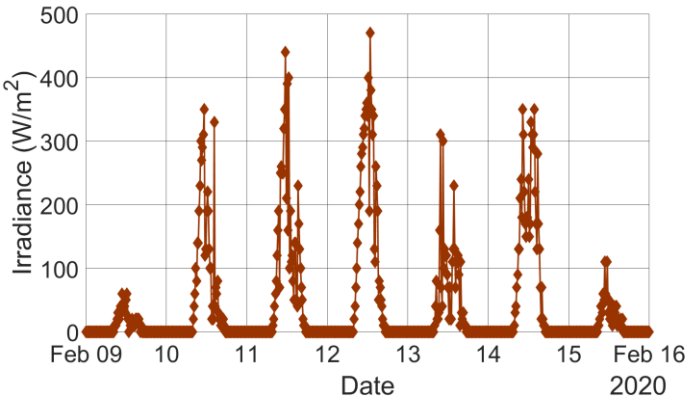

(d) Solar radiation

Figure 5.5 Example of Load, WTI measurement, wind speed, wind direction and solar radiation data for the local substation weather station.

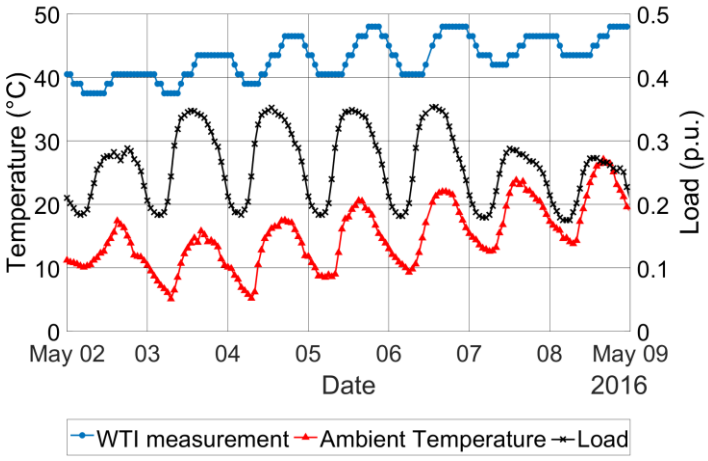

(a) Load, WTI measurement and ambient temperature

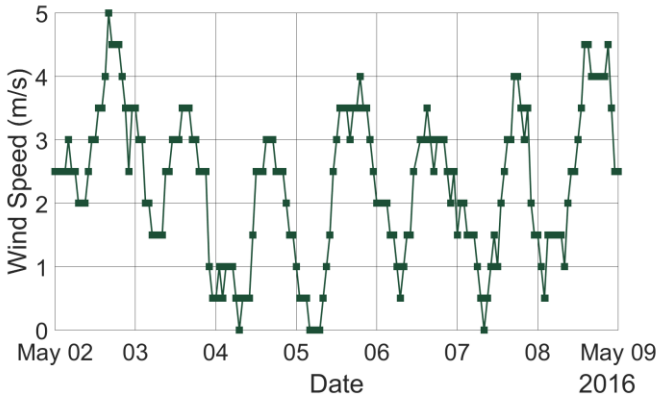

(b) Wind speed

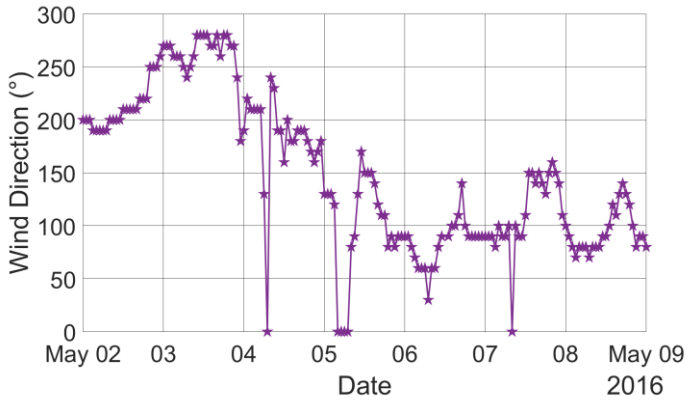

(c) Wind direction (0° = North, 90° = East, 180° = South and 270° = West)

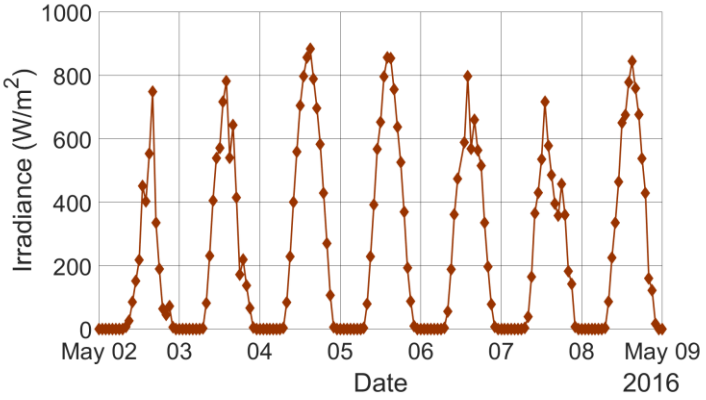

(d) Solar radiation

Figure 5.6 Example of Load, WTI measurement, wind speed, wind direction and solar radiation data for the Met office.

Table 5.1 Statistical quantities of measurements for Local substation dataset.

Transformer	**WTI (°C)**	**Load (MVA)**	**Tap**	**Ambient (°C)**	**Wind Speed (m/s)**	**Wind* Direction (°)**	**Solar (W/m^2)**
A	45.5±5.3	66±15	9±1	11.1±5.1	2.8±1.5	192±89	190±190
B	32.7±6.6	70.5±17.1	10±1	12±5.6	2.8±1.5	192±90	200±200
C	31.5±3.6	46.2±14.5	11±1	8.7±4.5	2.3±1.3	192±79	170±170

Mean±Standard deviation.

*Wind direction (0° = North, 90° = East, 180° = South and 270° = West)

Table 5.2 Statistical quantities of measurements for Met Office station dataset.

Transformer	WTI (°C)	Load (MVA)	Tap	Ambient (°C)	Wind Speed (m/s)	Wind* Direction (°)	Solar (W/m^2)
A	42.3±5.2	53.2±14.3	10±1	11.4±5.7	2.3±1.3	197±91	220±220
B	33.8±7.2	71±21.7	10±1	12.3±5.8	2.3±1.2	196±93	250±240
C	36.3±5.7	56.3±24.3	10±1	10.2±6	4.1±2.3	199±96	220±220
D	53.3±6.7	83.4±19.9	13±1	11.5±5.7	2.3±1.3	199±90	230±230
E	46.5±7.8	94.2±24.2	N/A	10±5.8	4.2±2.3	201±94	220±220
F	41.5±5.7	91.5±24	N/A	11±5.9	4.9±2.4	185±94	240±230
G	41.7±8.4	243±100	N/A	12±5.8	2.3±1.3	197±92	240±240
H	44±8.4	266±98	N/A	11.9±5.7	2.3±1.3	200±90	230±230
I	41.3±8.5	282±94	N/A	11.5±5.7	2.4±1.3	195±91	230±220
J	39±8.6	253±100	N/A	12.3±5.9	2.2±1.2	199±91	240±240
K	46.9±9.8	292±101	N/A	9.8±5.5	4.4±2.5	208±86	210±210

Mean±Standard deviation.

Wind direction* (0° = North, 90° = East, 180° = South and 270° = West)

5.3.3 Training and Testing Datasets

The provided datasets for each transformer are equally divided into two datasets, training (50% of the total data) and testing (50% of the total data). It should be noted that the cross-validation dataset is subset of the training dataset. The training dataset is used to develop the thermal model and the testing dataset is treated as unseen data and used to evaluate the accuracy of the model. Table 5.3 and Table 5.4 provide periods of the measurement data used as training and testing datasets for Local substation and Met office datasets.

Table 5.3 Periods of Training and Testing Datasets for Local substation dataset.

Transformer	Training Dataset	Testing Dataset
A	01/07/2019 – 17/12/2019	18/12/2019 – 30/04/2020
B	01/07/2019 – 29/11/2019	30/11/2019 – 30/04/2020
C	01/09/2019 – 17/12/2019	22/01/2020 – 30/04/2020

Table 5.4 Periods of Training and Testing Datasets for Met Office station dataset.

Transformer	Training Dataset	Testing Dataset
A	01/2013 – 10/2015	10/2015 – 06/2018
B	01/2015 – 10/2016	10/2016 – 06/2018
C	01/2013 – 10/2015	10/2015 – 06/2018
D	01/2013 – 10/2015	10/2015 – 06/2018
E	01/2013 – 10/2015	10/2015 – 01/2018
F	01/2013 – 04/2016	04/2016 – 06/2019
G	01/2013 – 04/2016	04/2016 – 06/2019
H	01/2013 – 04/2016	04/2016 – 06/2019
I	01/2013 – 10/2014	10/2014 – 06/2016
J	01/2013 – 04/2016	04/2016 – 06/2019
K	01/2013 – 04/2016	04/2016 – 06/2019

5.3.4 Data Preprocessing

Although the presence of load dependency of the WTI measurement has been checked by the algorithm proposed in Section 3.3, many of datasets still contained spurious data points including periods of constant load, periods of constant WTI temperatures and in some cases small intervals of missing data. This erroneous data, despite comprising a relatively small subset of the full dataset, was found to significantly reduce the performance of learning algorithms as it contaminated the training data. To resolve this the following post processing was performed to remove the following data from all sets:

- **A.** Periods of where WTI temperatures were unfeasibly high relative to the load (greater than 100°C)
- **B.** Periods of where WTI temperatures registered 0°C.
- **C.** Periods of where the load were the load reached zero. In these cases the load was typically recording sensible values and then returning zero for a single data point.
- **D.** Periods of where the load changed by more than 200 MVA in an hour.
- **E.** Periods of where the WTI temperature changed by more than 50°C in an hour.

In order to generate a continuous dataset for training the remaining periods of reliable data were spliced together assuming there was an hour gap, which is time interval of the data, between them. This does introduce spurious discontinuities in load and WTI data at these points. However, given the relatively short time constant of the transformer in comparison with the time periods of the whole dataset, and the fact that such points are discounted from “Thermally Stressful” events, which will be discussed later, it is unlikely to impact the findings of this work.

Furthermore, it is necessary to normalise the input data before using them to develop the thermal model. Scaling the data in the range between 0 and 1 avoid one or more independent variables which have larger numeric values dominating other variables with smaller values. In this work, the data are scaled as follows:

$$\hat{x}_{qj} = \frac{x_{qj} - \min(\boldsymbol{x_j})}{\max(\boldsymbol{x_j}) - \min(\boldsymbol{x_j})} \tag{5.8}$$

where x_{qj} is the q^{th} predictor of j^{th} input feature, $\hat{x}_{qj}$ is a normalised value of x_{qj} and $\boldsymbol{x_j}$ is all of j^{th} input feature. The data normalisation was applied to the input data into the alternatives introduced in this chapter.

5.4 Hyperparameter Optimisation

Hyperparameter optimisation is a method for tuning learning parameters. Training datasets, which in this work are half of the total dataset unless stated otherwise, are divided equally into five sections in this work. A model is trained with four sections which means 80% of the training dataset is used for training, or equivalently 40% of the total dataset. The remaining section of the training dataset is referred to as a cross-validation dataset, which is used to test the model for the purpose of the hyperparameter optimization. Each section is swapped for testing in turn. This means that there will be five trained models in total that use the same set of the hyperparameters. A set of optimized learning parameters that provides a minimum of the sum square errors against the cross-validation data for each trained model, is finally selected for the trained model.

5.4.1 Number of Hidden layers and Neurons

The number of the neurons are increased until no significant difference to the model performance is observed based on the cross-validation technique. The number of the neurons for each model varies with transformers, see Table 5.8 and Table 5.9. The highest number of the neurons was ten. This value was found to avoid overfitting and allow reasonably fast training of the network.

Furthermore, it is of interest whether the model with multi hidden layers could improve the performance. The models are trained with 3 different configurations as follows: 1) models based on single hidden layer, 2) models based on double hidden layers and 3) models based on triple hidden layers. For each hidden layer, the number of the neurons are between 1 and 10 and that means there are 10 models, 100 models and 1000 models for single, double and triple hidden layer configurations, respectively. The models with the lowest errors among the same configuration are selected. The performance of the selected models for each configuration is provided in Table 5.5 and Table 5.6 for Local substation and Met Office station datasets, respectively. It shows that by increasing the number of the hidden layers does not significantly improve the performance. Therefore, the model with a

single hidden layer was found to work effectively and have relatively low computational time for training the network about five minutes instead of several hours for multiple hidden layers.

Table 5.5 RMSE predicted by the models with single, double and triple hidden layer configurations for Local substation dataset.

Transformer ID	RMSE (°C)		
	1 Hidden Layer	2 Hidden Layers	3 Hidden Layers
A	1.2	1.4	1.3
B	1.2	1.3	1.1
C	1.4	1.4	1.6
All Transformers	1.3	1.4	1.3

Table 5.6 RMSE predicted by the models with single, double and triple hidden layer configurations using Met Office station dataset.

Transformer ID	RMSE (°C)		
	1 Hidden Layer	2 Hidden Layers	3 Hidden Layers
A	1.7	1.6	1.6
B	1.2	1.2	1.3
C	1.8	1.7	1.7
D	2.2	2.2	2.2
E	1.6	1.6	1.6
F	1.4	1.5	1.3
G	1.2	1.4	1.2
H	1.4	1.4	1.3
I	1.2	1.2	1.1
J	1.2	1.4	1.2
K	1.4	1.4	1.4
All Transformers	1.5	1.6	1.5

5.4.2 Hyperparameters of Support Vector Machine

There are three hyperparameters tuned to optimise the model accuracy for the SVM algorithm, i.e. the error margin (ε), kernel scale (γ) and the penalty factor (C). The restrictions of the hyperparameters are provided in Table 5.7. As the number of combinations of the hyperparameter is enormous, it requires relatively high computational resources to optimise the hyperparameter using the grid search, which sweeps each parameter from the lower to the upper limits. Instead, in this work, the Bayesian optimisation method is used to solve the hyperparameter optimisation [97]. The Bayesian method is usually used to determine global optimisation for black-box functions and functions that require high computational time to be evaluated [98]. It is based on two processes; a Gaussian process model which is a probabilistic regression model and an acquisition function which is a probability function used for selecting a next optimal combination [99]. Initially, several sets of the hyperparameters are evaluated to model the cost function using the Gaussian process model. Following this, the next candidate set of the hyperparameters is selected according to the acquisition function. The hyperparameters of the SVM algorithm are provided in Table 5.8 and Table 5.9.

Table 5.7 Restrictions of Hyperparameters

Algorithm	Parameter	Lower	Upper
SVM	Error margin (ε)	$10^{-3}\sigma(y_q)$	$10^{3}\sigma(y_q)$
	Kernel scale (γ)	10^{-3}	10^{3}
	Penalty factor (C)	10^{-3}	10^{3}

$\sigma(y_q)$ = Standard deviation of y_q

Table 5.8 Optimised Hyperparameters for Local Substation Dataset.

Transformer	ANN	SVM		
	Neurons	Error margin (C)	Kernel scale (γ)	Penalty factor (ε)
A	10	433.9	1.719	0.261
B	9	185.2	0.333	0.164
C	5	6.1	0.996	0.183

Table 5.9 Optimised Hyperparameters for Met Office Station Dataset.

Transformer	ANN	SVM		
	Neurons	Error margin (C)	Kernel scale (γ)	Penalty factor (ε)
A	9	207.5	17.18	0.8008
B	8	339.6	5.722	0.1264
C	10	16.9	1.599	0.0087
D	7	717.9	84.415	0.1182
E	8	26.5	0.731	0.1218
F	10	966.4	185.203	0.0159
G	7	22.2	1.271	0.008
H	9	891.3	1.91	0.0167
I	7	138.5	1.063	0.13
J	10	158	0.367	0.0083
K	7	324.6	4.673	0.0237

The variation in the hyperparameters of the SVM model is large even within the same transformer family. However, the accuracy is not compromised by the variation. It is unlikely that there is a universal combination of the hyperparameters that is suitable for any model, and the hyperparameters should therefore be optimized for each model. As a check, the optimized hyperparameters were swapped among the models to investigate how well they can be used for the other transformers. It appears that most of optimal combinations can be used for the other transformer and still yield reasonable accuracy, but a few combinations result in inaccurate models when transformers of a different family were considered. Furthermore, the trained models of the ANN and SVM algorithms for Transformer G, H and I, which are in the same family, are used to predict the temperature for the other transformer in the same family, see Chapter 6 for a further investigation. The performance is mostly similar. As the optimization algorithm usually provide local optimums, it is likely there might be different optimal combinations that provide similar performance.

5.5 Accuracy of WTI Temperature Prediction of Algorithms

The thermal models are developed using 5 different algorithms: IEEE-Annex G model, the transformer thermal model proposed in Chapter 4 referred to as TNM hereafter, ANN, SVM and MLR. The models are evaluated using the testing datasets. Examples of the measurement and prediction made by the algorithms and the errors between them for Transformer A are shown in Figure 5.7. As the measured WTI data are discretely recorded while the values predicted are continuous, there are

sometimes rapid and small rises in the errors between the measurement and prediction when the measurement changes from a discrete value to another. The root mean squared errors (RMSE) and error duration curves of absolute errors between the measurement and prediction made by the algorithms over the testing datasets for the 3 transformers are used to assess the model performance, see Table 5.10 and Figure 5.8. As the TNM algorithm is developed for transformers that operate in an ONAN state only, it is not applicable for Transformer B which is in an OFAF state. It appears that the ANN and MLR algorithms clearly outperform both IEEE-Annex G model and TNM, while the SVM algorithm surpass IEEE-Annex G, but it is not as accurate as the TNM algorithm.

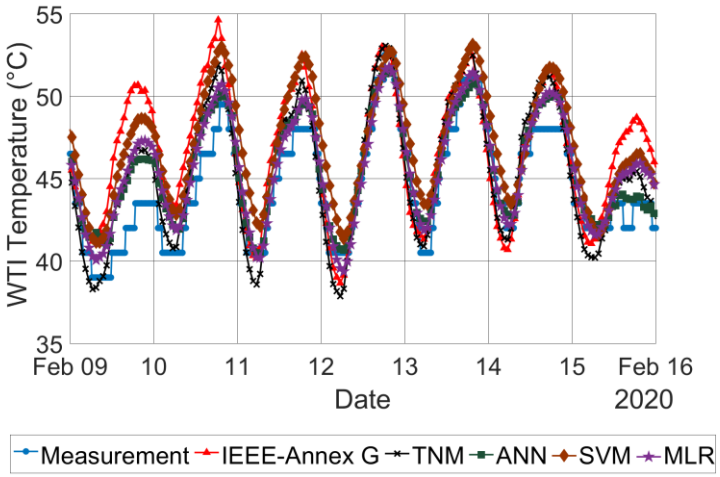

(a) Measurement and prediction

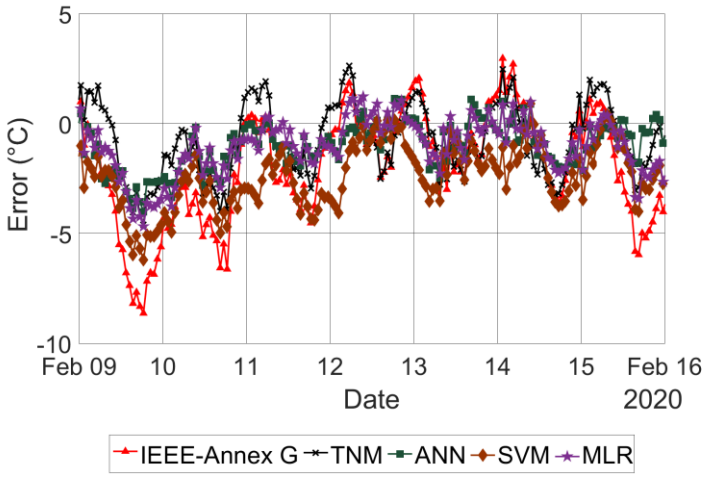

(b) Errors between the measurement and prediction

Figure 5.7 Examples of the measurement and prediction made by the algorithms for Transformer A: (a) measurement and prediction and (b) errors between the measurement and prediction.

Table 5.10 RMSEs between Measurements and Predictions made by the algorithms for each Transformer in Local substation dataset.

Transformer ID	RMSE (°C)				
	IEEE Annex G	TNM	ANN	SVM	MLR
A	2.0	1.8	1.2	2.2	1.2
B	2.1	N/A	1.2	1.9	1.4
C	3.0	2.0	1.4	1.7	1.6
All Transformers	2.3	1.9	1.3	2.0	1.4

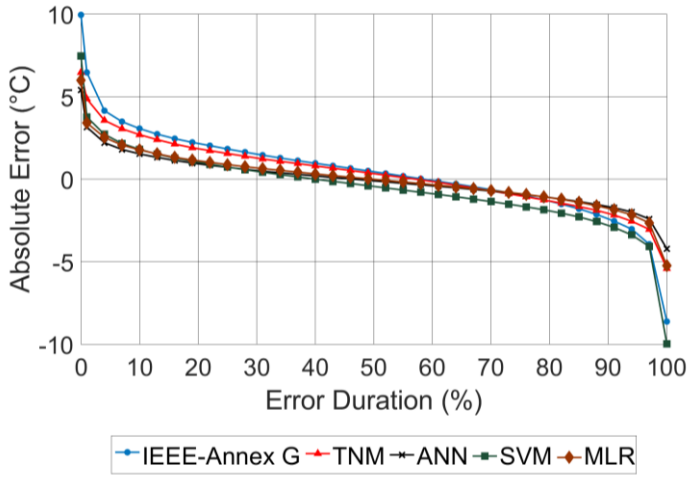

Figure 5.8 Error duration curves of errors produced by the algorithms for Local substation dataset of the three transformers.

Furthermore, the thermal models for the transformers in Met Office station dataset are developed using the same alternative algorithms to investigate whether they can be generally reproduced to other transformers. As there is not a local substation weather station in the substation of the transformers in Met Office station dataset, the weather information is derived from the nearest Met Office weather station. The number of transformers analysed in the Met Office station dataset are 11 transformers while there are only three transformers that have the weather data from the local substation. This increases confidence that they can be applied to any transformers if the algorithms work effectively and provide promising results for both Local substation and Met Office datasets.

Examples of the measurement and prediction made by the algorithms and the errors between them for Met Office station dataset are shown in Figure 5.9. It can be seen in Figure 5.9b that the errors made by the algorithms oscillated, especially in IEEE-Annex G and TNM. This implies that there is still an issue of the algorithms to capture complexity of changes in the thermal oil time constant due to temperature. According to the RMSEs for all the transformers, the ANN algorithm outperforms all other algorithms by a small margin. The overall RMSEs for the ANN, SVM and MLR algorithms

are 1.5°C, 1.6°C and 1.6°C, respectively, see Table 5.11. The error duration curves of absolute errors produced by the algorithms across all the transformers are shown in Figure 5.10.

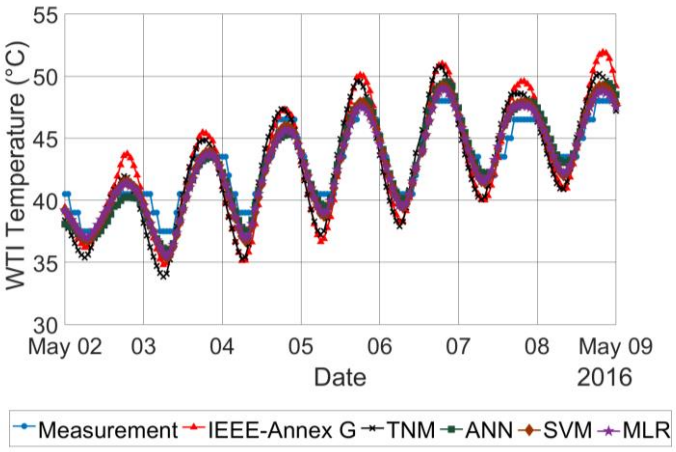

(a) Measurement and prediction

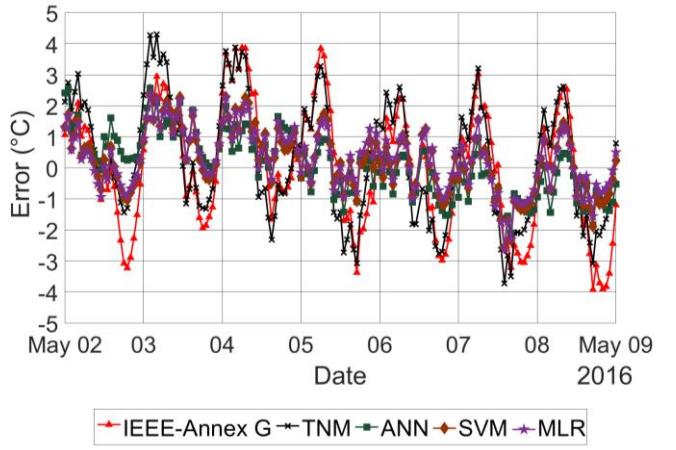

(b) Errors between measurement and prediction

Figure 5.9 Examples of the measurement and prediction made by the algorithms: (a) measurement and prediction and (b) errors between the measurement and prediction.

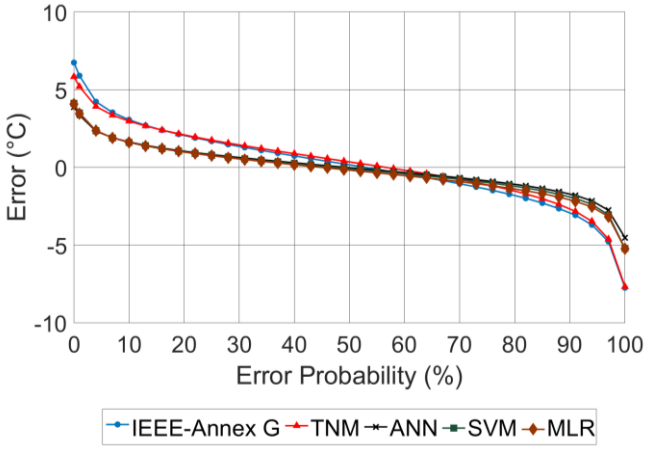

Figure 5.10 Error duration curves across all the transformers of Met Office station dataset for each algorithm.

Table 5.11 RMSEs between Measurements and Predictions made by the algorithms for each Transformer in Met Office station dataset.

Transformer ID	RMSE (°C)				
	IEEE Annex G	**TNM**	**ANN**	**SVM**	**MLR**
A	2.2	2.2	1.5	1.6	1.6
B	2.1	N/A	1.2	1.2	1.4
C	2.8	2.2	1.7	1.9	1.8
D	3.5	3.4	2.2	2.5	2.5
E	2.3	1.7	1.6	1.6	1.7
F	2.4	1.8	1.4	1.4	1.4
G	2.2	2.2	1.2	1.3	1.4
H	2.5	2.5	1.3	1.4	1.4
I	2.2	1.7	1.2	1.2	1.3
J	2.1	1.5	1.2	1.2	1.4
K	2.8	2.8	1.4	1.5	1.5
All Transformers	2.5	2.2	1.5	1.6	1.6

5.5.1 Calculating Thermal profile for "Thermally Stressful" Events

Abilities to calculate the transformer temperature at maximum capacity or even beyond are necessary [8, 9]. The degradation rate of solid insulation increases exponentially with temperature [100]. It is necessary to investigate the accuracy of the thermal model for predicting the transformer temperature during overloading conditions. This is because a miscalculation at the higher loading conditions could cause more severe consequences than at the lower loading conditions due to the exponential increase in the insulation deterioration rate.

As transmission transformers do not usually operate at maximum capacity for extended periods of time, it is unlikely to have the data to evaluate the model accuracy. Therefore, events that transformers are subjected to sufficiently high loading conditions are used instead and referred to as "Thermally Stressful" events or TS events. TS events are 100 events in the testing datasets that the 10-hour averaged load carried by the transformers are closest to their maximum capacity. Each event consists of 10 hours of data points and is at least one day apart from each other. An example of TS event is shown in Figure 5.11.

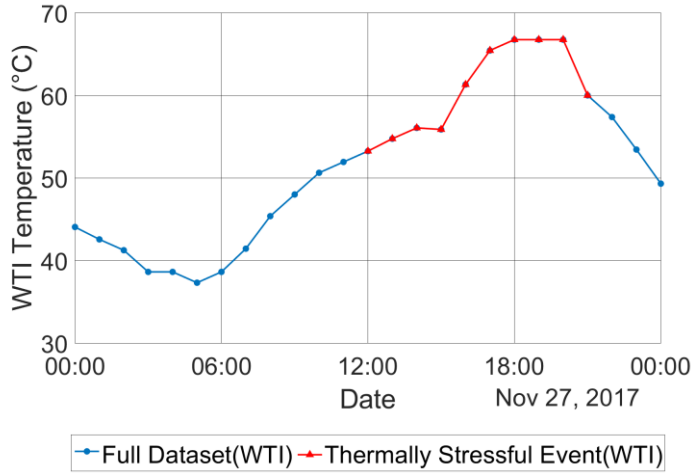

(a) WTI Measurement

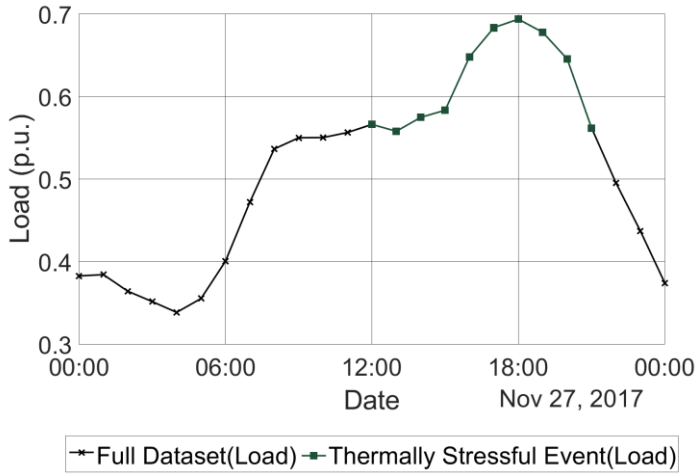

(b) Load profile

Figure 5.11 An example of 100 TS events from the WTI dataset of Transformer E. During this period, the transformer was operating in an ONAN model.

As the amount of the data in Local substation dataset is limited, the analysis is carried out for Met Office station dataset only. 100 TS events of 11 transformers are used to evaluate ability of the algorithms to estimate WTI profile while the transformers were being subjected to the thermal stress. The thermal models used to determine WTI profiles of TS events are the same as the models in 5.4. It should be noted that the TS events have never been seen by the trained models before, as they are all located within the testing dataset. For the ANN, SVM and MLR algorithms the initial point is simply taken from the data. The IEEE-Annex G and TNM algorithms require an appropriate initial condition. To achieve this the load for the first data point was altered such that a steady state solution outputted WTI temperature which matched the measured values. An example of the predictions made by the different algorithms is provided in Figure 5.12. A statistical analysis of the errors, discounting the initial data point which is set equal to the measured data and the averaged load of 100 TS events, are provided in Table 5.12. The RMSEs between the measurement and prediction made by the ANN,

SVM and MLR algorithms for TS events across all the transformers are 1.3°C, 1.4°C and 1.5°C, respectively.

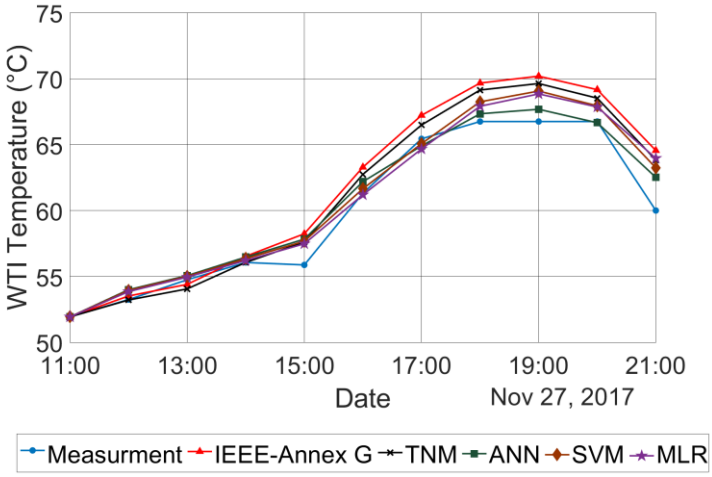

(a) Measurement and prediction

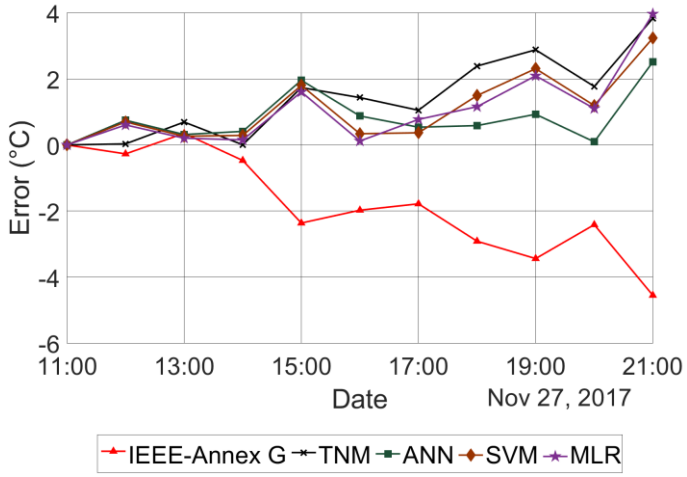

(b) Errors between measurement and prediction

Figure 5.12 Example of the predictions of different algorithms for a single TS event: (a) measurement and prediction and (b) errors between measurement and prediction. The rating event is the same as that shown in Figure 5.11.

Table 5.12 RMSEs between Measurements and Predictions on TS Events Based on the algorithms for each Transformer.

Transformer ID	Average load of TS events	RMSE (°C)				
		IEEE-Annex G	TNM	ANN	SVM	MLR
A	0.487	2.3	2.3	1.2	1.2	1.2
B*	0.599	1.9	N/A	1.1	1.1	1.3
C	0.480	2.2	1.9	1.6	1.5	1.5
D	0.524	2.2	2.0	1.4	1.8	1.8
E	0.602	2.3	2.3	1.6	1.7	2
F	0.493	2	1.9	1.2	1.3	1.2
G	0.435	2.9	2.9	1.2	1.2	1.4
H	0.459	2.8	2.8	1.4	1.4	1.5
I	0.419	2.4	2.0	1.2	1.2	1.2
J	0.443	3.4	3.1	1.3	1.5	1.5
K	0.461	2.9	2.7	1.3	1.3	1.5
All Transformers	0.491	2.5	2.4	1.3	1.4	1.5

* Transformer B is the only transformer that cooling systems are in operation.

5.5.2 Estimating Hot-Spot Temperature Rise above Ambient Temperature at Rated Load

The aim is to replicate the conditions of the heat run test by using the algorithms to determine the hot-spot temperature rise above ambient temperature at rated load. As WTI datasets of the provided transformers are recorded while the transformers are in an ONAN mode, the rated hot-spot temperature rise is calculated for the ONAN mode only excepting Transformer B that is in an OFAF state continuously. The ambient temperature is set equal to 20°C. The weather factors are set equal to zero value because the heat run test is usually undertaken indoors. The calculation assumes a nominal tap position. The calculated hot-spot temperature at rated load based on the algorithms are provided in Table 5.13.

Table 5.14 provides the percentages of the differences between the values determined from the heat run test and the alternative algorithms. The TNM algorithm outperforms the other algorithms for calculating transformer rating following with the MLR and ANN algorithms. The averaged difference between the values derived from the heat run test and the TNM algorithm for all the transformers is 4.3%.

Table 5.13 Hot-Spot Temperature at Rated Load Calculated by the Algorithms. Assuming ambient temperature of 20°C.

Transformer ID	Heat run test	Rated Hot-spot temperature (°C)				
		IEEE-Annex G	TNM	ANN	SVM	MLR
A	71.4	65.3	67.8	61.3	62.5	63.2
B	78.3	95.8	N/A	75.1	87	90.5
C	66.1	65.5	65.1	63.5	64.5	63.4
D	71.4	65.2	72	70.7	70.2	70.3
E	66.9	68.5	64.9	61.9	61.9	64.0
F	58.3	63.8	56.3	55.4	56	57.4
G	79.0	80.8	85.3	79.5	75	80.7
H	78.6	80.4	84.8	68	77.6	80.5
I	78.6	78.4	77.9	74.5	74.9	77.7
J	78.9	78.5	79.1	75.1	64.6	78.6
K	78.6	82	88	72.1	81.0	82.8

Table 5.14 Percentages of Difference between the Values Derived from the heat run test and alternative Algorithms.

Algorithm	Difference (%)
IEEE-Annex G	5.6
TNM	4.3
ANN	5.4
SVM	6.5
MLR	4.5

5.5.3 Abilities to Predict Thermal Profiles during Cooling Events

Power transformers are usually equipped with cooling pumps and fans to decrease the transformer temperature during heavily loaded conditions. While pumps and fans are working, the heat transfer is significantly enhanced because the air and transformer oil are forced to flow more quickly than when transformers cool naturally.

Thermal models developed using the operational measurement during natural cooling, and forced cooling due to prevailing wind, cannot be applied to predict the temperature during forced cooling by pumps and fans. It is necessary to develop another separate thermal model for predicting thermal profile during forced cooling periods. As operation status of pumps and fans are not usually recorded,

an algorithm to identify the cooling events will be developed first and discussed in the next section. Following that, the same algorithms are used to develop the thermal models for predicting the transformer temperature during cooling events.

5.5.3.1 Identifying Cooling Events

As cooling status of pumps and fans is not provided, periods where pumps and fans are in operation are identified by observing historical WTI time series along with load profiles. A cooling event is detected using a threshold method. The threshold values for activating and deactivating cooling system are usually set about 75°C and 50°C, respectively. However, due to sampling intervals or the other winding temperature triggering cooling system on rather than the provided WTI dataset in the same transformer, the turn-on thresholds can vary between 70°C and 75°C, whereas the turn-off threshold are between 45°C and 50°C. Using this information, an algorithm searches for a period where the WTI temperature is nearly 70°C and WTI temperatures for the next 24 hours are then captured. If the cooling system is active the WTI temperature should have decreased to the turn-off threshold value within 24 hours since the load pattern is diurnal. If WTI temperature have reached the lower threshold within the specified period, it is assumed that there is a cooling event.

Measurements recorded at hourly intervals cannot completely capture information during cooling events as the resolution is insufficient. Therefore, WTI and load measurements with 15-minute interval are used instead. An example of a cooling event from the WTI dataset of Transformer D with 15-minute interval is shown in Figure 5.13. The number of cooling events detected for Transformer D of the WTI dataset are provided in Table 5.15.

Table 5.15 Cooling Events.

Transformer ID	Data Period	Number of Cooling Events
D	01/2017 – 6/2019	50

5.5.3.2 Estimating WTI Profiles of Cooling Events from Historical Data

The same algorithms are used to develop thermal models to estimate the temperature response of the transformers during the cooling events, but the dataset is different. Only the data that are in periods of cooling events detected in the previous section are considered. Half of the number of cooling events are used to train the thermal models and the other half are used to test the models. As the number of cooling events occurring over the provided data is limited, only limited analysis can be performed. An example of the predictions made by the different algorithms is provided in Figure 5.14. A statistical analysis of the errors, discounting the initial data point which is set equal to the measured data and the number of cooling events for testing dataset, are provided in Table 5.16. Figure

5.15 shows the average absolute errors between the measurement and prediction made by the algorithms for each cooling event. There is not a sign of increase in the errors over the considered periods. This implies that the cooling performance has not changed during the considered periods. Although the ANN and SVM algorithms completely failed to estimate the WTI temperature during a cooling event occurred on 25th April 2019, the prediction made by the MLR algorithm is relatively close to the measurement as shown in Figure 5.15. This should be considered as the model failure rather than a cooling issue. This is unsurprising when there are such a limited number of datasets for training. More cooling events that occur in various load and weather conditions are required to train a more robust model.

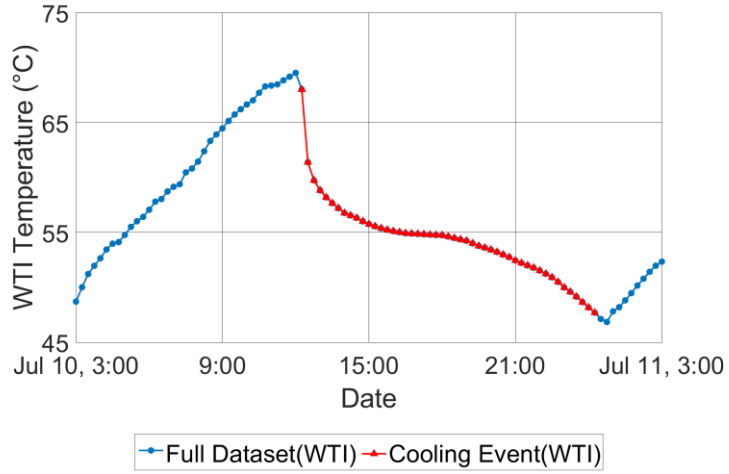

(a) WTI Measurement

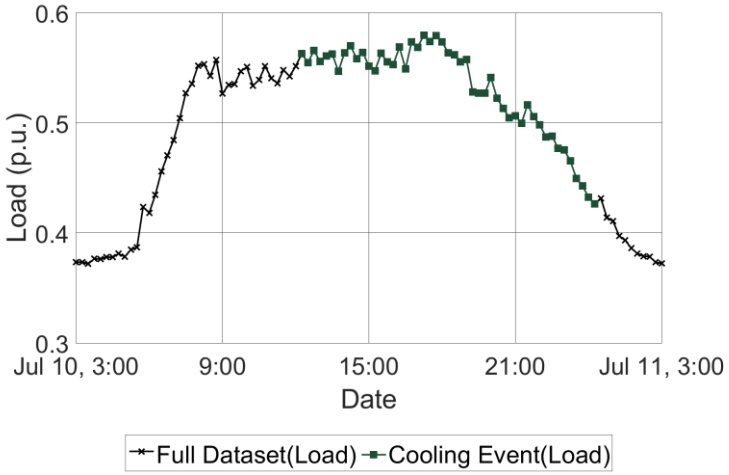

(b) Load Profile

Figure 5.13 An Example of Cooling Events from WTI dataset of Transformer D.

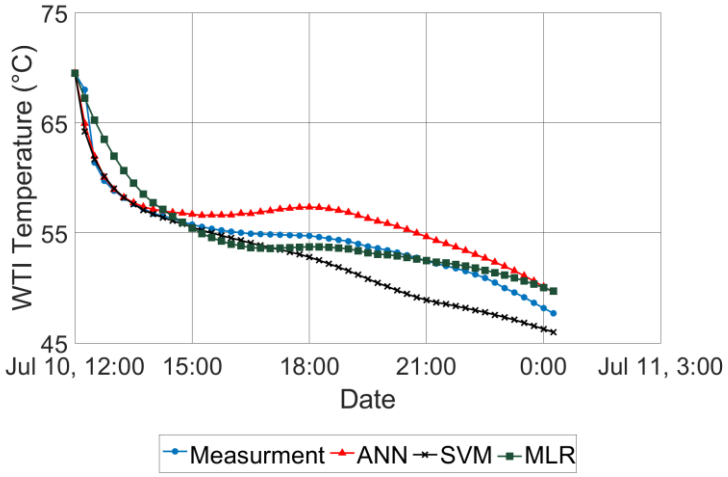

(a) Measurement and prediction

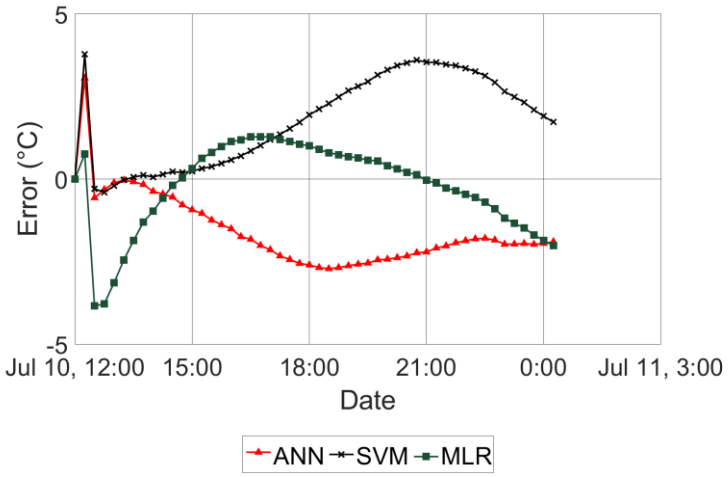

(b) Error between measurement and prediction

Figure 5.14 An Example of the measurement and predictions made by the algorithms for a cooling event: (a) Measurement and prediction and (b) errors between measurement and prediction. The cooling event is the same as that shown in Figure 5.13.

Table 5.16 RMSEs between Measurements and Predictions on Cooling Events Based on the algorithms for Transformer D.

Transformer ID	**Cooling Events**	**RMSE (°C)**		
		ANN	**SVM**	**MLR**
D	25	3	2.3	1.7

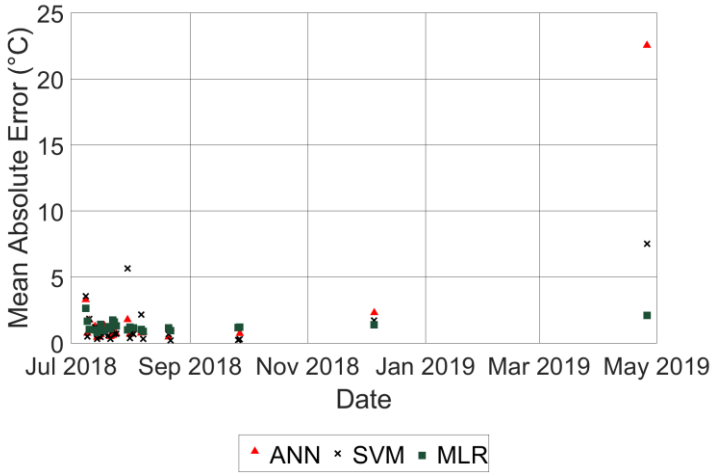

Figure 5.15 Average absolute errors of each cooling event from predictions made by the algorithms for Transformer D.

5.6 Robustness and Sensitivity

Robustness and sensitivity of the thermal models are also investigated. As the data quality is key to the algorithms' performance, sensitivity in the model performance to the number of input features (regression order), the amount of the data used to train a model and weather factors are analysed. Including all the data and input features as much as possible will not always be the most effective way as it would require longer computational time and more computational resources. The following analyses will provide useful results regarding to what extent the model performance is sensitive to the quantities of the data and the input features.

5.6.1 Regression orders

As the future WTI temperature is also dependent on the past conditions, it is of interest whether extending the inclusion of earlier data points, for example two or three time steps back could improve the performance. For the Local substation dataset which is recorded with 15-minute interval, it seems that including the data for the last 45 minutes could slightly reduce the errors from 1.3°C to 1.1°C, see Figure 5.16, however by including the data further than the last 45 minutes does not appear to improve the performance significantly. For the Met Office station dataset which is recorded with 1-hour interval, the performance does not improve any further by including more earlier data points and actually becomes less accurate, see Figure 5.17. This could be because of overfitting issues where the model tries to correlate the output data to the input data that do not have relationship with the output data.

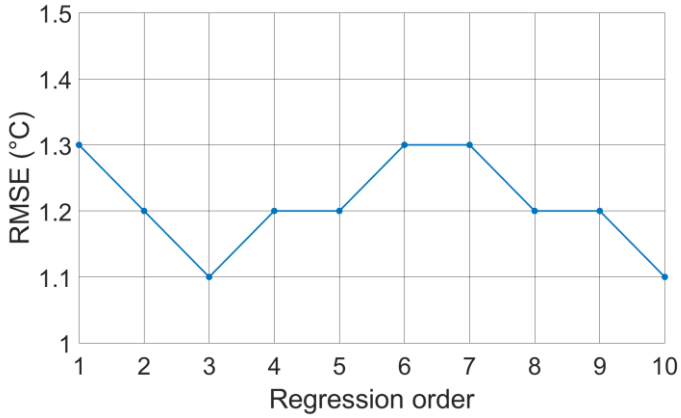

Figure 5.16 RMSE versus regression orders using Local substation dataset. Each regression order is equivalent to 15 minutes backward.

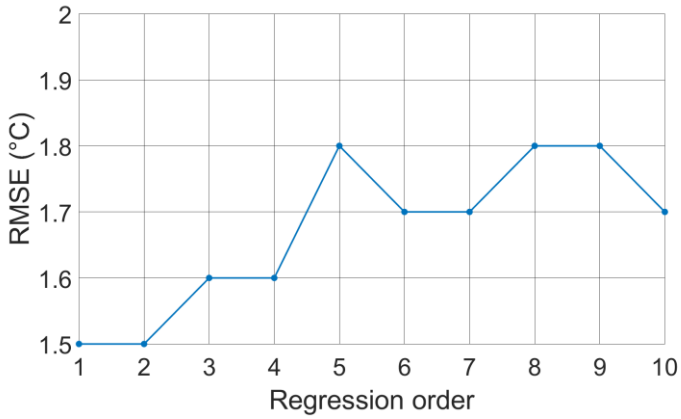

Figure 5.17 RMSE versus regression orders using Met Office station dataset. Each regression order is equivalent to one hour backward.

5.6.2 Weather Factors

An investigation on a combination of the weather factors which have the most significant impacts on the accuracy of the prediction is provided in this section. As the overall accuracy of the prediction made by the ANN algorithm has the lowest RMSE, it is used to build thermal models in this section. Basically, the models are trained with different sets of input features: 1) load, ambient temperature and previous WTI temperature, referred to as standard inputs hereafter, 2) standard inputs plus wind speed and direction, 3) standard inputs plus solar radiation and 4) standard inputs plus wind speed, wind direction and solar radiation. The RMSE between the measurement and prediction made by the different models for the Local substation and Met Office station datasets are provided in Table 5.17 and Table 5.18, respectively. It can be seen that the wind factors improve the accuracy significantly while the solar radiation does improve the accuracy for Transformer C only. This implies that the solar radiation received by Transformer C is significant compared to its total losses while it implies

the solar radiation received by the remaining transformers is an only small fraction compared to their total losses. Considering the weather factors in the model for Transformer B, which is continuously in an OFAF state and transformer tank is indoor, does not improve the performance but it seems to make it less accurate. This is likely to be because the effect of wind cooling is small compared with forced air from fans and solar radiation is only a small proportion of the total heating for this transformer which is more highly loaded.

For predicting thermal profile during cooling events for Transformer D, the evidence shows that without considering wind and solar radiation as inputs reduces the errors between the measurement and prediction see Table 5.19. It is consistent with the results of Transformer B.

Table 5.17 RMSEs between Measurements and Predictions Using Different Feature Inputs Based on the ANN algorithms for Local substation dataset.

Transformer ID	**RMSE (°C)**			
	Load, Ambient & WTI	**Load, Ambient, WTI & Wind**	**Load, Ambient, WTI & Solar**	**Load, Ambient, WTI, Wind & Solar**
A	1.5	1.3	1.7	1.2
B	1.0	1.1	1.1	1.2
C	2.2	1.6	2.1	1.4
All Transformers	1.6	1.3	1.6	1.3

Table 5.18 RMSEs between Measurements and Predictions Using Different Feature Inputs Based on the ANN algorithms for Met Office station dataset.

Transformer ID	**RMSE (°C)**			
	Load, Ambient & WTI	**Load, Ambient, WTI & Wind**	**Load, Ambient, WTI & Solar**	**Load, Ambient, WTI, Wind & Solar**
A	1.8	1.5	1.7	1.5
B	1.2	1.2	1.2	1.2
C	2.6	1.7	2.3	1.7
D	3.1	2.3	3.1	2.2
E	2	1.6	2	1.6
F	1.7	1.4	1.7	1.4
G	1.7	1.2	1.5	1.2
H	1.6	1.3	1.6	1.3
I	1.7	1.2	1.7	1.2
J	1.4	1.2	1.4	1.2
K	2.4	1.4	2.4	1.4
All Transformers	2.0	1.5	2.0	1.5

Table 5.19 RMSEs between Measurements and Predictions Using Different Feature Inputs Based on the ANN algorithms over cooling events.

Transformer ID	RMSE (°C)			
	Load, Ambient & WTI	Load, Ambient, WTI & Wind	Load, Ambient, WTI & Solar	Load, Ambient, WTI, Wind & Solar
D	1.5	3.3	2.2	3

5.6.3 Training Dataset Size

The sensitivity of the model performance against the amount of the training data is investigated. The number of training data points are varied as follows: 1) 2-year data points, 2) 1-year data points, 6-month data points, 3-month data points and 1-month data points. It is found that Model 1 trained with 2-year of data point have lowest errors between the measurement and prediction among the other models. However, the difference in the performance between Model 1 and Model 2 is insignificant. The errors increase significantly when the number of the training data is lower than 6 months. This should be because the training datasets with 2-year and 1-year data points allow the models to learn a yearly seasonal pattern which are naturally happen for weather conditions and load profile in some transformers, while the other models do not. Therefore, at least 1-year of data points for training a robust and accurate transformer thermal model are recommended.

Table 5.20 RMSEs between Measurements and Predictions Using the Different Amount of the Data Based on the ANN algorithms for Met Office station dataset.

Transformer ID	RMSE (°C)				
	2-year Data Points	1-year Data Points	6-month Data Points	3-month Data Points	1-month Data Points
A	1.5	1.6	1.8	1.8	2.6
B	N/A	1.1	1.3	2.4	2.4
C	1.7	2.6	3.2	2.4	2.8
D	2.2	2.2	2.9	3.4	4.5
E	1.6	1.6	1.9	3	3.4
F	1.4	1.4	1.8	2.4	1.9
G	1.2	1.3	1.5	2.2	2.4
H	1.4	1.4	1.7	1.8	2.2
I	N/A	1.1	1.5	2	3.9
J	1.4	1.2	1.3	2.9	3.3
K	1.4	2	1.6	3.2	4
All Transformers	1.5	1.7	2.0	2.6	3.2

5.7 Summary

The alternative algorithms based on the data driven modelling are proposed to predict the transformer temperature over various loading conditions. An overview of each algorithm is provided. The advantage of the alternative algorithms over the traditional model is that physical properties, thermal parameters and governing equations are not required. However, limitations of the proposed algorithms are that relationships between inputs and output are not explicitly understandable as the thermal model is treated as a black box, and the algorithms are prone to be less accurate for predicting loading conditions that lie outside of the range of the training dataset.

Following that, the performance of the algorithms to calculate WTI profiles for the unseen operational measurement are investigated. The alternative algorithms, ANN, SVM and MLR, outperform the IEEE-Annex G model. The RMSEs between the measurement and predictions of the alternative algorithms, ANN, SVM and MLR, TNM and IEEE Annex-G model over the three transformers based on Local substation dataset are 1.3°C, 2.0°C, 1.4°C, 1.9°C and 2.3°C, respectively.

The accuracy of the algorithms to estimate the transformer temperature during "Thermally Stressful" events is discussed. The results are promising, with the ANN algorithm capable of accurately predicting the thermal response during the TS events with the RMSE of 1.3°C. In addition, the ONAN hot-spot temperature rise above ambient temperature at rated load is calculated based on the algorithms. The results are compared with the heat run test data. The differences between the true and calculated values are about 5.4%, 6.5% and 4.5% for the ANN, SVM and MLR algorithms, respectively.

The performance of the algorithms to predict the transformer temperature during cooling events is discussed. The results are promising. Even though the number of cooling events is limited, the RMSEs between the WTI measurement and prediction made by the ANN, SVM and MLR algorithms during cooling events are 3.0°C, 2.3°C and 1.7°C. More datasets containing cooling events would improve the accuracy and robustness of the models. When wind and solar radiation are included in the ANN algorithm the performance for predicting cooling events decreases, with the RMSE increasing from 1.5°C to 3°C. This suggests that the algorithm is overfitting the data which it could be expected when the number of the training data is limited.

The sensitivity on the accuracy against the quantities of the data is investigated. The results show that including the input data only for the last 45 minutes and 1-hour is sufficient to predict the temperature at the present time for Local substation dataset and Met Office station dataset, which the sampling frequencies are 15-minute and 1-hour intervals, respectively. Considering the wind generally improves the accuracy of the prediction in all the units excepting Transformer B, which is in an OFAF state, while including the solar radiation improves the accuracy on Transformer C only. This is probably because the solar radiation might only be a small fraction compared to the total heat

losses in most transformers. The period of the training data should be at least one year so that the model can be exposed to yearly load and weather cycles.

Chapter 6

Thermal Condition Monitoring System

This Chapter presents a development of thermal condition monitoring system for power transformers that utilises the data driven thermal models developed in the previous Chapter. Due to abilities of the thermal model to estimate the transformer temperature with errors of a few Celsius given load profiles and weather information, it is feasible to develop an algorithm to identify thermal anomalies for power transformers. Relative cooling performance among transformer family could also be compared to each other using the thermal model. A comprehensive discussion of the proposed condition monitoring system is provided. The loss of insulation life of transformer, which is a useful indicator of the remaining life of the transformer, could be also calculated accurately due to the improved temperature prediction made by the data driven thermal models. The accuracy of the prediction of the loss of the life using the thermal model is provided.

6.1 Loss of Life Prediction

The end of life for power transformers is primarily due to the insulation paper no longer being able to withstand one of thermal, electrical or mechanical stresses. The degradation rate is usually dependent on the operating temperature. According to IEEE standards [8], well-dried insulation paper which is continuously subjected to a hot-spot temperature of 110°C and oxygen-free should last at least 20 years. Life expectancy could be extended if the operational temperature is less than the reference temperature and vice versa.

The relative ageing rate of the paper insulation that is given in the IEC standards [9] for non-thermally upgrade paper is then calculated using the measured and predicted transformer temperatures made by the ANN algorithm. Examples of comparisons of the cumulative loss of insulation life determined based on both the measured and predicted hot-spot temperature of Transformer A and Transformer K are shown in Figure 6.1 and Figure 6.4 for Local substation and Met Office station datasets, respectively. The total estimated cumulative loss of the insulation life over the whole testing periods for Local substation and Met Office station datasets are provided in Table 6.1 and Table 6.2, respectively.

Table 6.1 Estimated Cumulative Loss of Insulation Life Based on Measured and Predicted Temperatures over periods of Local substation testing dataset.

Transformer	Estimated Loss of Life (Hour)		
	Based on Measured Temperature	Based on Predicted Temperature	Error (%)
A	18.65	19.05	2.14
B	5.68	5.60	-1.32
C	2.25	2.20	-2.22

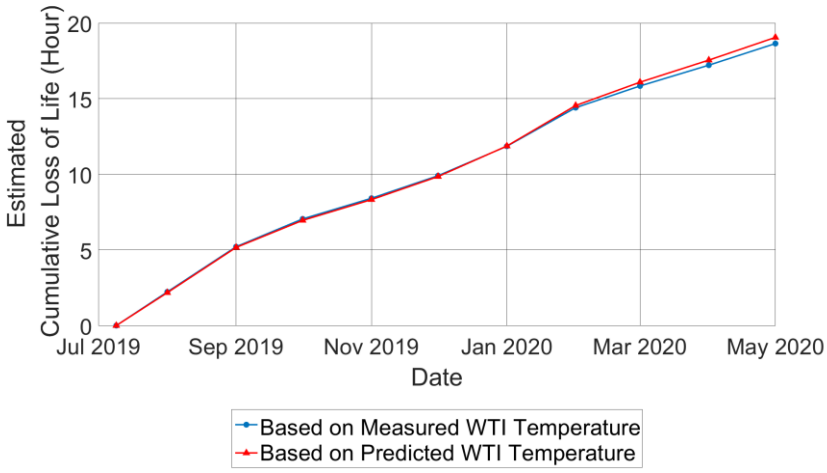

Figure 6.1 Estimated cumulative loss of insulation life over periods of Local substation testing dataset based on measured and predicted WTI temperature for Transformer A.

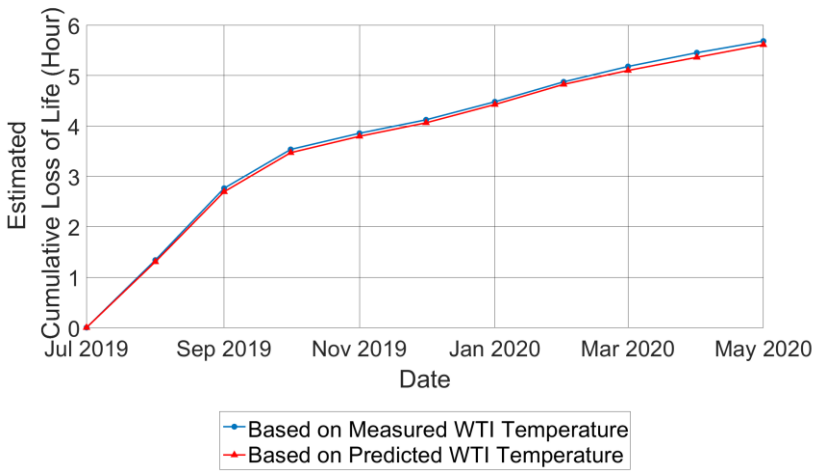

Figure 6.2 Estimated cumulative loss of insulation life over periods of Local substation testing dataset based on measured and predicted WTI temperature for Transformer B.

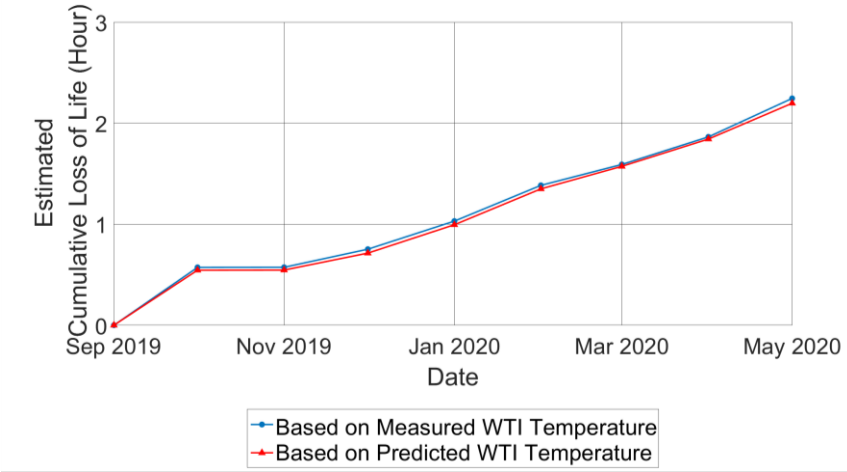

Figure 6.3 Estimated cumulative loss of insulation life over periods of Local substation testing dataset based on measured and predicted WTI temperature for Transformer C.

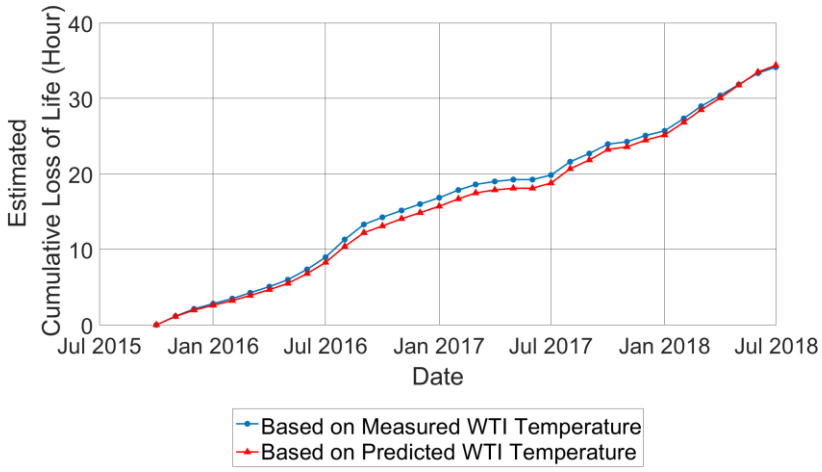

Figure 6.4 Estimated cumulative loss of insulation life over periods of Met Office station testing dataset based on measured and predicted WTI temperature for Transformer A.

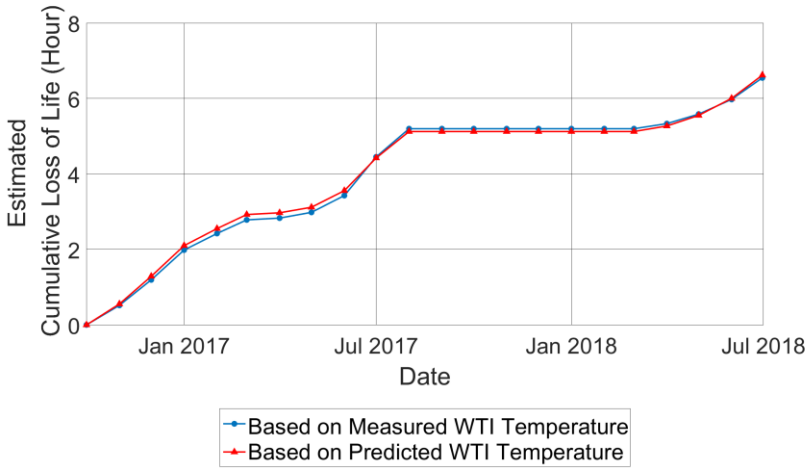

Figure 6.5 Estimated cumulative loss of insulation life over periods of Met Office station testing dataset based on measured and predicted WTI temperature for Transformer B.

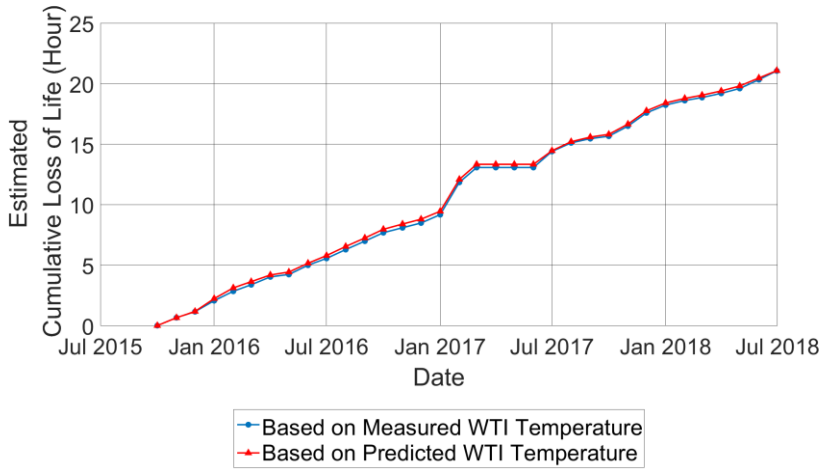

Figure 6.6 Estimated cumulative loss of insulation life over periods of Met Office station testing dataset based on measured and predicted WTI temperature for Transformer C.

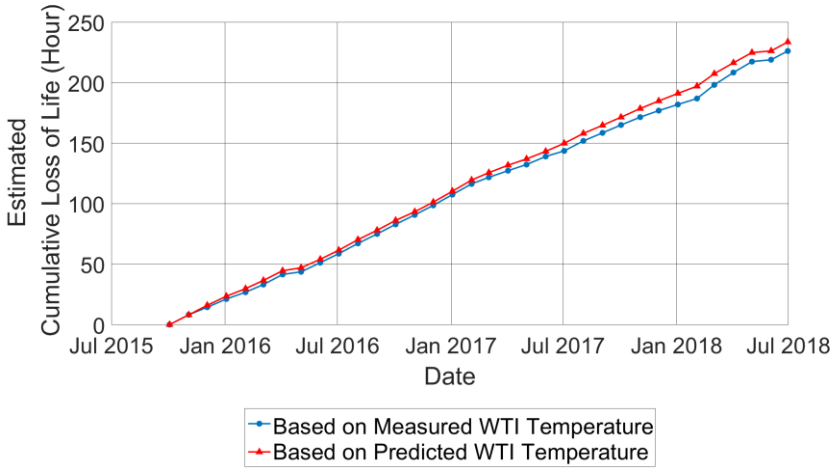

Figure 6.7 Estimated cumulative loss of insulation life over periods of Met Office station testing dataset based on measured and predicted WTI temperature for Transformer D.

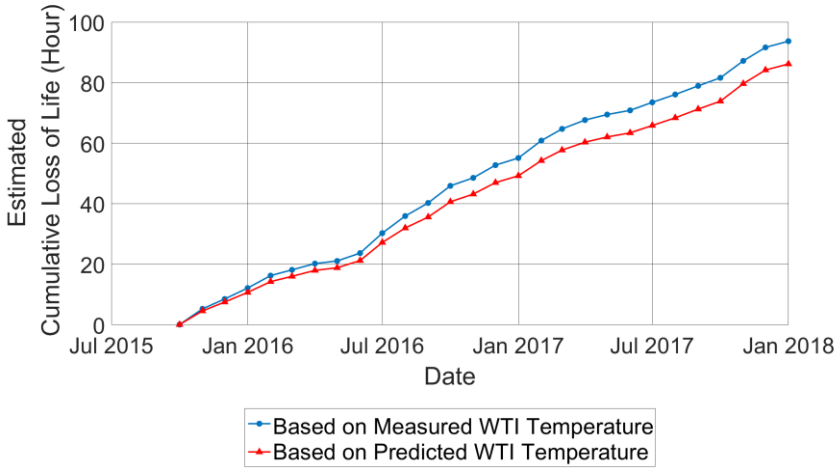

Figure 6.8 Estimated cumulative loss of insulation life over periods of Met Office station testing dataset based on measured and predicted WTI temperature for Transformer E.

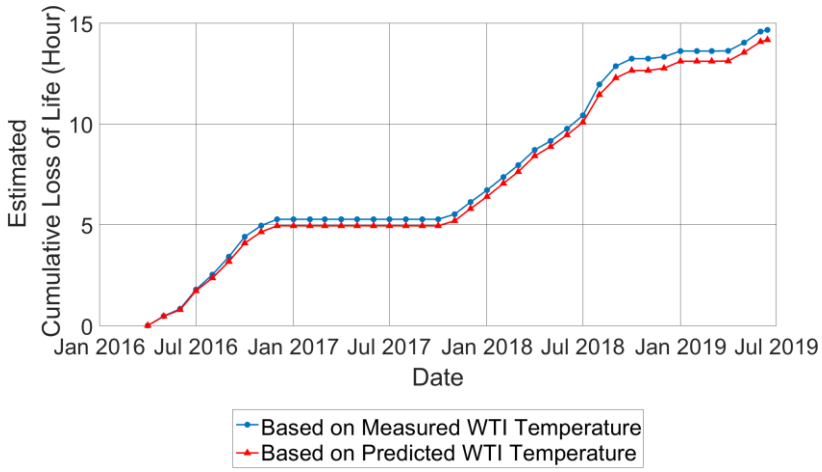

Figure 6.9 Estimated cumulative loss of insulation life over periods of Met Office station testing dataset based on measured and predicted WTI temperature for Transformer F.

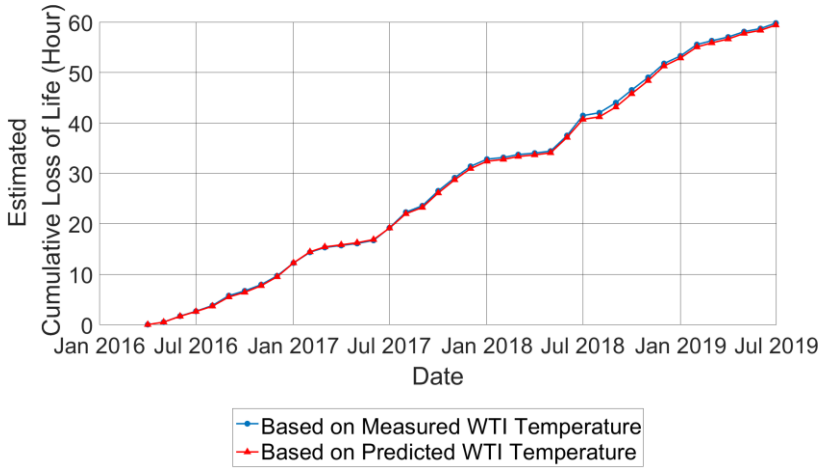

Figure 6.10 Estimated cumulative loss of insulation life over periods of Met Office station testing dataset based on measured and predicted WTI temperature for Transformer G.

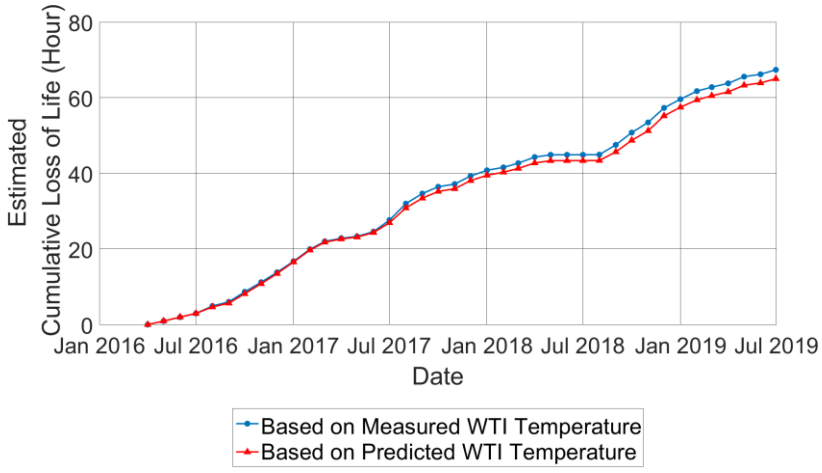

Figure 6.11 Estimated cumulative loss of insulation life over periods of Met Office station testing dataset based on measured and predicted WTI temperature for Transformer H.

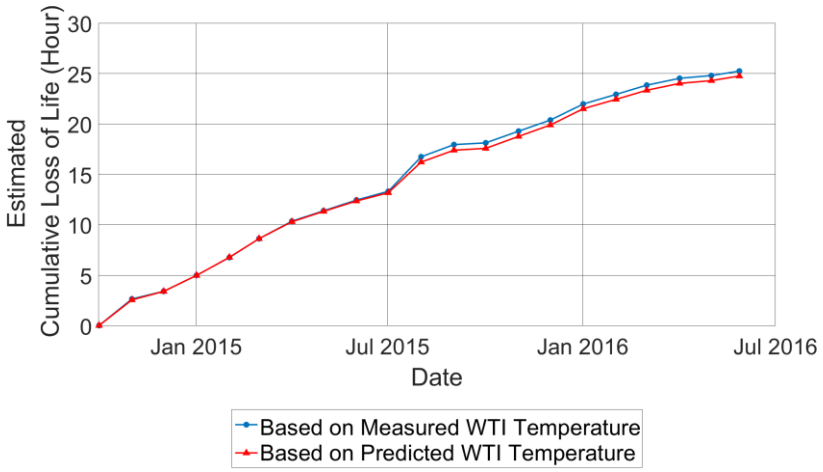

Figure 6.12 Estimated cumulative loss of insulation life over periods of Met Office station testing dataset based on measured and predicted WTI temperature for Transformer I.

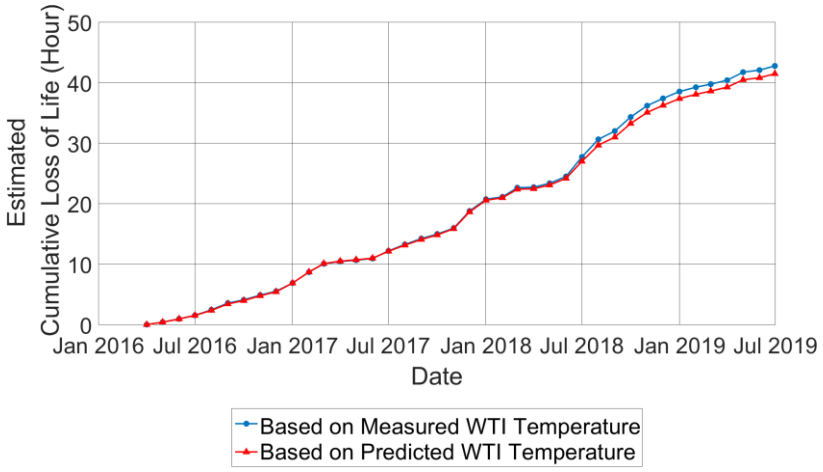

Figure 6.13 Estimated cumulative loss of insulation life over periods of Met Office station testing dataset based on measured and predicted WTI temperature for Transformer J.

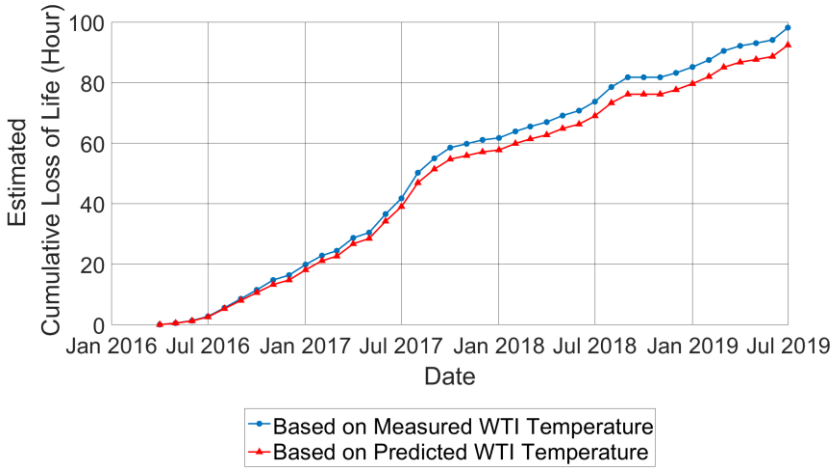

Figure 6.14 Estimated cumulative loss of insulation life over periods of Met Office station testing dataset based on measured and predicted WTI temperature for Transformer K.

Table 6.2 Estimated Cumulative Loss of Insulation Life Based on Measured and Predicted Temperatures over periods of Met Office station testing dataset.

Transformer	Estimated Loss of Life (Hour)		
	Based on Measured Temperature	**Based on Predicted Temperature**	**Error (%)**
A	34.2	35.9	4.97
B	6.5	6.6	1.54
C	21.1	21.8	3.32
D	226.1	233.6	3.32
E	93.7	86.2	-8.00
F	14.7	14.2	-3.4
G	59.8	59.4	-0.67
H	67.4	65.4	-2.97
I	25.2	24.8	-1.59
J	42.8	41.5	-3.04
K	98.2	92.4	-5.91

The errors of the estimated loss of life based on measured and predicted temperatures across 11 transformers are within ±10%. The estimated loss of life based on predicted temperature is likely to be underestimated when the loads carried by transformers on interested periods are significantly higher than the loads in the training dataset due to underestimation of the transformer temperature caused by poor extrapolation of the algorithm.

With the more accurate thermal models, the operators could use these thermal models to anticipate a new steady-state temperature caused by new higher or lower load conditions for planning, providing there is a sufficient volume of data points at this load in the training dataset. Subsequently, more accurate temperature prediction made by the thermal model improves the estimation of the loss of insulation life, and therefore it helps for planning the maintenance and replacement schedule.

6.2 Relative Thermal Performance

Typically, power transformers with the same designs are ordered in groups, which are referred to as transformer families. Theoretically, these transformers should have identical thermal behaviour. However, the transformers are subjected to loading conditions differently or are affected by imperfect manufacturing, and the ageing rate between them are therefore gradually divergent.

Using the proposed thermal model, relative thermal performance among the family could be determined. The thermal model, which is developed using the measurements of a unit in the fleet, should generally be able to be used for predicting the temperature of the other transformers in the same family, which are usually in the same substation, without significant errors if those transformers are subject to similar environmental conditions, for example they are all unaffected by solar radiation because they are in the shade. Building on this hypothesis, a thermally underperforming transformer could be distinguished from the family by creating an error matrix. The error matrix is a matrix of mean errors between the measurement and predictions made by the thermal model that is developed using its own historical data and the data of the other transformers in the same family. Typically, the mean errors between the measurement and prediction made by the thermal model using its own data should be approximately zero, however, the mean errors that are produced by the thermal model of the other transformer might be positive or negative, if the thermal behaviour between them is significantly different. If the mean error ($\bar{E}$) is positive, it means the transformer whose measurement data is used for testing is operating at a hotter temperature than the transformer used to train the model.

In the datasets considered, there are five transformers that are in the same family. The transformers could be ranked by their thermal performance using the thermal models. As the data are provided in different winding: two of them are the temperature of HV winding and three of them are the temperature of LV winding, there are two matrices: Matrix 1 (G and J) and Matrix 2 (H, I and K).

Transformer ID in the first column indicates the thermal model used for prediction and Transformer ID in the row headers indicates the measured data compared with the model prediction, see Table 6.3 and Table 6.4. It can been seen that the diagonal elements are approximately zero because the measurement and thermal model are derived from the same transformer while the elements outside the diagonal could be zero, positive or negative depending on the differences between their thermal behaviour. The results show that Transformer G is generally operating at a higher temperature than Transformer J about 4°C if the same loading conditions are applied to both transformers, see Figure 6.15. Table 6.4 suggests that Transformer K is operating hotter than its sister units followed by Transformer H and I. The temperature difference between Transformer K and I is about 7°C and the temperature difference between Transformer H and I is about 3.5°C, see Figure 6.16.

Table 6.3 Error matrix between Transformer G and J

	Measurement	
Model	**G**	**J**
G	-0.22°C	-4.12°C
J	3.87°C	-0.06°C

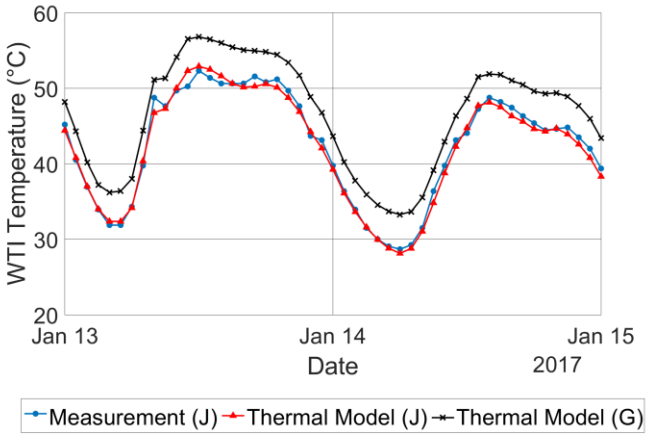

Figure 6.15 Examples of measurement of Transformer J and predictions based on the thermal models derived from Transformer J and G.

Table 6.4 Error matrix between Transformer H, I and K

	Measurement		
Model	**H**	**I**	**K**
H	-0.05°C	-3.67°C	3.95°C
I	3.66°C	-0.01°C	7.91°C
K	-3.28°C	-7.2°C	0.37°C

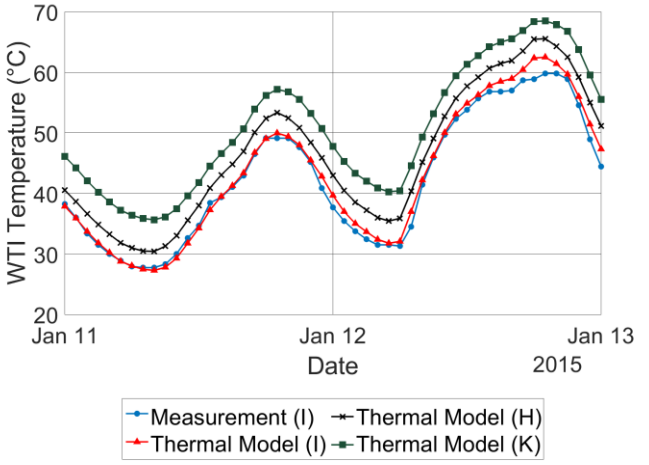

Figure 6.16 Examples of measurement of Transformer I and predictions based on the thermal models derived from Transformer I, H and K.

6.3 Incipient Thermal Fault Identification

As the alternative algorithm for calculating the transformer temperature proposed in Chapter 5 can generally predict the hot-spot temperature with the RMSEs of 1.5°C, it could be effectively used to identify anomalous thermal behaviour. An algorithm for identifying incipient thermal faults, such as restricted oil flow, is proposed using the alternative thermal model, see Figure 6.17 for a flow chart of the algorithm. Firstly, a transformer thermal model is developed using historical operational measurements. According to the previous results in 5.6.3, the models trained with 2-year data have the lowest RMSE in general. It is strongly recommended that the model should be trained with at least 1-year data so that the variations in loading condition and ambient temperature with seasons are properly captured. Secondly, a fault identification threshold (FIT) is calculated based on the training data as follows:

$$\mathrm{FIT} = \overline{|\mathrm{E}|} + 4\sigma(|E|) \qquad 6.1$$

where E are the errors between the measurement and prediction made by the algorithm for the training dataset. With regards to the error probabilities of the 11 transformers over the training datasets which contain 2-year of data for each transformer, typically 99.7% of the error lie within the values of the FIT.

Following that, the load profile, ambient temperature, solar radiation, wind speed, wind direction and the hot-spot temperature at the previous time step and the hot-spot temperature at the present time step are inputted and then the thermal model predicts the present hot-spot temperature which is compared with the measured hot-spot temperature. Subsequently, the difference between the measurement and prediction in the testing dataset ($\mathrm{E_t}$) is compared to the FIT to identify whether there is an incipient fault. There are 5 scenarios: 1) the difference between the measurement and prediction is less than FIT (No indication of an incipient fault), 2) the difference is greater than FIT but less than $\mathrm{FIT} + \mathrm{STD}$ (Level 1), 3) the difference is greater than $\mathrm{FIT} + \mathrm{STD}$ but less than $\mathrm{FIT} + 2\mathrm{STD}$ (Level 2), 4) the difference is greater than $\mathrm{FIT} + 2\mathrm{STD}$ but less than $\mathrm{FIT} + 3\mathrm{STD}$ (Level 3) and 5) the difference is greater than $\mathrm{FIT} + 3\mathrm{STD}$ (Level 4). The higher level means it is highly likely that there is an incipient thermal fault.

To ensure that reliability of the algorithm, A counting technique is introduced. A warning will be raised only if the errors have exceeded the thresholds for a certain period continuously. The periods of time vary with the magnitude of the divergence. The higher difference between the measurement and prediction is, the shorter period for that the excessive errors must have persisted is. For Level 1, to Level 4, the periods of time that the excessive errors must have persisted to raise a warning are 2 days (48 datapoints), 1 day (24 datapoints), 12 hours (12 datapoints) and 6 hours (6 datapoints), respectively. To reset all the counters, the errors must have been less than FIT for 1 day (24 datapoints) consecutively.

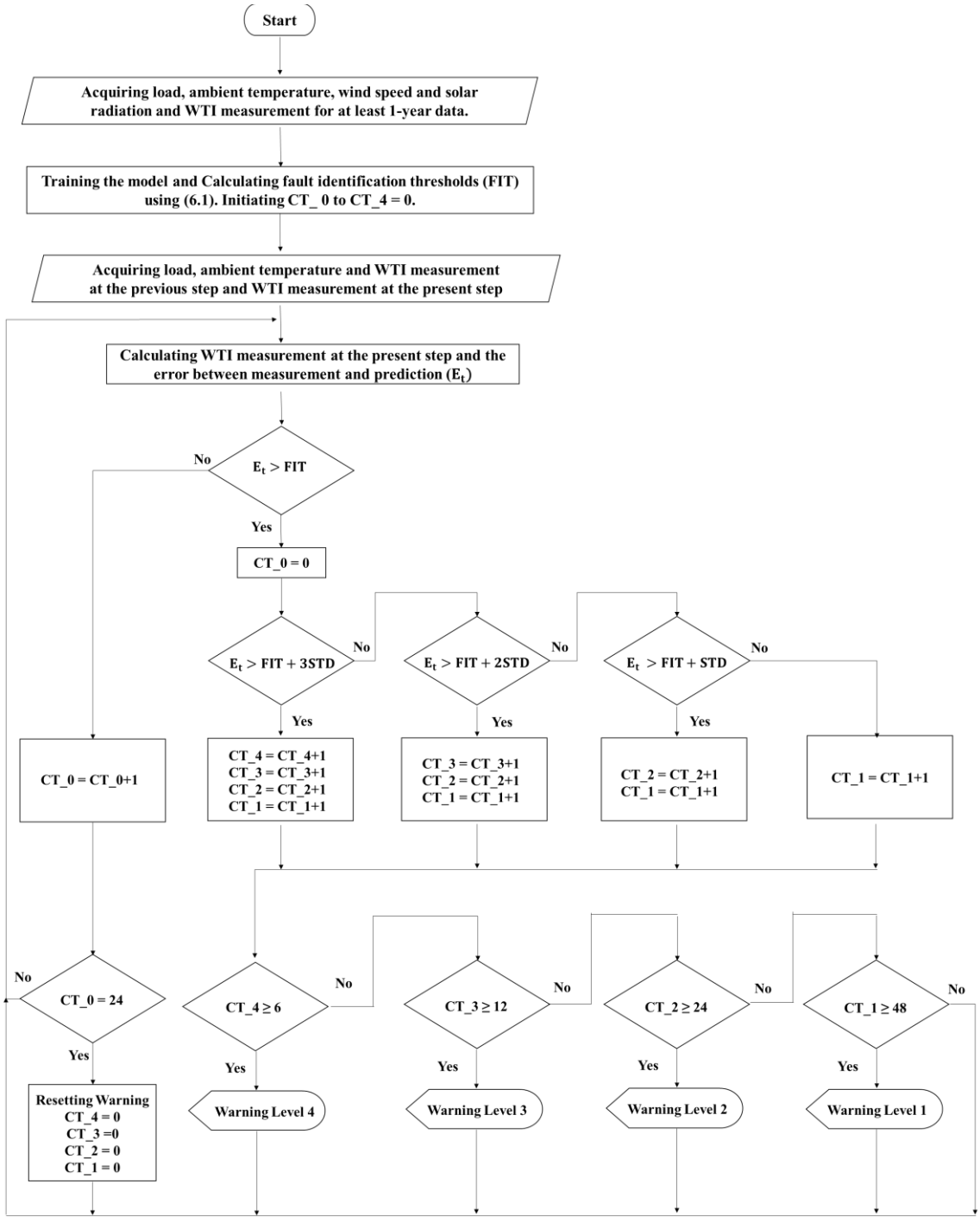

Figure 6.17 Flow chart of the algorithm of the incipient thermal fault identification

This algorithm has been applied to identify incipient faults from the measured data. It is found that there was one transformer where an incipient fault was detected by the algorithm, which is Transformer E. The model was developed using the data from 1st January 2013 and 31st December 2014 and then the threshold values were calculated, see Figure 6.18 and Figure 6.19. The predictions between 1st January 2015 and 31st December 2019 was then made by the algorithm using the load, thermal and weather measurements. There had not been a significant difference between the measurement and prediction until 3rd January 2018, after which a level 4 warning was raised. The divergence had persisted until mid-April 2019 and the measurement has approached to the prediction

again since then. Although the WTI temperature is not significantly higher than the WTI temperature in the adjacent year, the average load in the suspicious periods, 0.3 p.u., is relatively smaller than the average load in the adjacent year which is 0.4 p.u.

A list of maintenance activities for this transformer was reviewed but there were not any activities, which were carried regarding this incident. It is believed that there may have been a partial blockage of oil sludge in an oil pipe. The blockage in the oil pipe results in a reduction in the oil flow, which carries the heat away from a transformer tank to the environment via a cooler bank, causing a lower heat transfer rate. It is possibly that the blockage was cleared when the pumps were working.

Although the anomalous thermal fault was remedied without intervention, it took approximately 1 year before the problem disappeared. Using the algorithm, the issue could have been identified within one day and subsequently a proper maintenance could be planned to fix the fault. Even though there was not a catastrophic fault, the solid insulation of the transformer was aged with a higher rate for an extended period than it should be due to the higher operational temperature.

To ensure the result, another thermal model for this transformer was developed using a different training dataset instead, which is the data from 1st January 2015 to 31st December 2016, see Figure 6.21 and Figure 6.22. The similar results were observed. Besides, another thermal model was developed using the data during the periods that the thermal anomaly was identified. It is expected that the thermal model overestimates the temperature for normal periods because the thermal model was trained to capture the thermal behaviour while the cooling performance was affected by the fault, but predicts the temperature during the faulty period more accurately, see Figure 6.23 and Figure 6.24. Furthermore, another thermal model was developed using the data from another transformer which is in the same family as Transformer E. The results are shown in Figure 6.25 and Figure 6.26. Although it seems that the cooling performance of Transformer E is generally less effective than the sister transformer, during the faulty periods the cooling performance was even worse. According to those results, it infers that there was an incipient fault on that periods although it disappeared later. With the proposed algorithm, the fault could have been fixed sooner and an unnecessarily higher ageing rate could have been avoided.

It should be noted that the proposed approach will detect anomalous performance provided that the transformer is behaving “normally” in the training data. It would therefore be recommended that these algorithms are trained by the data from the commencement of service.

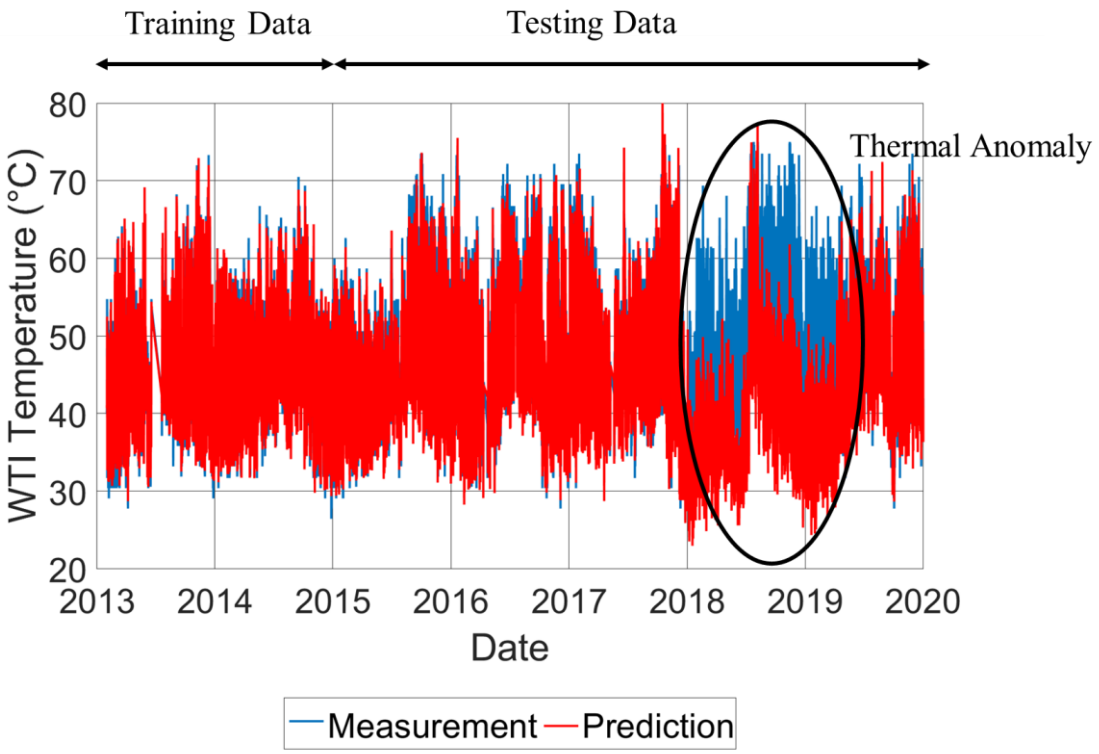

Figure 6.18 Time series of WTI measurement and prediction over training and testing datasets for Transformer E.

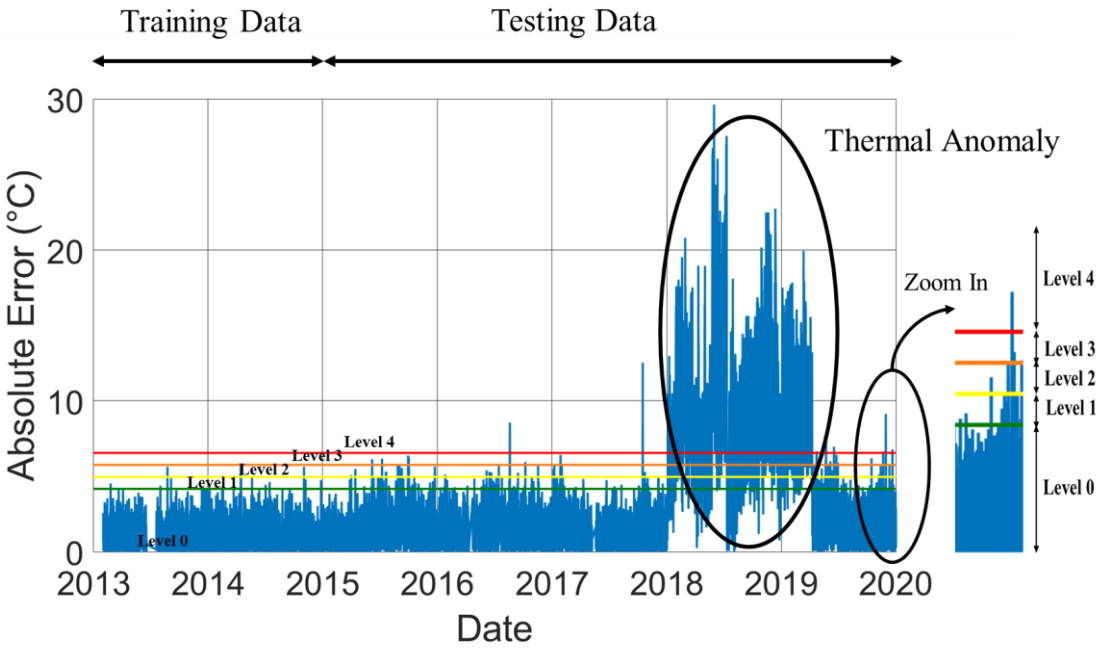

Figure 6.19 Time series of absolute errors between the measurement and prediction from Figure 6.18 showing periods that thermal anomaly was detected.

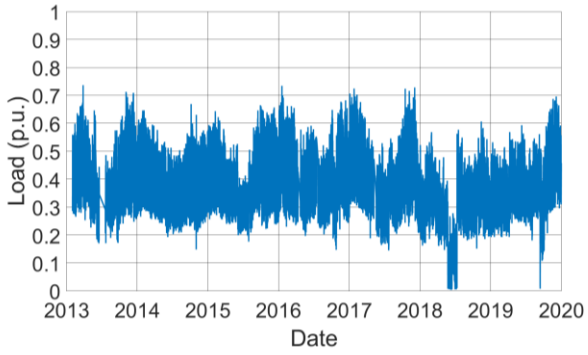

a) Load

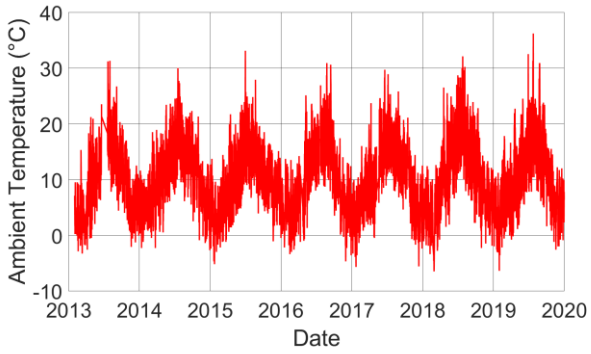

b) Ambient temperature

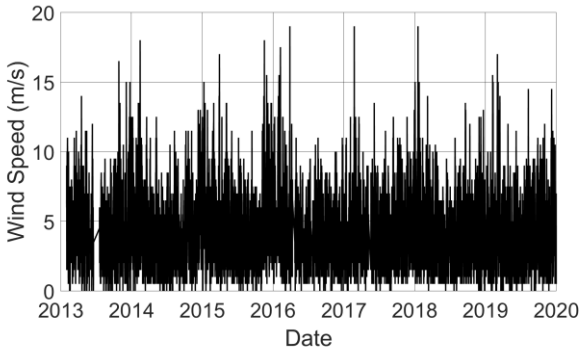

c) Wind speed

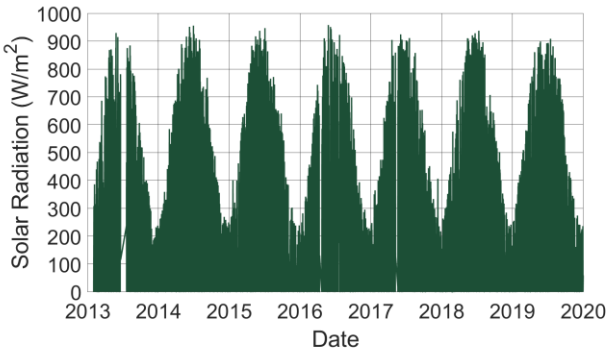

d) Solar radiation

Figure 6.20 Historical measurements for Transformer E: a) load, b) ambient temperature, c) wind speed and d) solar radiation.

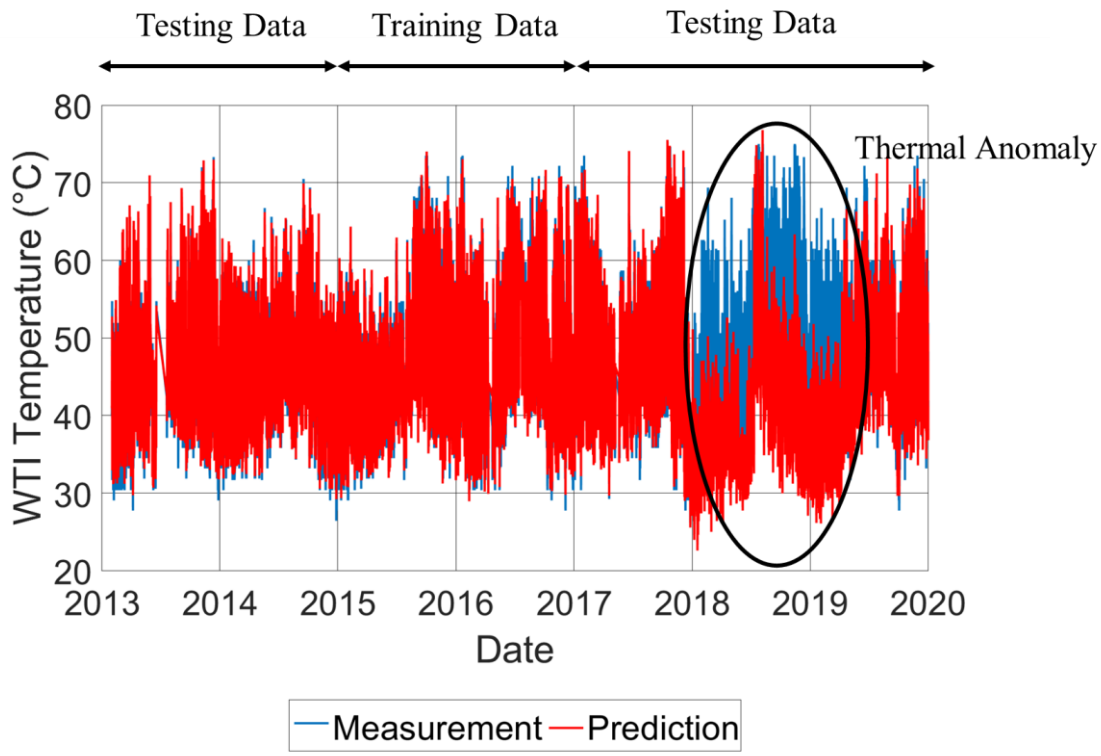

Figure 6.21 Time series of WTI measurement and prediction over training and testing datasets for Transformer E. The data is the same dataset as Figure 6.18 but the training dataset is between 1st January 2015 and 31st December 2016.

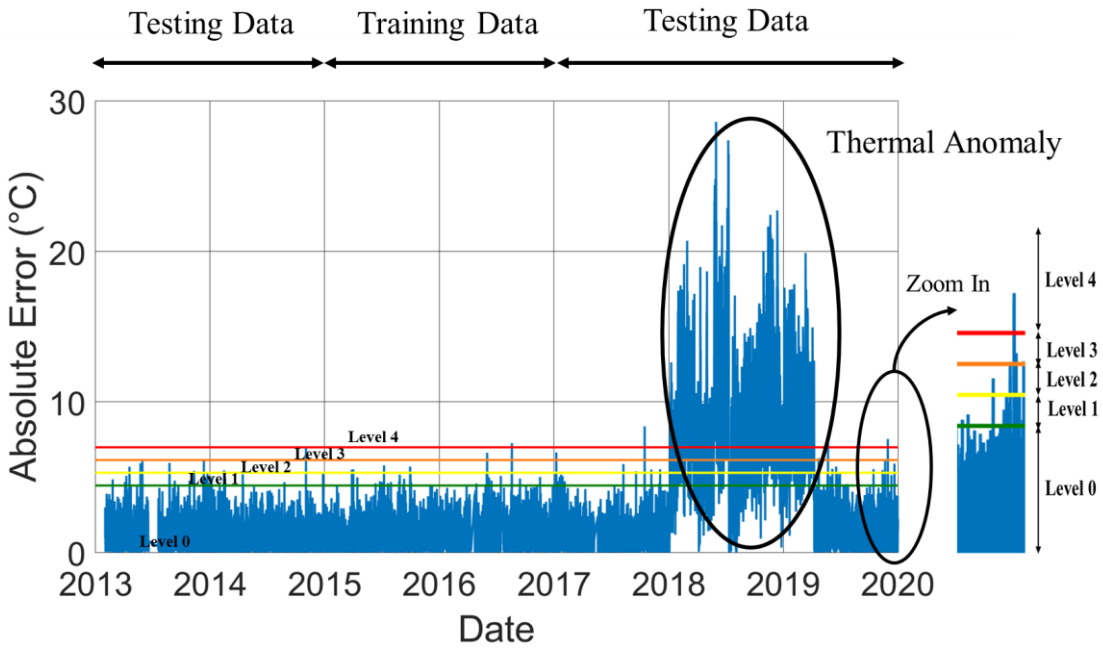

Figure 6.22 Time series of absolute errors between the measurement and prediction from Figure 6.21 showing periods that thermal anonaly was detected.

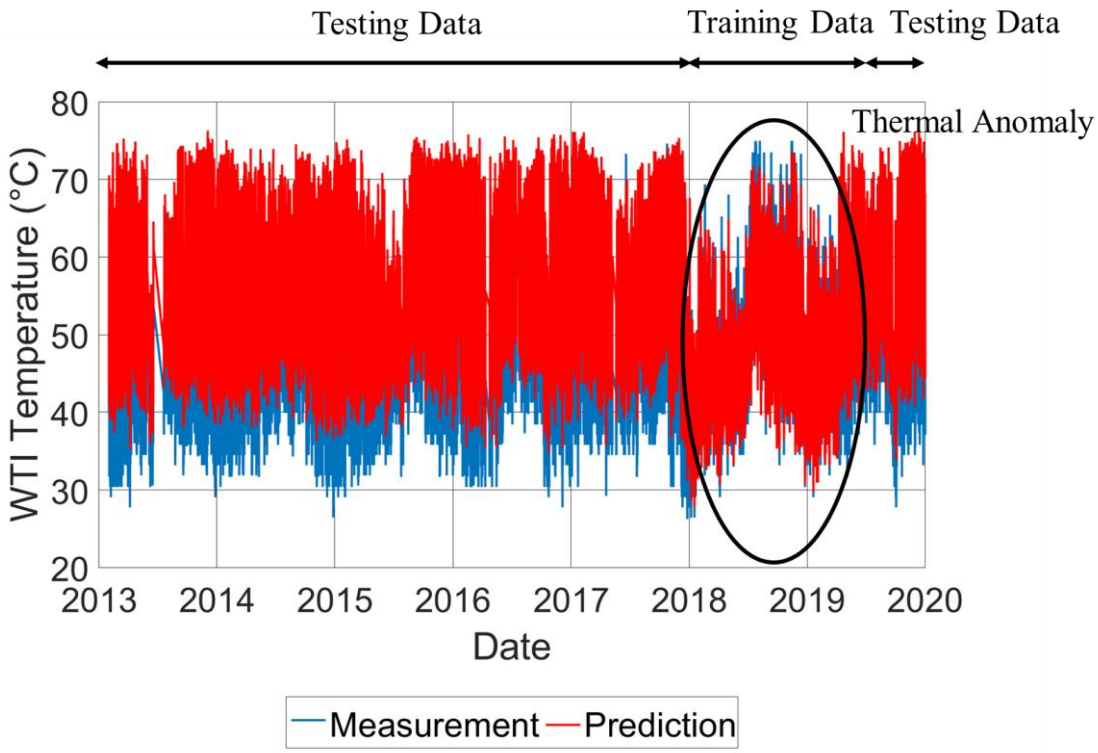

Figure 6.23 Time series of WTI measurement and prediction over training and testing datasets for Transformer E. The data is the same dataset as Figure 6.18 but the training dataset is between 3rd January 2018 and 16th April 2019.

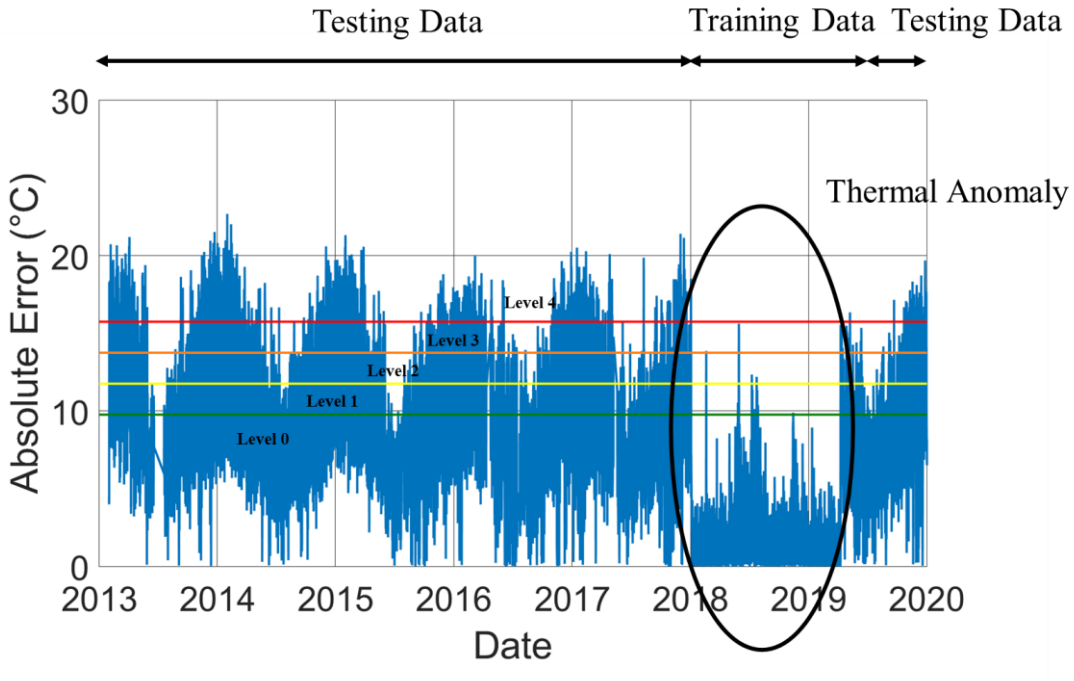

Figure 6.24 Time series of absolute errors between the measurement and prediction from Figure 6.23.

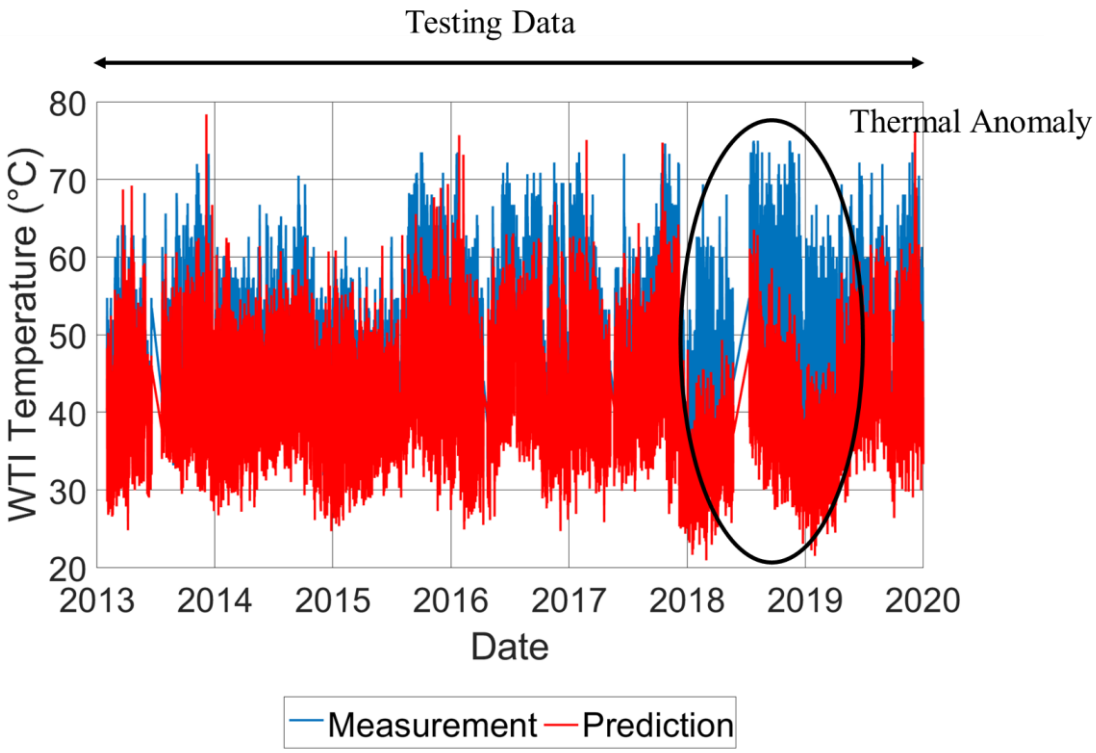

Figure 6.25 Time series of WTI measurement and prediction made by a thermal model of its sister transformer. The data is the same dataset as Figure 6.5 but the model is developed using the data from its sister transformer.

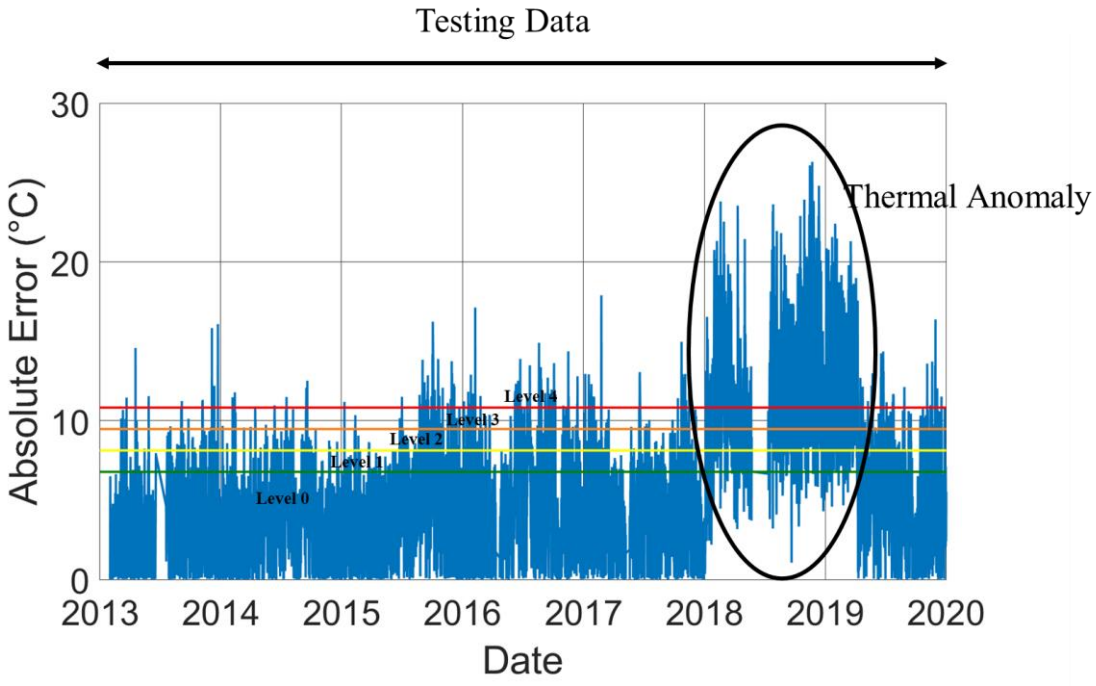

Figure 6.26 Time series of absolute errors between the measurement and prediction from Figure 6.25.

6.4 Summary

The ANN thermal models developed in Chapter 5 are used to predict the transformer temperature and the loss of the insulation life given load and weather conditions. The loss of the insulation for non-thermally upgraded insulation paper is calculated according to the IEC60076-7 [9]. The average difference between the loss of the insulation life calculated using the WTI measurement and prediction across 11 transformers is 3.52%. The accurate prediction of the loss of the insulation life is useful for the operators to plan maintenance and replacement schedules for their assets.

An error matrix is introduced to identify a transformer which is thermally underperforming from its same family. The thermal models are developed for each transformer in the same family. Following that, the thermal model for each transformer is used to predict the temperature for the other transformers. If the mean error between the measurement and prediction made by the thermal model developed from a sister transformer is approximately zero, it implies that the thermal characteristics between them are similar. On the other hand, if the mean error is significantly positive, it implies that the transformer from which the measurement is recorded would have a higher operational temperature for the same loading conditions than the transformer from which the thermal model is developed and vice versa. For example, Transformer K is typically operating at a higher temperature than Transformer I about 7°C regarding Table 6.4.

A method for incipient thermal fault identification is introduced using the thermal models. The ANN thermal model is created using the historical measurements where it is believed that the transformer is healthy. Following that, the thermal model is used to predict the transformer temperature and then compared with the measurement. The algorithm notifies the operators if the differences between measurement and prediction have been significantly greater than a specified threshold over a given period. A proper maintenance could be then planned and carried to address the issue and avoid a catastrophic failure.

Chapter 7

Conclusion and Future Work

This Chapter presents a conclusion of the thesis and a discussion of potential future work. A summary of the work undertaken is provided. A discussion of novel contributions of the work to the existing literature is provided. The implications for future thermal condition monitoring techniques are discussed.

7.1 Conclusion

The ultimate aims of this work are to develop a model to predict the thermal responses of power transformers over various loading, cooling and weather conditions using data driven modelling techniques, and to implement such an algorithm to a thermal condition monitoring system for power transformers.

Time series of WTI temperature, ambient temperature and load profiles were investigated using time series decomposition. For the transformers considered, the load was found to decrease with increasing ambient temperature, presumably because of heating demands. An algorithm was developed to check whether the WTI data exhibits expected load and ambient temperature dependency. WTI temperature rise above ambient was also found to vary with environmental conditions: wind speed, wind direction and solar radiation

The top-oil thermal model for power transformers that considers wind and solar radiation is proposed. It is based on the thermal-electrical analogy and heat transfer principles. Prevailing wind is considered as forced convection while solar radiation is taken into account as an additional heat source. The proposed model generally outperforms the traditional model, especially windy and sunny periods. It suggests that the calculation made by the traditional model may be a relatively conservative estimation for transformers in windy locations, e.g. wind farms and could lead to a decision to replace the transformers earlier than necessary on the loss of life criterion. Environmental effects should be considered if attempting to compare the as-installed transformer performance with factory heat run measurements.

Alternatively, hot-spot thermal models have been developed using data driven modelling techniques. The thermal models are treated as a black-box model and based on only the measured data. The

ANN, SVM and MLR algorithms are proposed. It appears that the ANN algorithm outperforms the other algorithms including the thermal model proposed in Chapter 4 and the IEEE-Annex G model. The RMSE between the measurement and prediction made by the ANN algorithms across 11 transformers is 1.5°C for the testing dataset. It is found that increasing the number of the hidden layers or regression order does not improve the model accuracy significantly. The accuracy of the model reduces with decreasing the amount of the training dataset and vice versa. For transformers considered that are in an ONAN state, excepting Transformer C, including the solar radiation in the alternative algorithms does not increase the accuracy significantly but considering prevailing wind does. For transformers that are in an OFAF state, inclusion of the weather factors does not improve the model accuracy. This is expected because the cooling wind is marginal compared to forced cooling by fans and the solar radiation is only a small proportional to the total heating for transformers in an OFAF state which are more highly loaded.

In addition, the algorithm of the incipient thermal fault identification has been proposed using the thermal models developed in Chapter 5. An incipient fault is identified by comparing the measurement and prediction made by the thermal model. If the differences between them are larger than the specified values for the certain periods, an alarm is raised by the algorithm to notify the operators. Proper maintenance could be then planned and carried to fix an incipient fault and a catastrophic failure is avoided. This moves us a one closer step from a dependency on time-based transformer maintenance to condition-based assessment/maintenance.

7.2 Future Work

This thesis has shown that it is viable to develop the transformer thermal models using the data driven modelling techniques and implement the algorithm to identify faulty transformers with thermal issues based on such models. In future, it is highly likely that direct fibre-optic hot-spot measurement will be available for most brand-new power transformers. Unlike WTIs, which are not direct measurement, fibre-optic sensors could be installed in multi-locations and measure local hot-spot temperatures in the winding directly. The ANN algorithm could be implemented but replacing WTI measurement with direct fibre-optic hot-spot measurement. This will improve understanding about dynamic thermal distribution inside the transformer winding and facilitate development of transformer winding thermal model.

It is found that cooling pumps and fans are rarely in operation because the transmission transformers are usually lightly loaded. This is difficult to evaluate cooling effectiveness. It will be useful for condition monitoring as well as rating calculation to develop a scheme where a number of heat run tests will be carried out on-site. Measurements gathered from the heat run tests will provide useful information of current transformer thermal conditions: cooling performance and maximum power

flow capacity. In addition, the thermal model could be developed using the data derived from the on-site heat run tests information using the data driven modelling techniques.

The same approach could be also applied to distribution transformers. An increasingly smart grid will require more reliable and effective power systems. That means that the traditional time-based maintenance needs to move forward to predictive condition-based maintenance, and an on-line rating system would be preferable to a traditional rating table. It is impossible to achieve those goals unless an accurate dynamic thermal model for transformers has been developed and its use accepted as an International Standard approach.

Appendix A Summary of Historical Data

Table A.1 Periods of Measurements for Local Substation Dataset

Transformer	Periods	Typical cooling	Comment
A	07/2019 – 05/2020	ONAN	Data comprise WTI at LV winding, tap position, load profile, ambient temperature, wind speed, wind direction and solar radiation. 15-minute sampling interval
B	07/2019 – 05/2020	OFAF	Data comprise WTI at LV winding, tap position, load profile, ambient temperature, wind speed, wind direction and solar radiation. 15-minute sampling interval
C	09/2019 – 05/2020	ONAN	Data comprise WTI at LV winding, tap position, load profile, ambient temperature, wind speed, wind direction and solar radiation. 15-minute sampling interval

Table A.2 Periods of Measurement for Met office Station Dataset

Transformer	Periods	Typical cooling	Comment
A	01/2013 – 06/2018	ONAN	Data comprise WTI at LV winding, tap position, load profile, ambient temperature, wind speed, wind direction and solar radiation. 60-minute sampling interval.
B	01/2015 – 06/2018	OFAF	Data comprise WTI at LV winding, tap position, load profile, ambient temperature, wind speed, wind direction and solar radiation. 60-minute sampling interval.
C	01/2013 – 06/2018	ONAN	Data comprise WTI at LV winding, tap position, load profile, ambient temperature, wind speed, wind direction and solar radiation. 60-minute sampling interval.
D	01/2013 – 06/2018	ONAN	Data comprise WTI at LV winding, tap position, load profile, ambient temperature, wind speed, wind direction and solar radiation. 60-minute sampling interval.
E	01/2013 – 01/2018	ONAN	Data comprise WTI at LV winding, load profile, ambient temperature, wind speed, wind direction and solar radiation. 60-minute sampling interval. Tap position is not available.
F	01/2013 – 06/2019	ONAN	Data comprise WTI at LV winding, load profile, ambient temperature, wind speed, wind direction and solar radiation. 60-minute sampling interval. Tap position is not available.
G	01/2013 – 06/2019	ONAN	Data comprise WTI at HV winding, load profile, ambient temperature, wind speed, wind direction and solar radiation. 60-minute sampling interval. There is not tap changer.
H	01/2013 – 06/2019	ONAN	Data comprise WTI at LV winding, load profile, ambient temperature, wind speed, wind direction and solar radiation. 60-minute sampling interval. There is not tap changer.
I	01/2013 – 06/2016	ONAN	Data comprise WTI at LV winding, load profile, ambient temperature, wind speed, wind direction and solar radiation. 60-minute sampling interval. There is not tap changer.

Table A.2 (continued).

J	01/2013 – 06/2019	ONAN	Data comprise WTI at HV winding, load profile, ambient temperature, wind speed, wind direction and solar radiation. 60-minute sampling interval. There is not tap changer.
K	01/2013 – 06/2019	ONAN	Data comprise WTI at LV winding, load profile, ambient temperature, wind speed, wind direction and solar radiation. 60-minute sampling interval. There is not tap changer.

Appendix B Transformer Specifications

Table B.1 Specifications of Transformers Analysed

Quantities	Transformers						
	A	**B**	**C**	**D**	**E**	**F**	**G to K**
Voltages(kV)	275/66		400/132				400/275
Nameplate Capacity (MVA)	180	180	240				1000
Typical cooling mode	ONAN	OFAF	ONAN	ONAN	ONAN	ONAN	ONAN
Load losses (kW)	992	992	748	596	792	848	1772
No-load losses (kW)	130	130	55	68	51	63	75
$\Delta\theta_{\mathrm{OR}}$ (K)	41.5	39.4	38.5	46.3	33.8	34.2	45.0
Hg_{R} (K)	7.3	22.0	8.7	5.7	14.5	5.2	15.4
Mass of coil and core, in kg	128000	128000	109000	109000	109000	109000	140000
Mass of tank and fitting, in kg	69200	69200	103750	103750	103750	103750	102000
Mass of oil, in kg	78250	78250	108850	108850	108850	108850	100000

Mass of coil, core, tank, fitting and oil for Transformer C, D and F are estimated from Transformer E because the data are not available.

Table B.2 Transformer Substation and Nearest Met Office Weather Station

Transformer ID	Transformer Location	Nearest MET Office Weather Station	Source ID
A	St. John's Wood, London	St. James's Park	697
B	St. John's Wood, London	St. James's Park	697
C	Braintree, Essex	Andrewfield	19188
D	West Ham, London	St. James's Park	697
E	Hoddesdon, Hertfordshire	Rothamsted	471
F	Walpole, Wisbech	Holbeach No2	395
G	Broxbourne, Hertfordshire	St. James's Park	697
H	Broxbourne, Hertfordshire	St. James's Park	697
I	Broxbourne, Hertfordshire	St. James's Park	697
J	Broxbourne, Hertfordshire	St. James's Park	697
K	Leeds, North Yorkshire	Bramham	534

List of References

[1] P. J. Baruah, et al., "Energy system impacts from heat and transport electrification," *Proc. Inst. Civ. Eng. Energy*, vol. 167, no. 3, pp. 139-151, 2014.

[2] W. Thuiller, "Climate change and the ecologist," *Nature,* vol. 448, pp. 550-552, 2007.

[3] K. Emanuel, "Increasing destructiveness of tropical cyclones over the past 30 years," *Nature,* vol. 436, pp. 686-688, 2005.

[4] M. Wang, A. J. Vandermaar and K. D. Srivastava, "Review of condition assessment of power transformers in service," *IEEE Electr. Insul. Mag.,* vol. 18, no. 6, pp. 12-25, 2002.

[5] T. A. Prevost and T. V. Oommen, "Cellulose insulation in oil-filled power transformers: Part I - history and development," *IEEE Electr. Insul. Mag.,* vol. 22, no. 1, pp. 28-35, 2006.

[6] T. V. Oommen and T. A. Prevost, "Cellulose insulation in oil-filled power transformers: part II maintaining insulation integrity and life," *IEEE Electr. Insul. Mag.,* vol. 22, no. 2, pp. 5-14, 2006.

[7] *Power transformer- Part 2: Temperature rise for liquid-immersed transformers,* IEC 60076-2, 2011.

[8] *IEEE Guide for Loading Mineral-Oil-Immersed Transformers and Step-Voltage Regulators,* IEEE std C57.91 2011.

[9] *Power transformer- Part 7: Loading guide for mineral-oil-immersed power transformers,* IEC 60076-7, 2018.

[10] CIGRÉ Working Group A2.24, *Thermal Peroformance of Power Transformers,* Technical Brochure 393, 2009.

[11] W. Zhan, A. E. Goulart, M. Falahi and P. Rondla, "Development of a Low-Cost Self-Diagnostic Module for Oil-Immerse Forced-Air Cooling Transformers," *IEEE Trans. Power Del.,* vol. 30, no. 1, pp. 129-137, 2015.

[12] M. Djamali and S. Tenbohlen, "Malfunction Detection of the Cooling System in Air-Forced Power Transformers Using Online Thermal Monitoring," *IEEE Trans. Power Del.,* vol. 32, no. 2, pp. 1058-1067, 2017.

[13] G. Swift, T. S. Molinski, R. Bray and R. Menzies, "A fundamental approach to transformer thermal modeling. II. Field verification," *IEEE Trans. Power Del.,* vol. 16, no. 2, pp. 176-180, 2001.

[14] G. Swift, T.S. Molinski and W. Lehn, "A fundamental approach to transformer thermal modeling. I. Theory and equivalent circuit," *IEEE Trans. Power Del.,* vol. 16, no. 2, pp. 171-175, 2001.

[15] D. Susa, M. Lehtonen and H. Nordman, "Dynamic thermal modelling of power transformers," *IEEE Trans. Power Del.,* vol. 20, no. 1, pp. 197-204, 2005.

[16] W.H. Tang, Q.H. Wu and Z. J. Richardson, "A Simplified Transformer Thermal Model Based on Thermal-Electric Analogy," *IEEE Trans. Power Delivery,* vol. 19, no. 3, pp. 1112-1119, 2004.

[17] H. Nordman, N. Rafsback and D. Susa, "Temperature Responses to Step Changes in the Load Current of Power Transformers," *IEEE Trans. Power Del.,* vol. 18, no. 4, pp. 1110-1117, 2003.

[18] D. Susa and M. Lehtonen, "Dynamic thermal modeling of power transformer: further Development-Part I," *IEEE Trans. Power Del.,* vol. 21, no. 4, pp. 1961-1970, 2006.

[19] *Power transformer- Part 1: General,* IEC 60076-1, 2011.

[20] CIGRÉ Working Group 05, "An international survey on failure in large power transformers in service," *Electra,* no. 88, 1983.

[21] CIGRÉ Working Group A2.37, *Transformer Reliability Survey,* Technical Brochure 642, 2015.

[22] *Fluid for electrotechnical applications- Unused mineral insulating oils for transformers and switchgear,* IEC60296, 2012.

[23] N. Lelekakis, D. Martin and J. Wijaya, "Ageing rate of paper insulation used in power transformers Part 1: Oil/paper system with low oxygen concentration," *IEEE Trans. Dielectr. Electr. Insul.,* vol. 19, no. 6, pp. 1999-2008, 2012.

[24] N. Lelekakis, D. Martin and J. Wijaya, "Ageing rate of paper insulation used in power transformers Part 2: Oil/paper system with medium and high oxygen concentration," *IEEE Trans. Dielectr. Electr. Insul.,* vol. 19, no. 6, pp. 2009-2018, 2012.

[25] J. Fabre and A. Pichon, “Deterioration Processes and Products of Paper in Oil. Application to Transformers,” *CIGRÉ paper,* 137, 1960.

[26] W. Lampe and E. Spicar, “The Oxygen-Free Transformer, Reduced Aging by Continuous Degassing,” *CIGRÉ paper,* 12-05, 1976.

[27] W. G. Lawson, M. A. Simmons and P. S. Gale, “Thermal Aging of Cellulose Paper Insulation,” *IEEE Trans. Electr. Insul.,* Vols. EI-12, no. 1, 1977.

[28] L. E. Lundgaard, W. Hansen, S. Ingebrigtsen, D. Linhjell and M. Dahlund, “Aging of Kraft paper by acid catalyzed hydrolysis,” *IEEE Int. Conf. Dielectr. Liq. (ICDL),* 2005, pp. 381-384.

[29] L. E. Lundgaard, W. Hansen and S. Ingebrigtsen, “Ageing of Mineral Oil Impregnated Cellulose by Acid Catalysis,” *IEEE Trans. Dielectr. Electr. Insul.,* vol. 15, no. 2, pp. 540-546, 2008.

[30] M. R. Hussain, S. S. Refaat and H. Abu-Rub, “Overview and Partial Discharge Analysis of Power Transformers: A Literature Review,” *IEEE Access,* vol. 9, pp. 64587-64605, 2021.

[31] N. A. Bakar, A. Abu-Siada and S. Islam, “A review of dissolved gas analysis measurement and interpretation techniques,” *IEEE Electr. Insul. Mag.,* vol. 30, no. 3, pp. 39-49, 2014.

[32] CIGRÉ Working Group A2.34, *Guide for Transformer Maintenance,* Technical Brochure 445, 2011.

[33] *Industrial platinum resistance thermometers and platinum temperature sensors,* IEC 60751, 2008.

[34] A. Bourgault, “Sturdy but sensitive to heat: the impact of a winding temperature on power transformer reliability,” *IEEE Power Energy Mag.,* vol. 3, no. 5, pp. 42-47, 2005.

[35] W. J. McNutt, J. C. McIver, G. E. Leibinger, D. J. Fallon and K. A. Wickersheim, “Direct Measurement of Transformer Winding Hot Spot Temperature,” *IEEE Power Eng. Rev.,* Vols. PER-4, no. 6, pp. 26-27, 1984.

[36] J. S. N’cho and I. Fofana, “Review of Fiber Optic Diagnostic Techniques for Power Transformers,” *Energies,* vol. 13, no. 7, 2020.

[37] H. Nordman and M. Lahtinen, “Thermal Overload Test on a 400-MVA Power Transformer With a Special 2.5-p.u. Short Time Loading Capability,” *IEEE Trans. Power Del.,* vol. 18, no. 1, pp. 107-112, 2003.

[38] A. Y. Arabul, F. K. Arabul and I. Senol, “Experimental thermal investigation of an ONAN distribution transformer by fiber optic sensors,” *Electr. Power Syst. Res.,* vol. 155, pp. 320-330, 2018.

[39] P. Lu et al, “Real-Time Monitoring of Temperature Rises of Energized Transformer Cores With Distributed Optical Fiber Sensors,” *IEEE Trans. Power Del.,* vol. 34, no. 4, pp. 1588-1598, 2019.

[40] CIGRÉ Working Group A2.38, *Transformer Thermal Modelling,* Technical Brochure 659, 2016.

[41] S. Tenbohlen, A. Weinläder and R. Wittmaack, “Prediction of the Oil Flow and Temperature Distribution in Power Transformers by CFD,” *CIGRE Biannual meeting 2010,* Paris, France, 2010.

[42] F. Torriano, M. Chaaban and P. Picher, “Numerical study of parameters affecting the temperature distribution in a disc-type transformer winding,” *Appl. Therm. Eng.,* vol. 30, no. 14-15, pp. 2034-2044, 2010.

[43] E.J. Kranenborg, C. O. Olsson, B. R. Samuelsson, L-Å. Lundin and R. M. Missing, “Numerical study on mixed convection and thermal streaking in power transformer windings,” *5th European Thermal Sciences Conference (EUROTHERM 2008),* 2008.

[44] P. Picher, F. Torriano, M. Chaaban, S. Gravel, C. Rajotte and B. Girard, “Optimization of transformer overload using advanced thermal modelling,” in *CIGRE 2010 A2-305*, Paris, 2010.

[45] A. Weinlader and S. Tenbohlen, “Thermal-hydraulic investigation of transformer windings by CFD modelling and measurements,” *Proceedings of the 16th International Symposium on High Voltage Engineering,* 2009.

[46] H. M. R. Campelo, M. A. Quintela, F. Torriano, P. Labbé and P. Picher, “Numerical thermofluid analysis of a power transformer disc-type winding,” *IEEE Electrical Insulation Conference,* 2016.

[47] X. Zhang, Z. Wang and Q. Liu, "Prediction of Pressure Drop and Flow Distribution in Disc-Type Transformer Windings in an OD Cooling Mode," *IEEE Trans. Power Del.,* vol. 32, no. 4, pp. 1655-1664, 2017.

[48] X. Zhang and Z. Wang, "Assessment of Hydraulic Network Models in Predicting Reverse Flows in OD Cooled Disc Type Transformer Windings," *IEEE Access,* vol. 7, pp. 139249-139257, 2019.

[49] X. Zhang, Z. Wang and Q. Liu, "Interpretation of Hot Spot Factor for Transformers in OD Cooling Modes," *IEEE Trans. Power Del.,* vol. 33, no. 3, pp. 1071-1080, 2018.

[50] S. B. Paramane, K. Joshi, W. Van der Veken and A. Sharma, "CFD Study on Thermal Performance of Radiators in a Power Transformer: Effect of Blowing Direction and Offset of Fans," *IEEE Trans. Power Del.,* vol. 29, no. 6, pp. 2596-2604, 2014.

[51] Y. J. Kim, M. Jeong, Y. G. Park and M. Y. Ha, "A numerical study of the effect of a hybrid cooling system on the cooling performance of a large power transformer," *Appl. Therm. Eng.,* vol. 136, pp. 275-286, 2018.

[52] Z. R. Radakovic and M. S. Sorgic, "Basics of Detailed Thermal-Hydraulic Model for Thermal Design of Oil Power Transformers," *IEEE Trans. Power Del.,* vol. 25, no. 2, pp. 790-802, 2010.

[53] J. Declercq and W. van der Veken, "Accurate hot spot modeling in a power transformer leading to improved design and performance," in *1999 IEEE Transmission and Distribution Conference (Cat. No. 99CH36333),* New Orleans, LA, USA, 1999.

[54] A. J. Oliver, "Estimation of transformer winding temperatures and coolant flows using a general network method," *IEE Proc. C (Gener. Transm. Distrib.),* vol. 127, no. 6, pp. 395-405, 1980.

[55] H. M. R. Campelo, L. F. Braña and X. M. Lopez-Fernandez, "Thermal hydraulic network modelling performance in real core type transformers," *2014 International Conference on Electrical Machines (ICEM),* pp. 2275-2281, 2014.

[56] V. Montsinger, "Loading Transformer By Temperature," *Trans. Am. Inst. Electr. Eng.,* vol. 49, no. 2, pp. 776-790, 1930.

[57] W. H. Tang, Q. H. Wu and Z. J. Richardson, "Equivalent heat circuit based power transformer thermal model," *IEE Proc. Electr. Power Appl.,* vol. 149, no. 2, pp. 87-92, 2002.

[58] L. W. Pierce, “Predicting Liquid Filled Transformer Loading Capability,” *IEEE Trans. Ind. Appl.,* vol. 30, no. 1, pp. 170-178, 1994.

[59] D. Susa and M. Lehtonen, “Dynamic thermal modeling of power transformers: further Development-part II,” *IEEE Trans. Power Del.,* vol. 21, no. 4, pp. 1971-1980, 2006.

[60] A. Seier, P. D. H. Hines and J. Frolik, “Data-Driven Thermal Modeling of Residential Service Transformers,” *IEEE Trans. Smart Grid,* vol. 6, no. 2, pp. 1019-1025, 2015.

[61] L. W. Pierce, “An investigation of the thermal performance of an oil filled transformer winding,” *IEEE Trans. Power Del.,* vol. 7, no. 3, pp. 1347-1358, 1992.

[62] J. Aubin and Y. Langhame, “Effect of oil viscosity on transformer loading capability at low ambient temperatures,” *IEEE Trans. Power Del.,* vol. 7, no. 2, pp. 516-524, 1992.

[63] D. Susa and H. Nordman, “A Simple Model for Calculating Transformer Hot-Spot Temperature,” *IEEE Trans. Power Del.,* vol. 24, no. 3, pp. 1257-1265, 2009.

[64] M. Djamali and S. Tenbohlen, “Hundred years of experience in the dynamic thermal modelling of power transformers,” *IET Gener. Transm. Distrib.,* vol. 11, no. 11, pp. 2731-2739, 2017.

[65] A. A. Taheri, A. Abdali and A. Rabiee, “A Novel Model for Thermal Behavior Prediction of Oil-Immersed Distribution Transformers With Consideration of Solar Radiation,” *IEEE Trans. Power Del.,* vol. 34, no. 4, pp. 1634-1646, 2019.

[66] B. Gorgan, P. V. Notingher, J. M. Wetzer, H. F. A. Verhaart, P. A. A. F. Wouters and A. V. Schijndel, “Influence of solar irradiation on power transformer thermal balance,” *IEEE Trans. Dielectr. Electr. Insul.,* vol. 19, no. 6, pp. 1843-1850, 2012.

[67] Bernardo Galletti, Andreas Blaszczyk, Wei Wu, “CFD Based Sensitivity Study of Cooling Performance of Transformer Radiators,” *2019 6th International Advanced Research Workshop on Transformers (ARWtr),* Cordoba - Spain, (6)7-9 October 2019.

[68] W. Van der Veken, S. B. Paramane, R. Mertens, V. Chandak and J. Coddé, “Increased Efficiency of Thermal Calculations via the Development of a Full Thermohydraulic Radiator Model,” *IEEE Trans. Power Del.,* vol. 31, no. 4, pp. 1473-1481, 2016.

[69] W. H. Tang, H. Zeng, K. I. Nuttall, Z. Richardson, E. Simonson and Q. H. Wu, “Development of power transformer thermal models for oil temperature prediction,” *Workshops on Real-*

World Applications of Evolutionary Computation, Springer, Berlin, Heidelberg, 2000, 195-204.

[70] Q. He, J. Si, and D. J. Tylavsky, "Prediction of Top-Oil Temperature for Transformers Using Neural Networks," *IEEE Trans. Power Del.,* vol. 15, no. 4, pp. 1205-1211, 2000.

[71] W. Bengang, W. Xinye, Y. Zhoufei and H. Hua, "A method of optimized neural network by L-M algorithm to transformer winding hot spot temperature forecasting," *2017 IEEE Electr. Insul. Conf. (EIC),* Baltimore, MD, USA, 2017, pp. 87-91.

[72] T. Qian, W. Tang, W. Jin, L. Gan, Y. Liu and G. Lu, "Comparisons of transformer top oil temperature calculation models using support vector regression optimised by genetic algorithm," *CIRED-Open Access Proceedings Journal,* pp. 69-73, 2017.

[73] Met Office (2006): MIDAS: UK Hourly Weather Observation Data. NCAS British Atmospheric Data Centre, Leeds, UK. [Online]. Available: https://catalogue.ceda.ac.uk/uuid/916ac4bbc46f7685ae9a5e10451bae7c. [Accessed 1 January 2019].

[74] Department for Business, Energy & Industrial Strategy, London, UK. [Online]. Available: https://www.gov.uk/government/statistical-data-sets/total-final-energy-consumption-at-regional-a. [Accessed 15 March 2021].

[75] Y. G. Yohanis, J. D. Mondol, A. Wright and B. Norton, "Real-life energy use in the UK: How occupancy and dwelling characteristics affect domestic electricity use," *Energy Build,* vol. 40, no. 6, pp. 1053-1059, 2008.

[76] K. Karsai, D. Kerenyi and L. Kiss, *Large Power Transformer,* Amsterdam, Elsevier, 1987.

[77] F. P. Incropera, D. P. DeWitt, T. L. Bergman and A. S. Lavine, *Fundamentals of Heat and Mass Transfer* , New York, Wiley, 2007.

[78] D. L. Siebers, R. G. Schwind and R. J. Moffat, "Experimental mixed-convection heat transfer from a large, vertical surface in a horizontal flow," United States, 1983.

[79] T. Coleman, "An Interior, Trust Region Approach for Nonlinear Minimization Subject to Bounds," *SIAM J. Optim,* vol. 6, pp. 418-445, 1996.

[80] J.A. Duffie and W.A. Beckman, *Solar Engineering of Thermal Processes 2nd edition* , New York, Wiley, 1991.

[81] A. C. P. Association, “Albedo: a measure of pavement surface reflectance,” *Concrete Pavement Research & Technology 3.05,* pp. 1-2, 2002 .

[82] I. Reda and A. Andreas, “Solar position algorithm for solar radiation applications,,” *Sol. Energy,* vol. 76, no. 5, pp. 577-589, 2004.

[83] T. Muneer, S. Etxebarria and E.J. Gago, “Monthly averaged-hourly solar diffuse radiation model for the UK,” *Build. Serv. Eng. Res. Technol.,* vol. 35, no. 6, pp. 573-584, 2014.

[84] A. Doolgindachbaporn, G. Callender, J. Pilgrim, P. Lewin and G. Wilson, “The Use of Thermal and Load Data to Identify Large Autotransformers that Have Aged and Degraded Electrical Insulation,” *2020 IEEE Electr. Insul. Conf. (EIC),* Knoxville, TN, USA, 2020, pp. 313-316.

[85] P. A. Gonzalez and J. M. Zamarreno, “Prediction of hourly energy consumption in buildings based on a feedback artificial neural network,” *Energy Build.,* vol. 37, no. 6, pp. 595-601, 2005.

[86] S. Christou, “Thermal Prognostic Condition Monitoring for MV Cable,” Ph.D. Thesis, Dept. Elect. Comput. Sci., Univ. Southampton, Southampton, UK, 2016.

[87] S. C. Chu, T. R. Hsiao, J. K. Lin, C. Wang and H. K. Chiang, “Comparison of the Performance of Linear Multivariate Analysis Methods for Normal and Dyplasia Tissues Differentiation Using Autofluorescence Spectroscopy,” *IEEE Trans. Biomed. Eng.,* vol. 53, no. 11, pp. 2265-2273, 2006.

[88] P. A. Jansson, “Neural Networks: An Overview,” *Anal. Chem.,* vol. 63, no. 6, pp. 357-362, 1991.

[89] R. Aggarwal and Y. Song, “Artificial neural networks in power systems. II. Types of artificial neural networks,” *Power Engineering Journal,* vol. 12, no. 1, pp. 41-47, 1998.

[90] Y. LeCun, Y. Bengio and G. Hinton, “Deep learning,” *Nature,* vol. 521, pp. 436-444, 2015.

[91] MathWorks, [Online]. Available: https://uk.mathworks.com. [Accessed 20 January 2019].

[92] M. T. Hagan and M. B. Menhaj, “Training feed-forward networks with the Marquardt algorithm,” *IEEE Trans. Neural Networks,* vol. 5, no. 6, pp. 989-993, 1994.

[93] A. J. Smola and B. Scholkpf, “A tutorial on support vector regression,” *Stat. Comput,* vol. 20, no. 1, pp. 199-222, 2004.

[94] J. Shawe-Taylor and N. Cristianini, “Basic kernels and kernel types,” in *Kernel Methods for Pattern Analysis*, Cambridge, Cambridge University Press, 2004, pp. 291-326.

[95] B. Scholkopf and A. J. Smola, *Learning with Kernels: Support Vector Machines, Regularization, Optimization and Beyond ,* Cambridge, MIT Press, 2002.

[96] D. Freedman, *Statistical Models: Theory and Practice,* Cambridge, Cambridge University Press, 2009.

[97] J. Močkus, “On Bayesian methods for seeking the extremum,” *Optimization techniques IFIP technical conference 1975,* Springer, Berlin, Heidelberg, pp(400-404).

[98] J. Snoek, H. Larochelle and R.P. Adams , “Practical Bayesian optimization of machine learning algorithms,” *NIPS'12: Proceedings of the 25th International Conference on Neural Information Processing Systems,* vol. 2, p. 2951–2959, 2012.

[99] C. E. Rasmussen and C. Williams, *Gaussian Processes for Machine Learning,* Cambridge, MIT Press, 2006.

[100] CIGRÉ Task Force D1.01.10, *Ageing of Cellulose in Mineral-Oil Insulated Transformers,* Technical Brochure 323, 2007.